Broad-spectrum antiviral activity of 3CLpro inhibitors against bat coronaviruses utilizing ACE2 or DPP4 receptors

by

Uttama Acharjee

D.V.M., Sylhet Agricultural University, Bangladesh, 2022

M. S., Sylhet Agricultural University, Bangladesh, 2024

A THESIS

Submitted in partial fulfillment of the requirements for the degree

MASTER OF SCIENCE

Department of Veterinary Biomedical Sciences

College of Veterinary Medicine

KANSAS STATE UNIVERSITY

Manhattan, Kansas

2026

Approved by:

Major Professor

Yunjeong Kim

Copyright

© Uttama Acharjee 2026.

Abstract

Coronaviruses are positive-sense RNA viruses that cause important diseases in both humans and animals. In humans, they cause infections ranging from a self-limiting, mild common cold to severe, life-threatening diseases, such as those caused by severe acute respiratory syndrome coronavirus (SARS-CoV), severe acute respiratory syndrome coronavirus 2 (SARS-CoV-2), and Middle East respiratory syndrome coronavirus (MERS-CoV). The coronaviruses responsible for these severe human diseases are believed to have originated in bats. Some bat coronaviruses have been shown to use human and/or bat angiotensin-converting enzyme 2 (ACE2) or dipeptidyl peptidase 4 (DPP4) receptors, highlighting their potential for future spillover into humans and the need for preparedness. Coronavirus 3C-like protease (3CLpro) is a viable therapeutic target because of its essential role in viral polyprotein processing and its conserved function and structure. In this study, we conducted multiple sequence alignment and phylogenetic analyses of all available bat coronavirus 3CLpros and evaluated the inhibitory activity of a panel of 3CLpro inhibitors against expressed recombinant 3CLpros of bat coronaviruses, including those that can utilize ACE2 or DPP4 receptors, using a fluorescence resonance energy transfer (FRET) assay. In addition, two co-crystal structures of 3CLpro-inhibitor complexes were determined. The results showed that 3CLpro was highly conserved within the subgenera *Sarbecovirus* and *Merbecovirus* but exhibited greater diversity among the analyzed subgenera and genera of coronaviruses, consistent with their

phylogenetic clustering. Despite this diversity, several 3CLpro inhibitors exhibited broad-spectrum antiviral activity against 3CLpros of bat coronaviruses across different genera. Structural analyses of 3CLpro-inhibitor co-crystal complexes provided insights into inhibitor binding and antiviral potency. These findings highlight the potential of broad-spectrum 3CLpro inhibition as a therapeutic strategy against coronaviruses with zoonotic spillover potential.

Table of Contents

List of figures vii

List of tables viii

Acknowledgments ix

Dedication xi

Chapter 1 Review of literature on coronavirus 1

1.1 Classification of coronavirus 1

1.2 Structure and genomic organization of coronavirus 4

1.2.1 Genome structure of coronavirus 4

1.2.2 Structural protein of coronavirus 5

1.2.3 Nonstructural proteins of coronavirus 7

1.2.4 Accessory proteins of coronavirus 8

1.3 Coronavirus replication 10

1.4 Coronavirus 3CLpro 13

1.4.1 Structure and function of coronavirus 3CLpro 13

1.4.2 Coronavirus 3CLpro as a therapeutic target 18

1.4.3 Antiviral resistance against 3CLpro inhibitors 20

1.5 Human coronaviruses 22

1.5.1 Human common cold associated coronaviruses 22

1.5.2 Severe Acute Respiratory Syndrome Coronavirus (SARS-CoV) 23

1.5.3 Middle East Respiratory Syndrome Coronavirus (MERS-CoV) 23

1.5.4 Severe Acute Respiratory Syndrome Coronavirus-2 (SARS-CoV-2) 24

1.5.5 Potential animal origins of human coronaviruses 24

1.6 Bat coronaviruses 27

Chapter 2 Broad-spectrum antiviral activity of 3CLpro inhibitors against bat coronaviruses utilizing ACE2 or DPP4 receptors 34

2.1 Abstract 34

2.2 Introduction 36

2.3 Materials and Methods 40

2.3.1 Multiple sequence alignment and phylogenetic analysis of bat coronavirus 3CLpros 40

2.3.2 Cloning and expression of coronavirus 3CLpro 41

2.3.3 FRET (Fluorescence resonance energy transfer) assay 46

2.3.4 3CLpro inhibitors used in the FRET assay 48

2.3.5 X-ray crystallography 51

2.4 Result 53

2.4.1 Multiple sequence alignment and phylogenetic analysis of bat coronavirus 3CLpros 53

2.4.2 FRET assay of 3CLpro inhibitors against expressed recombinant bat coronavirus 3CLpros 58

2.4.3 X-ray crystallography structure of bat coronavirus 3CLpro in complex with GC376 64

2.5 Discussion 70

2.6 Conclusion 77

References 78

List of figures

Figure 1. Taxonomic classification of coronavirus 3
Figure 2. Structure and genome organization of coronavirus.....9
Figure 3. Monomeric structure of SARS-CoV-2 3CLpro.....14
Figure 4. Sequence conservation at 3CLpro cleavage sites in human coronaviruses.....16
Figure 5. Potential animal origin of human coronaviruses 26
Figure 6. Geographic distribution of bat coronavirus sampling sites 30
Figure 7. Principle of FRET- based 3CLpro inhibition assay.....47
Figure 8. Conservation of the catalytic dyad in bat coronavirus 3CLpro sequences 54
Figure 9. Sequence conservation at 3CLpro cleavage sites in bat coronaviruses 55
Figure 10. Phylogenetic tree of coronavirus 3CLpro amino acid sequences.....57
Figure 11. Structure of bat coronavirus NL140422 3CLpro in complex with GC376 64
Figure 12. Comparison of Bat coronavirus NL1404 3CLpro with MERS-CoV 3CLpro ...65
Figure 13. Electrostatic surface of bat coronavirus NL1404 3CLpro and MERS-CoV 3CLpro.....66
Figure 14. Structure of bat coronavirus MZ1901 3CLpro in complex with GC376 68

List of tables

Table 1. Coronavirus 3CLpro used in FRET assay 43
Table 2. Structure of 3CLpro inhibitors used in FRET assay 48
Table 3. IC_{50} values of 3CLpro inhibitors against MERS-CoV, SARS-CoV, SARS-CoV-2 and FIPV 3CLPro, determined by FRET assay 62
Table 4. IC_{50} values of 3CLpro inhibitors against bat coronavirus 3CLpros, determined by FRET assay 63
Table 5. Crystallographic data for bat coronavirus 3CLpro NL1404 and MZ1908 in complex with GC376 69

Acknowledgments

First and foremost, I would like to express my sincere gratitude to my major professor, Dr. Yunjeong Kim, for her invaluable guidance, continuous support, patience, and encouragement throughout my graduate studies and research. I am forever grateful to had the opportunity to learn from her and grow as a researcher under her mentorship.

I am deeply grateful to my committee members, Dr. Kyeong-Ok Chang and Dr. Janine Seetahal for their valuable suggestions, guidance, and constructive feedback, which have contributed to my academic and professional growth. I would also like to extend my heartfelt appreciation to David George for teaching me laboratory protocols, guiding me through various experimental procedures, and always being there whenever I needed help with my laboratory work. His willingness to share his knowledge and provide support has been invaluable to me. My sincere thanks also go to my labmates, Luija Nathali, and Dr. Alexandira Zabiegala, for their friendship, cooperation, and support throughout my research journey.

I am profoundly grateful to my family for always believing in me, having faith in my abilities, and supporting me through every challenge, even from afar. I would also like to thank all my friends here in Manhattan, Kansas, who have made my life away from home happier, easier, and more meaningful through their friendship, kindness, and encouragement.

Finally, I offer my deepest gratitude to Almighty God for His blessings, strength, and guidance throughout this journey and for helping me overcome the challenges I encountered along the way.

Dedication

I dedicate this thesis to my beloved parents and my siblings, whose unconditional love, endless sacrifices, unwavering faith and constant support have been the foundation of my journey.

Chapter 1 Review of literature on coronavirus

1.1 Classification of coronavirus

Coronaviruses belong to the subfamily *Orthocoronavirinae* within the family *Coronaviridae* and the order *Nidovirales* (Figure 1) Based on comparative protein sequence analyses and phylogenetic relationships, the *Orthocoronavirinae* subfamily is classified into four genera: *Alphacoronavirus*, *Betacoronavirus*, *Gammacoronavirus* and *Deltacoronavirus* (Cui et al., 2019). Alphacoronaviruses are a highly diverse group, both genetically and in the range of hosts they infect. The genus *Alphacoronavirus* comprises fifteen subgenera whose members have been identified across multiple mammalian groups, including bats, rodents, shrews, carnivores, and ungulates (Woo et al., 2023). Examples include Lucheng Rn rat coronavirus (*Luchacovirus*) in brown rats (Wang et al., 2015), mink coronavirus (*Minacovirus*) in American mink (Vlasova et al., 2011), common shrew coronavirus Tibet-2014 (*Soracovirus*) in common shrews (Wu et al., 2018), and *Suncus murinus* coronavirus Xingguo-74 (*Sunacovirus*) in Asian house shrews. Members of *Tegacovirus* include canine coronavirus, feline coronavirus, and transmissible gastroenteritis virus (TGEV), which infect dogs, cats, and pigs, respectively. Enteric disease in pigs is caused by porcine epidemic diarrhea virus (*Pedacovirus*) (Pensaert and de Bouck, 1978) and swine acute diarrhea syndrome coronavirus (SADS-CoV) (*Rhinacovirus)* (Zhou et al., 2018). In humans, HCoV-229E (*Duvinacovirus)* and HCoV-NL63 (*Setracovirus)* are associated with mild common cold illness (Hamre and Procknow, 1966; van der Hoek et al., 2004). The genus *Betacoronavirus* includes three highly pathogenic human coronaviruses, SARS-CoV and SARS-CoV-2, which belong to the subgenus *Sarbecovirus,* and MERS-CoV, which

belongs to the subgenus *Merbecovirus.* Two additional common-cold-associated human coronaviruses, HCoV-OC43 and HCoV-HKU1, belong to the subgenus *Embecovirus* (LaTourrette et al., 2021). *Embecovirus* also includes animal coronaviruses such as murine hepatitis virus (MHV), bovine coronavirus (BCoV), and canine respiratory coronavirus (CRCoV). Bats also harbor diverse alphacoronaviruses and betacoronaviruses (Woo et al., 2012). Gammacoronaviruses and deltacoronaviruses primarily infect avian species. An important gammacoronavirus is avian infectious bronchitis virus (IBV), which causes severe respiratory disease in domestic chickens (Rafique et al., 2024). The genus *Deltacoronavirus* includes porcine deltacoronavirus (PDCoV), which is responsible for enteric disease and mortality in neonatal piglets. Human PDCoV (Hu-PDCoV) strains were identified in plasma samples from children showing acute febrile illness in Haiti (Lednicky et al., 2021), highlighting the potential for zoonotic transmission of PDCoV.

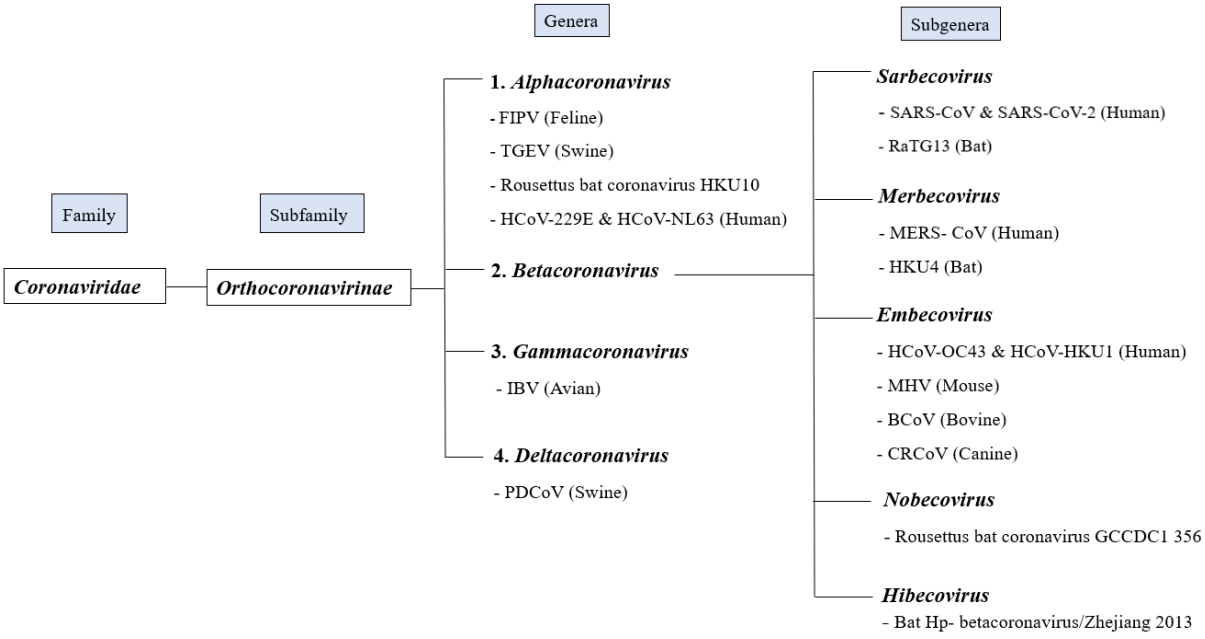


Figure 1. Taxonomic classification of coronavirus

The figure shows the taxonomic classification of coronaviruses according to the International Committee on Taxonomy of Viruses (ICTV), along with important human and animal coronaviruses within these taxonomic groups.

1.2 Structure and genomic organization of coronavirus

1.2.1 Genome structure of coronavirus

Coronaviruses are enveloped, positive-sense, single-stranded RNA viruses that possess one of the largest known genomes among RNA viruses, ranging from approximately 26 to 32 kilobases (Brant et al., 2021; Rohaim et al., 2021). The viral genome contains a 5' methylated cap and a 3' poly(A) tail (Al-Qaaneh et al., 2021). Approximately two-thirds of the genome consists of two large overlapping open reading frames (ORFs), ORF1a and ORF1b, at the 5' end. These ORFs are translated to produce two large polyproteins, pp1a and pp1ab, which are subsequently processed into 15–16 nonstructural proteins essential for viral replication and transcription. At the 3' end, the remaining one-third of the genome encodes the major structural proteins, spike (S), envelope (E), membrane (M), and nucleocapsid (N), as well as a varying number of accessory proteins (Nakagawa et al., 2016; Shamsi et al., 2021). The genomic organization follows a conserved arrangement: 5'-ORF1a/1b (replicase)-spike (S)-envelope (E)-membrane (M)-nucleocapsid (N)-3', with accessory protein genes interspersed among or within the structural genes (Fang et al., 2021) (Figure 2).

1.2.2 Structural protein of coronavirus

Coronaviruses possess prominent spike glycoproteins, approximately 20 nm in length, on their envelope surface. Under electron microscopy, these projections create a distinctive crown-like appearance, from which the family derives its name, "coronavirus" (Fehr and Perlman, 2015). The spike protein is a homotrimeric class I fusion protein composed of two functional subunits, S1 and S2 (Bosch et al., 2003; Walls et al., 2020). The S1 subunit has a receptor-binding domain (RBD), which binds to a host cell receptor and helps to determine host range and tissue tropism (Fehr and Perlman, 2015). Receptor usage varies across coronavirus species. Angiotensin-converting enzyme 2 (ACE2) is used as the functional entry receptor for SARS-CoV (Li et al., 2003), SARS-CoV-2 (Wan et al., 2020), and HCoV-NL63 (Hofmann et al., 2005). Aminopeptidase N (APN) is used by various alphacoronaviruses, including HCoV-229E (Yeager et al., 1992), TGEV (Delmas et al., 1992), and serotype II feline coronaviruses (Tekes and Thiel, 2016). Human dipeptidyl peptidase 4 (hDPP4) is used by MERS-CoV (Raj et al., 2013). Some bat coronaviruses have demonstrated the ability to utilize ACE2 (Ge et al., 2013) or DPP4 receptors (Lau et al., 2021) for host cell entry. The S2 subunit contains the fusion peptide, which is required for fusion between the viral envelope and the host cell membrane and enables the viral genome to enter host cells (Bosch et al., 2003). Membrane fusion requires proteolytic activation and conformational rearrangement of the spike protein. Several host proteases, including endosomal cathepsins, trypsin, and type II transmembrane serine proteases (TTSPs) such as TMPRSS2, can activate the coronavirus spike protein by cleaving it at the S1/S2 boundary and/or the S2' site (Belouzard et al., 2009; Hoffmann et

al., 2020b). Several coronaviruses contain a furin cleavage site (FCS) at the S1/S2 boundary, which enables proteolytic activation by the host proprotein convertase furin. Furin typically recognizes basic amino acids within the motif (R/K)-(2X)n-(R/K), where n = 0, 1, 2, or 3 (Coutard et al., 2020). Human coronaviruses HCoV-OC43 and HCoV-HKU1 encode canonical FCS motifs at their S1/S2 boundaries (Jaimes et al., 2020). MERS-CoV contains a dibasic R-X-X-R motif at both the S1/S2 and S2' sites (Millet and Whittaker, 2014). SARS-CoV-2 has a polybasic cleavage site, PRRAR, at the S1/S2 boundary that permits efficient furin-mediated pre-cleavage and subsequent spike activation (Hoffmann et al., 2020a; Walls et al., 2020).

The coronavirus membrane (M) protein is a major structural protein and plays key roles in viral morphogenesis (Zhang et al., 2022), assembly, budding, and immunomodulation (Jiang et al., 2026). The envelope protein is a small integral membrane protein that plays roles in assembly, budding, and envelope formation. It also functions as an ion channel-forming viroporin and modifies host cellular membranes to facilitate viral release from infected cells (Schoeman and Fielding, 2019). The nucleocapsid (N) protein binds to viral RNA, packages it into the ribonucleocapsid, and plays important roles in viral RNA replication and transcription (Minigulov et al., 2024). In addition to its role in the viral life cycle, the SARS-CoV-2 N protein contributes to immune evasion by suppressing pyroptosis through inhibition of gasdermin D (GSDMD) cleavage (Ma et al., 2021).

Members of the subgenus *Embecovirus*, including bovine coronavirus (BCoV) (Zhang et al., 1991), HCoV-OC43, HCoV-HKU1, and MHV, possess a fifth structural protein,

hemagglutinin-esterase (HE), which is thought to assist spike-mediated cell entry as a secondary attachment factor and act as a receptor-destroying enzyme (Lang et al., 2020). In MHV, HE also enhances neurovirulence (Kazi et al., 2005).

1.2.3 Nonstructural proteins of coronavirus

The nonstructural proteins (NSPs) of coronaviruses work together to regulate viral replication, transcription, assembly, and immune evasion. NSP3 and NSP5 are proteases that process viral polyprotein into functional non-structural proteins. NSP3, which contains the viral papain-like protease (PLpro) domain, helps coronavirus evade host antiviral immunity by its deubiquitinating activity (Barretto et al., 2005). SARS-CoV-2 PLpro cleaves interferon-stimulated gene 15 (ISG15) from host proteins, thereby suppressing type I interferon signaling and interferon regulatory factor 3 (IRF3)-mediated antiviral responses (Shin et al., 2020). NSP3, NSP4, and NSP6 remodel the host endoplasmic reticulum to form double-membrane vesicles that serve as replication sites (Kifer et al., 2025; Zhao et al., 2025). NSP12 (RNA-dependent RNA polymerase), together with its cofactors NSP7 and NSP8, drives viral RNA replication (Hillen et al., 2020). NSP13 (helicase) unwinds the viral RNA strands and forms the replication complex together with NSP8 and NSP12 (Jia et al., 2019). NSP14 possesses 3'→5' exoribonuclease activity that contributes to proofreading during viral RNA synthesis and maintains genome stability (Ferron et al., 2018). NSP1 suppresses host gene expression and innate

immune responses. NSP15 acts as an endoribonuclease that cleaves viral RNA internally, thereby limiting its recognition by host immune sensors. NSP16, together with NSP10, methylates the 5' cap of viral mRNA, allowing viral RNA to resemble host mRNA and reducing innate immune recognition (Rohaim et al., 2021).

1.2.4 Accessory proteins of coronavirus

The coronavirus accessory proteins are genus-specific or even species-specific, and the number of these accessory proteins also varies among different coronaviruses (Fang et al., 2021). For example, FIPV possesses five accessory proteins, TGEV has three, and PEDV has only one. SARS-CoV encodes eight, and SARS-CoV-2 possesses approximately nine putative accessory proteins (Cruz et al., 2011; Jantraphakorn et al., 2021; Liu et al., 2014). Although accessory proteins are nonessential for viral replication *in vitro*, cell-based studies have demonstrated their involvement in coronavirus pathogenesis by altering host cellular homeostasis, inducing apoptosis, and modulating the host innate immune system (Fang et al., 2017, 2021; McBride and Fielding, 2012).

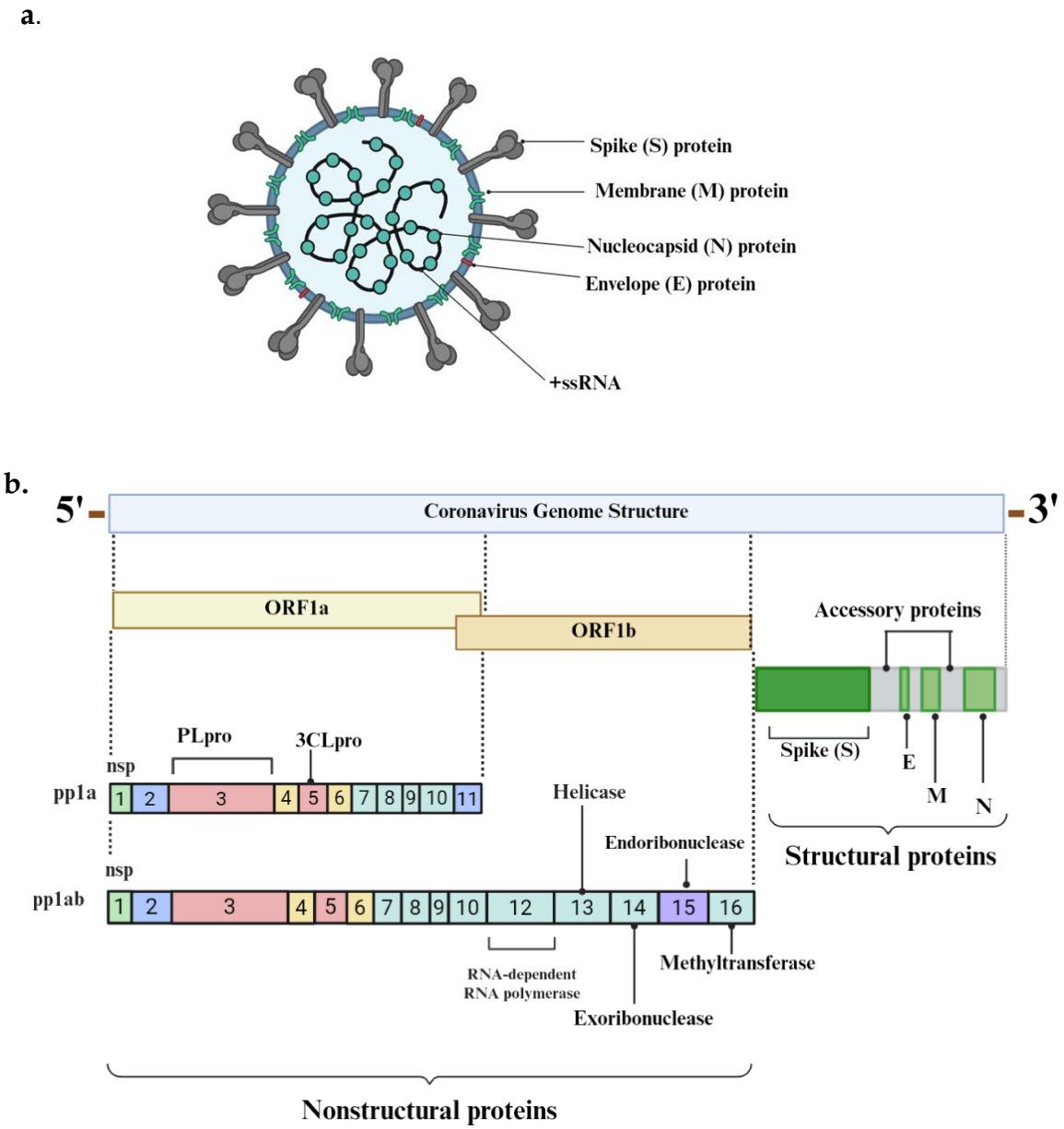


Figure 2. Structure and genome organization of coronavirus

a. Coronavirus virion showing the four major structural proteins: spike (S), membrane (M), envelope (E), and nucleocapsid (N) and the positive-sense single-stranded RNA (+ssRNA) genome.

b. Organization of the coronavirus genome. The 5' region of the genome contains ORF1a and ORF1b, which encode the polyproteins pp1a and pp1ab. These polyproteins are cleaved to generate non-structural proteins (nsp1-nsp16). The 3' region encodes the structural and accessory proteins. Created with BioRender.com.

1.3 Coronavirus replication

The initial step of coronavirus infection involves the specific binding of the viral spike protein to cellular receptors such as ACE2, DPP4, or APN (V'kovski et al., 2021). The availability of specific host cell proteases that cleave and activate the S protein to mediate membrane fusion helps to determine the predominant viral entry route. When surface proteases such as TMPRSS2 are present on the plasma membrane, spike activation can occur at the cell surface, allowing direct fusion between the viral envelope and the host cell membrane through the early entry pathway (Hoffmann et al., 2020b; Jackson et al., 2022; Koch et al., 2021). In the absence of these surface proteases, entry can occur through the late entry pathway, also known as the endosomal pathway, in which virions are internalized by endocytosis and spike activation is mediated by cathepsins within endosomal compartments (Jackson et al., 2022; Koch et al., 2021).

Following cell entry and uncoating, the positive-sense genomic RNA is translated by host ribosomes. Translation of ORF1a at the 5' end of the genome produces the replicase polyprotein pp1a, whereas translation extending into ORF1b produces pp1ab. The formation of pp1ab occurs through a programmed -1 ribosomal frameshift at the short overlapping region between ORF1a and ORF1b (Brierley and Dos Ramos, 2006). The replicase polyproteins must undergo proteolytic processing to generate functionally active nonstructural proteins. Nsp1–nsp11 are generated by cleavage of pp1a, while cleavage of pp1ab results in the formation of nsp1–nsp10 and nsp12–nsp16 (Madhugiri et al., 2026; Malone et al., 2022). The papain-like protease (PLpro) within nsp3 cleaves the

nsp1/nsp2, nsp2/nsp3, and nsp3/nsp4 junctions (Lei et al., 2025). Following autoproteolytic release from its polyprotein precursor, the coronavirus main protease (3CLpro) processes the remaining cleavage sites (Fehr and Perlman, 2015). These cleavage reactions generate 15 or 16 nonstructural proteins from the replicase polyproteins. Nsp12 (RNA-dependent RNA polymerase, RdRp), nsp13 (helicase), nsp14 (3'→5' exoribonuclease), and nsp16 (methyltransferase), along with cofactors nsp7, nsp8, and nsp10, assemble into membrane-associated replication-transcription complexes (RTCs) (Malone et al., 2022). RTCs are anchored in double-membrane vesicles (DMVs), which are most likely derived from the endoplasmic reticulum (ER) (Hagemeijer et al., 2010). Coronavirus RNA synthesis involves two coordinated processes: genome replication and transcription. The RTC synthesizes full-length negative-sense RNA in a continuous process, and this serves as the template for new positive-sense genomic RNA (gRNA) (Sola et al., 2015). This gRNA has three major roles: it is packaged into newly formed virions, serves as a template for additional RNA synthesis, and acts as the mRNA for translation of the replicase polyproteins (Madhugiri et al., 2026). Coronavirus subgenomic RNAs (sgRNAs), which encode the structural and accessory proteins in the 3′ region of the genome, are produced through a discontinuous process mediated by transcription-regulatory sequences (TRSs) (Sola et al., 2015). The viral genome contains a leader TRS (TRS-L) at the 5' end and multiple body TRSs (TRS-Bs) upstream of the structural and accessory protein genes. During negative-strand RNA synthesis, the RTC pauses at a TRS-B and switches to the TRS-L, which has a complementary nucleotide sequence. This template-switching process generates negative-strand sgRNAs containing

a common 5' leader sequence (Williams et al., 2025). These negative-strand sgRNAs then serve as templates for the synthesis of positive-sense sgRNAs, which form a nested set of mRNAs sharing the same 5' leader and 3' end. These mRNAs are translated into the structural and accessory proteins. Following translation, the structural proteins accumulate at the endoplasmic reticulum–Golgi intermediate compartment (ERGIC), where they, together with the N-encapsidated genome, assemble into mature virions that bud into the ERGIC lumen (Stertz et al., 2007). Assembled virions are then carried to the cell surface in vesicles and released by exocytosis.

1.4 Coronavirus 3CLpro

1.4.1 Structure and function of coronavirus 3CLpro

Coronavirus main protease is termed 3C-like protease (3CLpro) because it shares substrate specificity and structural features with picornavirus 3C protease (3Cpro), including a chymotrypsin-like fold and a catalytic cysteine residue (Anand et al., 2002). Picornavirus 3Cpro is generally monomeric and contains a catalytic triad composed of cysteine (Cys), histidine (His), and glutamic acid (Glu) residues (Cys–His–Glu), whereas coronavirus 3CLpro usually functions as a homodimer with a catalytic Cys–His dyad (Kumar et al., 2017). Crystal structures show that the coronavirus 3CLpro dimer is composed of two protomers arranged nearly perpendicular to one another. Each protomer contains three structural domains (Figure. 3). Domains I and II form antiparallel β-barrel structures, while domain III is mainly α-helical, consisting of five α-helices arranged into a globular structure, and is connected to domain II by a long loop region (Anand et al., 2002). The catalytic site of 3CLpro is located in the cleft between domains I and II. In SARS-CoV and SARS-CoV-2, the catalytic dyad is formed by His41 and Cys145, and in MERS-CoV it is formed by His41 and Cys148 (Dampalla et al., 2021; Jin et al., 2020; Yang et al., 2003). In alphacoronaviruses, including feline, ferret, and mink coronaviruses and transmissible gastroenteritis virus (TGEV), the catalytic cysteine instead occupies position 144, with conserved His41 (Perera et al., 2018).

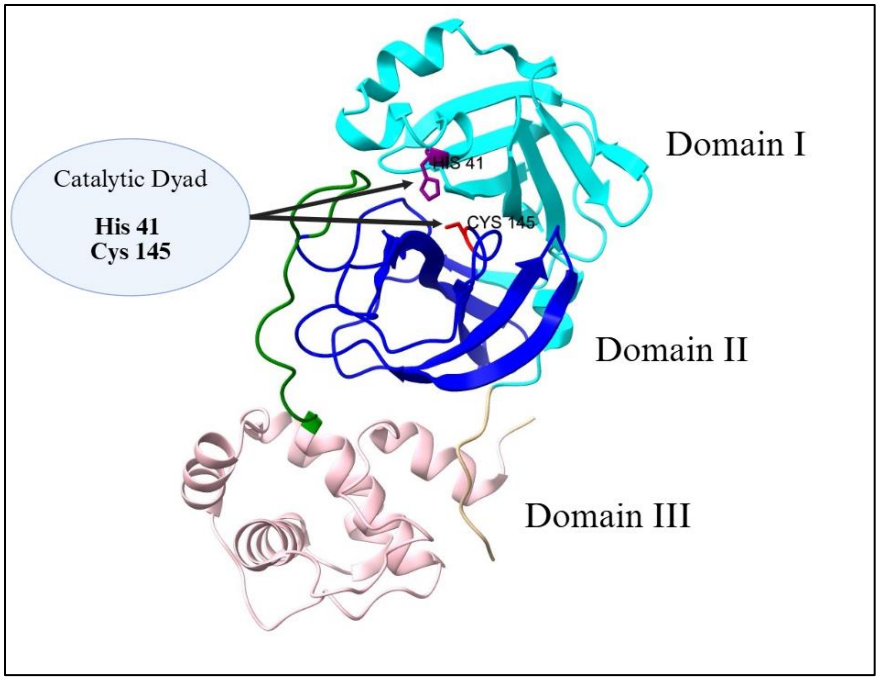


Figure 3. Monomeric structure of SARS-CoV-2 3CLpro

Ribbon representation of the SARS-CoV-2 3CLpro monomer (Protein Data Bank accession number 6Y84) rendered in UCSF ChimeraX. The enzyme is organized into three structurally distinct domains: domain I (residues 8–101, cyan), domain II (residues 102–184, blue) and domain III (residues 201–303, pink) (Jin et al., 2020). Domain II and III are connected by a long linker loop (green). The catalytic dyad formed by His41 (purple) and Cys145 (red), lies within the cleft between domains I and II (indicated by arrows).

The active site of 3CLpro is organized into a series of substrate-binding subsites S1', S1, S2, S3, and S4. The S1 subsite is highly selective for the P1 glutamine residue of the substrate. The adjacent S1' subsite, formed in part by the catalytic histidine, is shallow and accommodates small P1' residues such as alanine, serine, or glycine (Dampalla et al., 2024). The S2 subsite is predominantly hydrophobic and shows a strong preference for a hydrophobic P2 residue, typically leucine. The S3 and S4 subsites, by contrast, are more solvent-exposed and structurally flexible, allowing them to accommodate a wider range of substrate side chains (Amorim et al., 2024). This substrate preference is broadly conserved across human (Figure 4) and animal coronaviruses such as TGEV, PEDV, MHV, BCoV, IVB (Chen et al., 2022; Chuck et al., 2011; Kiemer et al., 2004). Although glutamine is nearly invariant at P1,the nsp6/nsp7 cleavage site in HCoV-NL63 and the nsp13/nsp14 cleavage sites in both HCoV-NL63 and HCoV-HKU1 contain histidine instead (Chuck et al., 2011; Wang et al., 2016; Xiong et al., 2021).

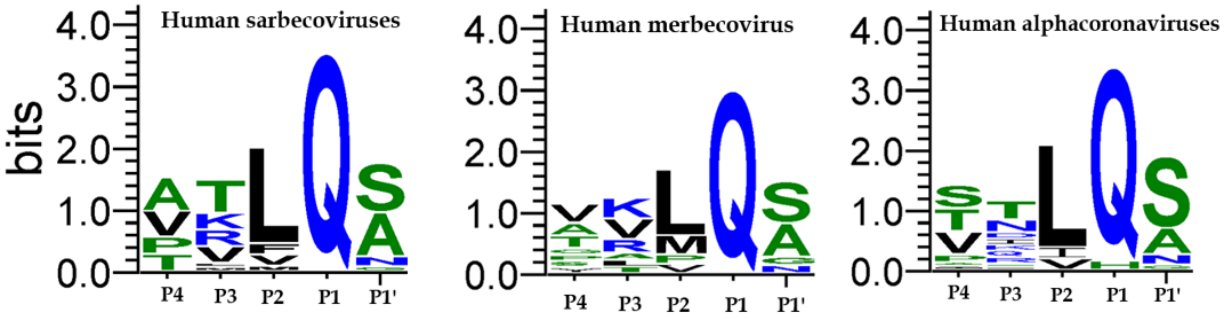


Figure 4. Sequence conservation at 3CLpro cleavage sites in human coronaviruses

Sequence logos generated with WebLogo (version 3.9) show residue conservation at the eleven 3CLpro cleavage sites (nsp4/nsp5 through nsp15/nsp16) in human sarbecoviruses (SARS-CoV and SARS-CoV-2), and the human merbecovirus (MERS-CoV), and human alphacoronaviruses (HCoV-NL63 and HCoV-229E). Positions are numbered according to the Schechter–Berger nomenclature as P4–P3–P2–P1↓P1' (Schechter and Berger, 1967). At each position, the total stack height (bits) reflects the degree of sequence conservation, and the height of each single-letter amino acid symbol within a stack is proportional to its relative frequency.

Coronavirus 3CLpro is a cysteine protease that cleaves peptide bonds through nucleophilic attack by its catalytic cysteine (Xiong et al., 2021; Zhang et al., 2025). The enzyme is first released from the polyprotein precursor by autoprocessing, which yields the mature active dimer (Aniana et al., 2023). The active 3CLpro cleaves the replicase polyproteins pp1a and pp1ab at 11 sites to release functional nonstructural proteins nsp4 through nsp16. These proteins are essential for viral replication, transcription, and immune evasion, which makes 3CLpro indispensable for the viral life cycle (Lee et al., 2020; Zhang et al., 2025). In addition to its proteolytic role, 3CLpro modulates host cellular pathways to promote viral replication. It cleaves host transcription-related factors, including RPAP1, hnRNP U, CSTF2, and PTBP1, which may suppress host transcription and create a cellular environment favorable for viral replication (Pablos et al., 2021; Zhang et al., 2025). Coronavirus 3CLpro also contributes to immune evasion by suppressing innate antiviral signaling. MERS-CoV 3CLpro cleaves the adaptor protein MAVS (mitochondrial antiviral signaling protein). These cleavages inhibit IFN-β and NF-κB responses (van Huizen et al., 2024). 3CLpro from several coronaviruses, including PEDV, PDCoV, FIPV, SARS-CoV, and SARS-CoV-2, can cleave NEMO (NF-κB essential modulator), a central regulator of both NF-κB and interferon signaling pathways. Cleavage of NEMO disrupts downstream signaling and reduces type I interferon production (Zhang et al., 2025). Overall, these mechanisms allow coronaviruses to suppress innate immunity, evade host defense, and replicate more efficiently in infected cells.

1.4.2 Coronavirus 3CLpro as a therapeutic target

The essential role of 3CLpro in the coronavirus life cycle, together with its conserved three-dimensional structure, substrate specificity, and the absence of a homologous human enzyme with the same substrate specificity, makes 3CLpro a key antiviral target for coronaviruses (Anand et al., 2003; Dampalla et al., 2022). GC376 is a peptidomimetic 3CLpro inhibitor developed by our research group, built around a γ-lactam glutamine surrogate at P1 and a leucine residue at P2 that mimic the conserved substrate-recognition elements of coronaviral 3CLpro (Kim et al., 2012). GC376 is the bisulfite adduct of the aldehyde GC373. After conversion to the aldehyde form, its electrophilic warhead forms a reversible covalent bond with the catalytic cysteine of 3CLpro. GC376 exhibited broad-spectrum activity against 3Cpro or 3CLpro from coronaviruses, caliciviruses, and picornaviruses in biochemical and cell-based assays (Kim et al., 2012). Therapeutic efficacy of GC376 was subsequently demonstrated against both experimentally induced (Kim et al., 2016) and naturally occurring (Pedersen et al., 2018) FIPV in cats, providing the first *in vivo* validation that inhibiting coronavirus 3CLpro can suppress a lethal coronavirus infection in a live host. Several GC376 analogues incorporating structure-guided modification of the R1 cap and/or electrophilic warhead, developed by our research group, exhibited potent inhibitory and antiviral activity against different animal coronaviruses including feline, ferret, and mink coronaviruses (Perera et al., 2018). Most of these inhibitors were active against SARS-CoV-2 and MERS-CoV in biochemical and/or cell-based assays (Dampalla et al., 2021a, 2022, 2023, 2024; Nguyen et al., 2026). Selected inhibitors further demonstrated *in vivo* therapeutic efficacy

in transgenic mouse models infected with MERS-CoV (Rathnayake et al., 2020) or SARS-CoV-2 (Dampalla et al., 2021b). Pfizer's drug Paxlovid, a combination of nirmatrelvir and ritonavir, became the first FDA-approved oral 3CLpro-targeting treatment for mild-to-moderate COVID-19 in adults at high risk of progression to severe disease (Hammond et al., 2022). Its demonstrated clinical efficacy further established the clinical validity of 3CLpro as a target. Nirmatrelvir, the antiviral component of Paxlovid, is a peptidomimetic inhibitor containing a γ-lactam glutamine surrogate that occupies the conserved S1 subsite and a nitrile warhead that forms a reversible covalent bond with the catalytic cysteine of SARS-CoV-2 3CLpro (Owen et al., 2021). Ritonavir inhibits hepatic and intestinal CYP3A, slowing nirmatrelvir's metabolism and sustaining therapeutic plasma concentrations. This CYP3A inhibition can substantially raise the concentrations of other medications, producing clinically important drug-drug interactions (Gerhart et al., 2023; Khan et al., 2026). Dysgeusia and diarrhea are the most frequently reported adverse effects of Paxlovid, with nausea and vomiting also reported (Hammond et al., 2022).

Ensitrelvir fumarate (Xocova) is a non-peptidic, non-covalent inhibitor of SARS-CoV-2 3CLpro and can be dosed orally as a single agent (Unoh et al., 2022). It received approval in Japan in 2024 (MHLW, 2024) and has been FDA-approved in the United States for post-exposure prophylaxis of COVID-19 in patients 12 years of age and older following contact with an individual who has COVID-19 (Shionogi, 2026). Ensitrelvir is itself a CYP3A

inhibitor and can produce clinically significant drug-drug interactions (Shimizu et al., 2023).

1.4.3 Antiviral resistance against 3CLpro inhibitors

Emergence of antiviral resistance is an important consideration in the development of coronavirus inhibitors. Like other RNA viruses, coronaviruses can generate genetic variants during replication and can exist within a host as a quasispecies, a population of closely related but genetically distinct genomes produced by the error-prone viral polymerase, as has been shown for both SARS-CoV and SARS-CoV-2 (Karamitros et al., 2020; Xu.D. et al., 2004). These populations may contain pre-existing variants with reduced drug susceptibility that gain a selective advantage during antiviral treatment, allowing them to replicate under drug pressure, or can favor the development of acquired resistance with the generation of new resistant variants in the population. Resistance to the 3CLpro inhibitor GRL-001 emerged in mouse hepatitis virus (MHV) after only four passages in cell culture and was associated with amino acid substitutions, including T26I, D65G/A, and A298D. Variants containing single substitutions showed an approximately threefold increase in EC_{50}, whereas viruses carrying double substitutions exhibited greater than sixfold resistance. Some resistant variants showed reduced replication efficiency *in vitro* and attenuation in mice, suggesting that resistance mutations may impose a substantial fitness cost (Deng et al., 2014). Resistance has also been reported for

feline infectious peritonitis virus (FIPV) exposed to the 3CLpro inhibitor NPI52. After 10 passages, the EC_{50} of NPI52 increased approximately 15-fold, and the resistant virus contained an S131C substitution in domain II of 3CLpro. In contrast, resistance to GC376 could not be selected even after 20 passages, and the NPI52-resistant FIPV remained fully susceptible to GC376, indicating a lack of cross-resistance (Kim et al., 2016). However, a subsequent study of a cat with FIP that received prolonged GC376 treatment identified the substitutions N25S, A252S, and K260N. Only the N25S resulted in a modest decrease in GC376 susceptibility in FRET assay (Perera et al., 2019). More recently, passage of FIPV in the presence of GC376 identified a different mechanism of reduced susceptibility involving a mutation at the nsp12/nsp13 cleavage site rather than within 3CLpro itself. This mutation conferred up to a threefold increase in resistance to both GC376 and nirmatrelvir in cell culture and reduced the therapeutic efficacy of GC376 in an FIP-infected cat model (Jiao et al., 2022). Resistance of SARS-CoV-2 to nirmatrelvir has been identified by *in vitro* serial passaging (Heilmann et al., 2023; Iketani et al., 2023; Zhou et al., 2022) and screening of naturally occurring variants (Hu et al., 2023; Moghadasi et al., 2023; Noske et al., 2023). Resistance-associated substitutions mainly occur at positions E166, S144, L167, T21, and L50. These substitutions can reduce susceptibility to nirmatrelvir and often reduce viral fitness. Reported reductions in susceptibility include an approximately 100-fold increase in EC_{50} for E166V (Iketani et al., 2023) and a greater than 20-fold increase in EC_{50} for L50F/E166A/L167F (Jochmans et al., 2023).

1.5 Human coronaviruses

Seven coronaviruses are known to infect humans. Four seasonal HCoVs (HCoV-229E, HCoV-NL63, HCoV-OC43, and HCoV-HKU1) are primarily associated with common cold respiratory illness. In contrast SARS-CoV, SARS-CoV-2, and MERS-CoV have caused major outbreaks of severe respiratory disease with substantial morbidity and mortality.

1.5.1 Human common cold associated coronaviruses

Seasonal human coronaviruses (HCoVs) are the most important cause of human common cold disease (Sipulwa et al., 2016). Infections range from asymptomatic to mild or moderate upper respiratory tract infections. Common symptoms include rhinorrhea, nasal congestion, sneezing, sore throat, cough, headache, malaise, and occasional fever (Su et al., 2016). Most infections are mild and self-limiting, but seasonal HCoVs can sometimes reach the lower respiratory tract and cause bronchiolitis or pneumonia, especially in young children, older adults, and immunocompromised individuals (Killerby et al., 2018). Mortality from seasonal HCoV infection is generally low in healthy individuals. Reinfection with seasonal coronaviruses can occur because protective immunity declines over time (Edridge et al., 2020). Seasonal HCoVs circulate worldwide, and infections can occur throughout the year but are generally more frequent during winter and early spring in temperate regions. In the United States, the circulation of seasonal HCoVs was reported to peak mainly between December and March (Killerby et al., 2018).

1.5.2 Severe Acute Respiratory Syndrome Coronavirus (SARS-CoV)

SARS-CoV emerged in Guangdong Province, China, in late 2002 and caused an epidemic in 2003. The outbreak spread to multiple countries through international travel and healthcare-associated transmission. Approximately 8,096 probable SARS cases and 774 deaths were reported globally during the 2002–2003 outbreak. The overall case–fatality rate was 9.6%(WHO, 2015). SARS commonly begins with fever, chills, headache, malaise, and myalgia. In later stages, patient often develop a dry cough, dyspnea, and pneumonia. Severe cases can progress to acute lung injury, acute respiratory distress syndrome (ARDS), and multiorgan dysfunction, accompanied by dysregulated inflammatory responses (Ye et al., 2020). The SARS outbreak was controlled through public health interventions, and no cases have been reported since 2004 (CDC, 2026).

1.5.3 Middle East Respiratory Syndrome Coronavirus (MERS-CoV)

MERS-CoV was first identified in Saudi Arabia in 2012 (Zaki et al., 2012). The majority of laboratory-confirmed infections have occurred in the Middle East, particularly in Jordan, Qatar, Saudi Arabia, and the United Arab Emirates, while travel associated secondary cases have been documented in several European countries, Tunisia, and South Korea (Hilgenfeld and Peiris, 2013; Ye et al., 2020). The clinical manifestations of MERS-CoV infection include progressive acute pneumonia and, in many cases acute renal failure as well as gastrointestinal symptoms such as diarrhea and vomiting (Ye et al., 2020). Between April 2012 and November 2026, a total of 2,655 laboratory confirmed MERS cases and 960 associated deaths, were reported worldwide (ECDC, 2026).

1.5.4 Severe Acute Respiratory Syndrome Coronavirus-2 (SARS-CoV-2)

SARS CoV-2, the virus that causes COVID-19, was first identified in late December 2019 in Wuhan, China (Zhu et al., 2020), and subsequently spread rapidly worldwide. WHO declared the disease a pandemic on March 2020 (WHO, 2020). COVID-19 commonly begins with fever and cough and can progress to severe pneumonia and acute respiratory distress syndrome (ARDS) (Huang et al., 2020). Several variants have emerged since 2020, including Alpha, Beta, Gamma, Delta and Omicron (Wasim et al., 2025). Omicron and its subvariants have remained dominant worldwide since late 2021 (Kung et al., 2025). By October 2026, more than 779 million confirmed cases and more than seven million confirmed deaths had been reported globally to WHO (WHO,2026). In May 2023, WHO declared that COVID-19 no longer constituted a public health emergency of international concern (PHEIC) (WHO, 2023).

1.5.5 Potential animal origins of human coronaviruses

Bats harbor diverse coronaviruses, including viruses closely related to several human coronaviruses. For SARS-CoV, closely related viruses were found in Himalayan palm civets sold in live-animal markets in Guangdong, China, and animal traders who worked closely with these civets had notably higher levels of SARS-CoV antibodies (Guan et al., 2003), supporting the role of civets as an intermediate host between bats and humans. Later studies found that horseshoe bats carry a wide variety of SARS-like coronaviruses, suggesting bats as the original source (Lau et al., 2005; Li et al., 2005). MERS-CoV is

closely related to bat coronaviruses HKU4 and HKU5 (Lau et al., 2013; Woo et al., 2006). MERS-CoV, genetically identical to the human virus, has been isolated directly from camels, and camels across the Middle East and parts of Africa have tested positive for MERS-CoV antibodies, confirming their role as the intermediate host and direct source of human infection (Tolah et al., 2020; Yusof et al., 2017). SARS-CoV-2 is 96% identical at the whole genome level to Rhinolophus bat coronavirus RaTG13 (Zhou et al., 2020). Pangolins have been proposed as a possible intermediate host for SARS-CoV-2, since pangolin coronaviruses show high similarity to SARS-CoV-2 in the receptor binding domain (RBD) of the spike protein (Lam et al., 2020; Xiao et al., 2020). Both human coronaviruses 229E and NL63 are believed to have originated from bats (Tao et al., 2017). Camelids, including alpacas and dromedary camels, have been proposed as a possible intermediate host for HCoV-229E (Lau et al., 2021). In contrast, HCoV-OC43 is thought to have emerged from a bovine coronavirus spillover (Corman et al., 2018; Vijgen et al., 2005), with rodents proposed as more distant ancestral hosts and cattle as likely intermediate host (Corman et al., 2018; Ghai et al., 2021). A study also reported a close evolutionary relationship between HCoV-OC43 and the porcine coronavirus PHEV (Xu et al., 2024). In addition, multigene and complete genome analyses suggest several possible ancestral origins for OC43, including ungulate, canine and rabbit coronaviruses depending on the gene analyzed (Otieno et al., 2022). HCoV-HKU1 is also thought to have a rodent-associated ancestral origin and its intermediate host remains unidentified (Corman et al., 2018). The proposed evolutionary pathways of human coronaviruses are showing in figure 5.

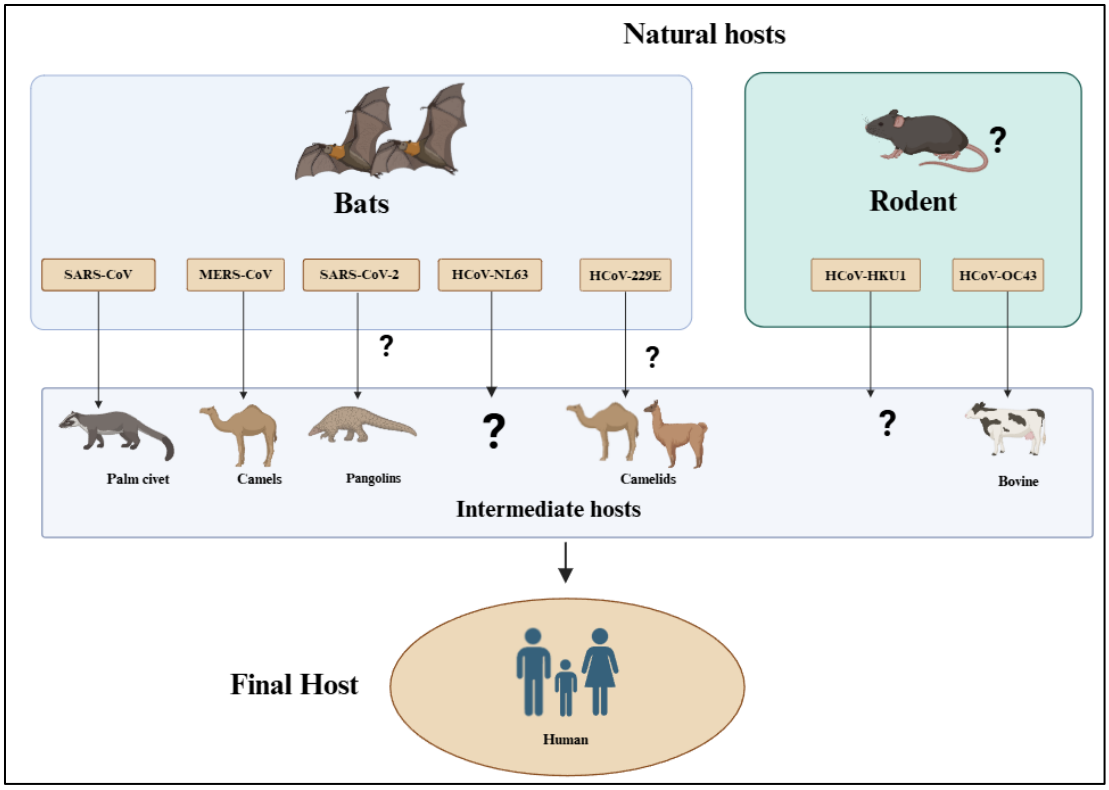


Figure 5. Potential animal origin of human coronaviruses

Bats are the proposed natural reservoir of SARS-CoV, SARS-CoV-2, MERS-CoV, HCoV-NL63, and HCoV-229E, and rodents of HCoV-HKU1 and HCoV-OC43. Arrows indicate the proposed route of each virus from its natural host through an intermediate host to humans. Question marks denote links that remain unconfirmed or intermediate host that have not been identified. Created with BioRender.com.

1.6 Bat coronaviruses

Bats harbor diverse viruses, and their ecological and biological traits create ideal conditions for viral maintenance and transmission. Bats belong to the order Chiroptera and represent the second largest (Wong et al., 2019) and most diverse group of mammals, with more than 1500 known species (Simmons, N.B. and A.L. Cirranello. 2026). This large number of species provides diverse host populations in which pathogens can survive, circulate, and evolve (Luis et al., 2013). Bats have existed for more than 50 million years, which has allowed long-term coevolution with many microorganisms, including viruses (Luis et al., 2013; Teeling et al., 2005). Many bats are highly social and tend to live in large dense colonies facilitating pathogen transmission within bat populations. Their ability to fly allows infected individuals to carry viruses between geographically separated locations, although transmission depends on viral shedding and opportunities for exposure. Some bats species readily use human-made structures, including buildings and tunnels, as roosts, increasing their opportunities for contact with humans, domestic animals (Calisher et al., 2006). The dietary habits of some frugivorous bats, such as *Artibeus jamaicensis* may result in saliva contamination of partially eaten fruit and discarded seeds, creating a possible source of pathogen exposure for other animals.

Bats can harbor several viruses that may be well adapted and non-virulent in the bat host, are highly pathogenic in humans (Baker et al., 2013). For example bats experimentally infected with Ebola virus (Swanepoel et al., 1996), a bat coronavirus (Watanabe et al., 2010) or Nipah virus (Middleton et al., 2007) showed no or minimal clinical signs, even

when virus replication was detectable in tissues and serum samples. This suggest disease tolerance, allowing bats to survive infection despite ongoing viral replication. Bats maintain a unique balance between antiviral defense and immune tolerance. In the black flying fox (*Pteropus alecto*) type I interferon locus is contracted, with only three functional INF-α genes, that are constitutively expressed even in the absence of detectable viral infection (Zhou et al., 2016). This baseline IFN-α expression induces a distinct subset of interferon-stimulated genes (ISGs) and may help maintain an antiviral state (Zhou et al., 2016). Enhanced autophagy in bats may similarly support the clearance of viral components and damaged cellular material acting as an additional antiviral mechanism (Laing et al., 2019). In contrast, dampened STING signaling, reduced NLRP3 inflammasome activation, loss or modification of PYHIN DNA sensing pathways and decrease downstream of IL-1 β may contribute to the bat immune response (Irving et al., 2021).

Bats harbor a wide diversity of alphacoronaviruses and betacoronaviruses. Sequences deposited in NCBI GenBank have been recovered from hosts spanning at least seven chiropteran families. Horseshoe bats (*Rhinolophus* spp.) are the most frequently represented and carry diverse betacoronaviruses of the subgenus *Sarbecoviurs*, including Chinese horseshoe bat (*R. sinicus*), intermediate horseshoe bat (*R. affinis*), and greater horseshoe bat (*R. ferrumequinum*). Merbecoviruses were identified largely in vesper bats, including the lesser bamboo bat (*Tylonycteris pachypus*), Japanese pipistrelle (*Pipistrellus abramus*), Chinese pipistrelle (*Hypsugo pulveratus*), and great evening bat. Nobecoviruses

were identified in Old World fruit bats, including Leschenault's rousette (*Rousettus leschenaultii*) and the straw-colored fruit bat (*Eidolon helvum*). Alphacoronaviruses were identified in diverse bat hosts, including bent-winged bats (*Miniopterus* spp.), leaf-nosed bats (*Hipposideros* spp.), *Myotis* and *Eptesicus* species, free-tailed bats (*Chaerephon* spp.), and the common vampire bat (*Desmodus rotundus*).

Bat coronaviruses have been detected across diverse geographical regions worldwide (Figure 6). Analysis of NCBI GenBank records showed that most of the bat coronavirus sequences were collected in China. However, these viruses were also detected in other parts of Asia, Europe, Africa, the United States, Latin America and the Caribbean.

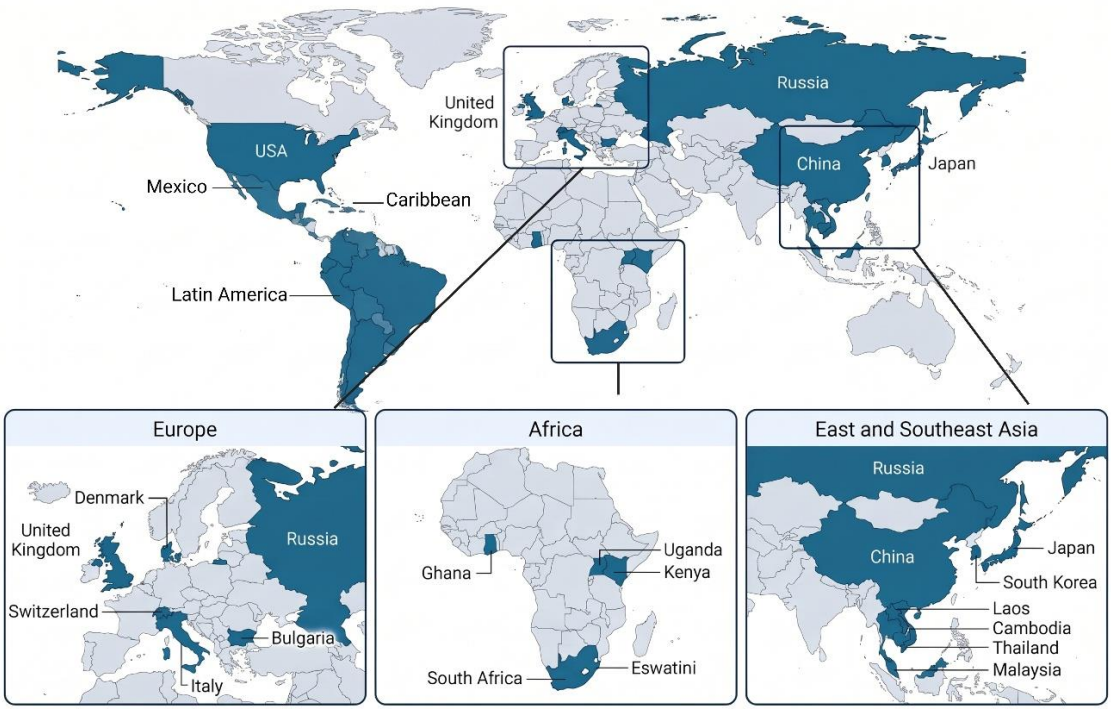


Figure 6. Geographic distribution of bat coronavirus sampling sites

Geographic locations of bat coronavirus collection sites retrieved from GenBank. Countries from which the viruses were collected are shaded blue, with regional insets for Europe, Africa, and East and Southeast Asia. Map created with BioRender.com.

Although civets were initially identified as animal origin of SARS-CoV (Guan et al., 2003), bats were soon found to be the most likely natural reservoir hosts of this virus (Lau et al., 2005). Bat SARS-like coronavirus WIV1 is closely related to SARS-CoV, sharing approximately 95% whole-genome nucleotide sequence identity (Ge et al., 2013). Bat coronavirus RaTG13, detected in *Rhinolophus affinis*, exhibits approximately 96.1% whole-genome sequence identity with SARS-CoV-2 (Zhou et al., 2020b). BANAL-52 identified in *Rhinolophus malayanus*, shares approximately 96.8% whole genome sequence identity with SARS-CoV-2 (Temmam et al., 2022). For MERS-CoV, the closest known bat coronavirus is NeoCoV (shares approximately 85% whole-genome nucleotide sequence identity with MERS-CoV) identified in African vesper bats (Xiong et al., 2022).

Some bat sarbecoviruses and merbecoviruses have shown the ability to use ACE2 or DPP4 receptors. Bat SARS-like coronavirus WIV1 (Ge et al., 2013) and WIV16 (Yang et al., 2016), isolated from Chinese horseshoe bats (*Rhinolophus sinicus*), used ACE2 as a cellular entry receptor and replicated in HeLa cells expressing humans, civets and Chinese horseshoe bats ACE2. The isolate Rs4874, collected from the same bat population, likewise replicated efficiently in HeLa cells expressing human ACE2 (Hu et al., 2017). Two chimeric viruses constructed using a WIV1 backbone and carrying the spike gene of Rs4231 or Rs7327 also replicated efficiently in HeLa cells expressing human ACE2, confirming human ACE2 usage by their spike proteins (Hu et al., 2017). Although a lentivirus pseudotyped with the RsSHC014 spike failed to enter human ACE2-expressing cells, a chimeric virus bearing that spike in a mouse-adapted SARS-CoV

backbone used human, civet and bat ACE2 and replicated in Calu-3 cells (Menachery et al., 2015). Khosta-2, identified in the lesser horseshoe bat (*Rhinolophus hipposideros*) in Russia, also showed human-ACE2 dependent entry in pseudovirus assays. A chimeric spike was generated by replacing the SARS-CoV RBD with the Khosta RBD and pseudotyped it onto a vesicular stomatitis virus. This construct infected BHK cells expressing human ACE2 cells (Seifert et al., 2022). BANAL-20-236 was identified in Marshall's horseshoe bat (*Rhinolophus marshalli*). A lentivirus pseudotyped with its full spike protein entered human ACE2 expressing HEK-293T cells. BANAL-236 also replicated in the human cell lines Calu-3 and Caco-2, which express ACE2 at endogenous levels (Temmam et al., 2022).

NL140422 (BtCoV/li/GD/2014-422) is a bat mervecoviurs identified in great evening bats. The RBD of its spike protein bound human and bat DPP4 in protein-protein binding and dot blot assays, and retrovirus pseudotyped with its spike, entered bat cells exogenously expressing human or bat DPP4. Pseudovirus entry was inhibited by anti-DPP4 antibodies, confirming DPP4-dependent entry (Luo et al., 2018). Hp-BatCoV HKU25 was detected in Chinese pipistrelle bats (*Hypsugo pulveratus*) and its S1 receptor-binding domain bound human DPP4 on the surface of Huh7 cells expressing the receptor endogenously. Retrovirus pseudotyped with HKU25 spike entered human DPP4 expressing HEK293T cells (Lau et al., 2018). Live *Ty*-BatCoV HKU4 SM3A, detected from lesser bamboo bat, used DPP4 as receptor and replicated efficiently in HEK-293T cells expressing human or dromedary camel DPP4 receptors, but not in HEK-293T cells

expressing *Tylonycteris pachypus* DPP4 expressing HEK-293T or in bat kidney or lung cells. *Ty*-BatCoV HKU4 infected transgenic mice expressing human DPP4. (Lau et al., 2021). Interestingly, NeoCoV and PDF-2180, despite their close whole-genome relationship to MERS-CoV, used ACE2 rather than DPP4 for cell entry. Pseudoviruses bearing their spike proteins efficiently entered HEK293T cells expressing ACE2 from most Yangochiropteran bat species, whereas entry into cells expressing human ACE2 was comparatively weak. No human or bat DPP4 ortholog tested supported detectable entry (Xiong et al., 2022).

Chapter 2 Broad-spectrum antiviral activity of 3CLpro inhibitors against bat coronaviruses utilizing ACE2 or DPP4 receptors

2.1 Abstract

The emergence of SARS-CoV, SARS-CoV-2, and MERS-CoV has highlighted the threat posed by coronaviruses to human health. SARS-CoV and SARS-CoV-2 use human ACE2, whereas MERS-CoV uses human DPP4 to enter host cells. Bats are considered the natural reservoir of SARS-CoV, SARS-CoV-2, and MERS-CoV, and several bat coronaviruses have been shown to use bat and/or human ACE2 or DPP4 receptors for cell entry. The ability of some bat coronaviruses to utilize these receptors highlights their spillover potential and the need for antivirals effective against them. The coronavirus 3CLpro is an attractive target for such broad-spectrum intervention because it is essential for viral polyprotein processing, contributes to innate immune evasion, has a conserved three-dimensional structure and catalytic dyad, and has no closely related human homolog. In this study, we performed multiple sequence alignment and phylogenetic analyses of all available bat coronavirus 3CLpro sequences in NCBI GenBank belonging to the subgenera *Sarbecovirus* and *Merbecovirus* and the genus *Alphacoronavirus* to characterize their conservation and evolutionary relationships. We then expressed the 3CLpros of eleven bat coronaviruses from different groups, including several viruses with demonstrated bat and/or human ACE2 or DPP4 receptor usage, and evaluated the inhibitory activity of a panel of 3CLpro inhibitors against recombinant 3CLpro using a FRET assay. In addition, two cocrystal structures of bat 3CLpro-inhibitor complexes were determined. The results showed that bat sarbecovirus and bat merbecovirus 3CLpro

sequences shared amino acid identities of 87.58–99.67%, 78.10–99.67% within each group, respectively, and 48.84–53.80% between the two *Betacoronavirus* subgenera. Bat *Alphacoronavirus* 3CLpros showed less than 50% amino acid identity with both bat *Sarbecovirus* and bat *Merbecovirus* 3CLpros. Despite this sequence divergence between groups, the catalytic dyad (Cys145/His41 in *Sarbecovirus*, Cys148/His41 in *Merbecovirus*, and Cys144/His41 in *Alphacoronavirus*) and the preference for glutamine at the P1 position of the cleavage site were conserved across all three groups. Four 3CLpro inhibitors bearing *gem*-dimethyl (GC1207 and GC1213) or pyrrolidinone-based (GC1400 and GC1406) scaffolds were found to potently inhibit all eleven bat 3CLpros (IC_{50} = 0.15–3.36 μM). Cocrystal structures of GC376 bound to a bat *Merbecovirus* 3CLpro (RMSD = 0.83 Å relative to MERS-CoV 3CLpro) and a bat *Sarbecovirus* 3CLpro (RMSD = 0.95 Å relative to SARS-CoV-2 3CLpro) revealed conserved protease structures and a shared mode of covalent binding of GC376 to the catalytic cysteine. Overall, these findings support coronavirus 3CLpro as a potential target for broad-spectrum antiviral development and identify several tested 3CLpro inhibitors as potential candidates for further development as broad-spectrum direct-acting antivirals against coronaviruses with zoonotic spillover potential.

2.2 Introduction

Coronaviruses belong to the family *Coronaviridae*, and subfamily *Orthocoronavirinae*. They are enveloped, positive-sense, single-stranded RNA viruses responsible for a wide range of clinically important diseases in both humans and animals (Cui et al., 2019; V'kovski et al., 2021). Since the beginning of the twenty-first century, the world has experienced three major human outbreaks caused by SARS-CoV, MERS-CoV, SARS-CoV-2. The COVID-19 pandemic caused by SARS-CoV-2 has killed millions of people worldwide and caused massive economic disruption. Four additional human coronaviruses (HCoV-229E, HCoV-NL63, HCoV-OC43, and HCoV-HKU1) circulate endemically and typically cause comparatively mild upper respiratory diseases.

Bats harbor diverse alphacoronaviruses and betacoronaviruses (Woo et al., 2012), the two genera to which all known human coronaviruses belong. Owing to distinctive features of their immune systems, many bats are able to tolerate coronavirus infection without developing clinical disease (Irving et al., 2021; Zhou et al., 2016). Their species diversity, long lifespans, capacity for flight, and colonial roosting behavior further facilitate the maintenance, circulation, and cross-species transmission of these viruses (Calisher et al., 2006; Luis et al., 2013; Wong et al., 2019). As a consequence, bat populations worldwide harbor an extraordinarily diverse and largely uncharacterized pool of coronaviruses.

Coronavirus entry into host cells is governed primarily by interactions between the viral spike (S) glycoprotein and host cell surface receptors such as ACE2, DPP4, or aminopeptidase N. SARSS-CoV and SARS-CoV-2 use human ACE2 (Li et al., 2003; Zhou

et al., 2020), whereas MERS-CoV use human DPP4 (Raj et al., 2013)receptor to enter host cell. Some bat coronaviruses can utilize bat and/or human ACE2 receptors (Ge et al., 2013; Hu et al., 2017; Seifert et al., 2022; Temmam et al., 2022; Yang et al., 2016) or bat and/or human DPP4 receptors (Lau et al., 2021, 2018; Luo et al., 2018). This receptor uses ability of some bat coronaviruses raising the likelihood that additional bat coronaviruses could spill over into humans. Preparedness strategies must therefore be developed proactively, rather than only in response to outbreaks after they occur.

A range of viral and host-directed targets have been explored for coronavirus therapeutics, including the spike protein (Tai et al., 2020), RNA-dependent RNA polymerase (Beigel et al., 2020), papain-like protease (Osipiuk et al., 2021), 3CLpro, the host protease TMPRSS2 (Hoffmann et al., 2020), and cathepsin L (Zhao et al., 2021). Among these, coronavirus 3CLpro, also known as main protease, remains one of the most important due to its essential role in both viral replication and innate immune evasion. Following translation of the positive-sense viral genomic RNA by host ribosomes, the resulting polyproteins (pp1a and pp1ab) must be proteolytically processed into individual functional nonstructural proteins (nsps) that participate in viral replication and transcription. The 3CLpro performs the majority of this processing. The three-dimensional structure of 3CLpro, along with its catalytic dyad formed by cysteine (Cys145 in SARS-CoV, and SARS-CoV-2, Cys148 in MERS-CoV and Cys144 in *Alphacoronavirus*) and histidine (His41) residues, is highly conserved across diverse coronaviruses (Dampalla et al., 2021a; Jin et al., 2020b; Kiemer et al., 2004; Needle et al.,

2015; Perera et al., 2018; Wang et al., 2016). The enzyme's substrate specificity is similarly conserved, particularly its strong preference for glutamine at the P1 position of cleavage sites (Anand et al., 2002). This combination of a conserved structure, an essential role in viral replication and contribution to immune evasion, and the absence of closely related human homologs establishes coronavirus 3CLpro as an attractive target for broad-spectrum antiviral development.

GC376 is a peptidomimetic 3CLpro inhibitor, showed antiviral activity against feline infectious peritonitis virus (FIPV) *in vitro* (Kim et al., 2012), and therapeutic efficacy in cats with experimentally induced FIPV (Kim et al., 2016) or naturally occurring disease (Pedersen et al., 2018). Our research group has generated multiple series of 3CLpro inhibitors, including GC376 and its derivatives and several of these have demonstrated inhibitory activity against multiple human and animal coronaviruses including, SARS-CoV, MERS-CoV, SARS-CoV-2, TGEV, FIPV, and mink, and ferret coronaviruses in FRET-based enzyme assays and/or cell culture studies (Dampalla et al., 2021a, 2022, 2023, 2024; Perera et al., 2018). Selected compounds also significantly increased survival of transgenic mice with fatal SARS-CoV-2 (Dampalla et al., 2021b) or MERS-CoV infection (Rathnayake et al., 2020).

Given the demonstrated ability of certain bat coronaviruses to utilize human and/or bat ACE2 or DPP4 receptors, and the resulting concern over future zoonotic spillover, in this study, we conducted multiple sequence alignment and phylogenetic analyses of all available bat coronavirus 3CLpro sequences belonging to the subgenera *Sarbecovirus* and

Merbecovirus and the genus *Alphacoronavirus*. We evaluated the inhibitory activity of a panel of 3CLpro inhibitors against expressed recombinant 3CLpros from eleven bat coronaviruses, and including those that can utilize bat and/or human ACE2 or DPP4 receptors using FRET assay. In addition, two co-crystal structures of bat coronavirus 3CLpro-inhibitor complexes were determined. The results showed that 3CLpro was highly conserved within the subgenera *Sarbecovirus* and *Merbecovirus* but exhibited greater diversity among the analyzed subgenera and genera of coronaviruses, consistent with their phylogenetic clustering. Despite this diversity, several 3CLpro inhibitors exhibited broad-spectrum inhibitory activity against 3CLpros of bat coronaviruses across different genera. Structural analyses of 3CLpro-inhibitor co-crystal complexes provided insights into inhibitor binding and antiviral potency. These findings highlight the potential of broad-spectrum 3CLpro inhibition as a therapeutic strategy against coronaviruses with zoonotic spillover potential.

2.3 Materials and Methods

2.3.1 Multiple sequence alignment and phylogenetic analysis of bat coronavirus 3CLpros

All available bat coronavirus 3CLpro sequences belonging to the subgenera *Sarbecovirus* and *Merbecovirus* within the genus *Betacoronavirus* and the genus *Alphacoronavirus* were retrieved from the National Center for Biotechnology Information (NCBI) GenBank. The 3CLpro sequences of the human coronaviruses SARS-CoV, SARS-CoV-2, and MERS-CoV and feline infectious peritonitis virus (FIPV) were included for comparative analysis. Duplicate or identical sequences were removed from the dataset to eliminate redundancy.

The retrieved 3CLpro sequences were aligned using Clustal Omega multiple sequence alignment program (EMBL-EBI; https://www.ebi.ac.uk/jdispatcher/msa/clustalo) with default alignment parameters (McWilliam et al., 2013).

The positions of the catalytic histidine and cysteine residues of bat coronavirus 3CLpro were identified in the sequence alignment by comparison with their known positions in reference proteases: SARS-CoV-2 (His41 and Cys145) for bat *Sarbecovirus* (Zhang et al., 2020), MERS-CoV (His41 and Cys148) (Galasiti Kankanamalage et al., 2018) for bat *Merbecovirus,* and HCoV-229E and TGEV 3CLpros (His41 and Cys144) for bat *Alphacoronavirus* (Anand et al., 2003; Kim et al., 2012).

A phylogenetic tree comprising 194 bat coronavirus 3CLpro amino acid sequences (98 from the genus *Alphacoronavirus*, 44 from subgenus *Sarbecovirus*, and 52 from

Merbecovirus), together with the human coronavirus 3CLpro sequences, was generated using the neighbor-joining method on the MAFFT web server (https://mafft.cbrc.jp/alignment/server/) (Katoh and Standley, 2013), and the resulting tree was annotated using iTOL version 6.4 (https://itol.embl.de/) (Letunic and Bork, 2024).

The 3CLpro cleavage sites in bat coronavirus polyproteins (corresponding to nsp4/5, nsp5/6, nsp6/7, nsp7/8, nsp8/9, nsp9/10, nsp11/12, nsp12/13, nsp13/14, nsp14/15, and nsp15/16) were manually identified. For each cleavage site, the substrate-recognition motif encompassing the P4–P3–P2–P1↓P1' positions was extracted, and sequence logos were generated using WebLogo 3 (https://weblogo.berkeley.edu/) to visualize amino acid conservation and frequency at each position within the substrate-recognition motif.

2.3.2 Cloning and expression of coronavirus 3CLpro

A total of eleven bat coronavirus 3CLpros were used in the enzymatic assay in this study, along with the 3CLpros of three human coronaviruses (SARS-CoV, SARS-CoV-2, and MERS-CoV), and FIPV (Table 1). Among the bat coronaviruses, the 3CLpros of ZXC21, MZ1901, YD1313, NL1404, KYNL, and HKU33 were expressed in this study, and the remaining proteases were previously expressed by our research group.

Six of the eleven bat coronavirus included in this study have demonstrated the ability to use human and/or bat ACE2 or DPP4 receptors. MZ1901 (Khosta-2), showed human ACE2-dependent entry in pseudovirus assay, in which SARS-CoV RBD was replaced

with khosta-2 RBD and pseudotyped onto vesicular stomatitis virus, this construct infected BHK cells expressing human ACE2 (Seifert et al., 2022). The RsSHC014 spike, in mouse-adapted SARS-COV backbone, used human, bat and civet ACE2 and replicated in human Calu-3 cells (Menachery et al., 2015). Among the included bat merbecoviruses, NL1404 ((BtCoV/li/GD/2014-422) bound human and bat DPP4 in protein-protein binding and dot blot assays, and a pseudovirus bearing its spike protein entered bat cells expressing human or bat DPP4 (Luo et al., 2018). The receptor-binding domain of the YD1313 (Hp-BatCoV HKU25) spike bound human DPP4 of Huh7 cells and a pseudovirus with its spike entered human DPP4 expressing HEK2293T cells (Lau et al., 2018). SM3A (*Ty*-BatCoV HKU4) isolate replicated efficiently in HEK293T cells expressing human or dromedary camel DPP4 ,but not in those expressing *Tylonycteris pachypus* DPP4 (Lau et al., 2021). Although NeoCov is classified as a merbecovirus, it showed ACE2-dependent cell entry. Pesudoviruses bearing its spike proteins efficiently entered cells expressing ACE2 from most Yangochiropteran bats, whereas entry into cells expressing human ACE2 was comparatively weak. No human or bat DPP4 ortholog tested supported detectable entry (Xiong et al., 2022). Pairwise amino acid identity among the expressed bat coronavirus 3CLpros ranged from 91.50%–95.10% for the sarbecoviruses, 78.76%–90.52% for the merbecoviruses and 67.55%–69.87% for the alphacoronaviruses.

Table 1. Coronavirus 3CLpro used in FRET assay

Betacoronaviruses				
Subgenus	**Virus**	**Accession number**	**Host**	**Receptor usage**
Sarbecovirus	SARS-CoV	NC_004718	Human	hACE2
	SARS-CoV-2	MN908947	Human	hACE2
	ZXC21	MG772934.1	Least horseshoe bat (*R. pusillus*)	NI
	MZ1901	MZ190138	Lesser horseshoe bat (*R. hipposideros*)	hACE2
	RsSHC014	KC881005	Chinese rufous horseshoe bat (*R. sinicus*)	hACE2, bACE2 & cACE2
Merbecovirus	MERS-CoV	KM210277	Human	hDPP4
	HKU5-2	EF065510	Pipistrelle bat (*Pipistrellus sp*)	NI
	YD1313	KX442564	Chinese pipistrelle (*Hypsugo pulveratus*)	hDPP4
	NeoPML	KC869678	Cape house bat (*Neoromicia capensis*)	bACE2
	SM3A	MW218395	Lesser bamboo bat (*Tylonycteris pachypus*)	hDPP4 & dcDPP4
	NL1404	MG021452	Great evening bat (*la io*)	hDPP4 & bDPP4
Alphacoronaviruses				
Nyctacovirus	HKU33	MK720944	Greater bamboo bat (*Tylonycteris robustula*)	NI
Pedacovirus	GX2018	MK211370	Lesser Asiatic yellow bat (*Scotophilus kuhlii*)	NI
Setracovirus	KYNL	NC_048216	African Trident bat (*Triaenops afer*)	NI
Tegacovirus	FIPV (m3c-2)	Kim et al., 2016	Feline	NI

h, human; b, bat; c, civet; dc, dromedary camel. Receptor usage refer to the ability of the virus or its spike protein to utilize the particular receptor tested in experimental study. NI, undefined.

The full-length 3CLpro sequences were codon-optimized for expression in *E. coli* synthesized as double-stranded DNA by Integrated DNA Technologies (IDT, Coralville, IA, USA). Both the 3CLpro genes and expression vectors were digested with appropriate restriction endonucleases at 37 °C for 30 min. For bacterial expression, the 3CLpro genes were cloned into either the pET28a(+) vector or the pET His6 Sumo TEV LIC cloning vector (1S). The digested products were purified by column-based DNA purification using the Wizard® SV Gel and PCR Clean-Up System (Promega, Madison, WI, USA), and the lengths of 3CLpro inserts and vectors were confirmed by agarose gel electrophoresis. The digested 3CLpros and vectors were ligated at room temperature for 30 min using T4 DNA ligase (Rapid DNA Ligation Kit, Thermo Scientific, Waltham, MA, USA) and transformed into *E. coli* DH5α competent cells by heat-shock transformation: incubation on ice for 30 min, heat shock at 42 °C for 1 min, and immediate return to ice for 2 min. The transformed cells were recovered in pre-warmed SOC medium and incubated at 37 °C in a shaker incubator for one hour. Transformed cultures were plated on Luria–Bertani (LB) agar containing the appropriate selection antibiotics (kanamycin) and incubated at 37 °C for 24 hours. Distinct, well-formed colonies were selected for plasmid extraction using the GeneJET Plasmid Miniprep Kit (Thermo Scientific, Waltham, MA, USA). The sequence and orientation of each 3CLpro insert were confirmed by Sanger sequencing (GENEWIZ, Azenta Life Sciences, South Plainfield, NJ, USA).

The plasmids containing the 3CLpro genes were transferred into *E. coli* BL21(DE3) competent cells. Transformed colonies were inoculated into LB broth supplemented with

kanamycin and incubated at 37 °C with shaking for 1 hour. The starter culture was then transferred into a larger volume of LB medium for large-scale protein expression. Bacterial growth was monitored by measuring optical density at 600 nm (OD_{600}) at 15-minute intervals, and protein expression was induced with 1 mM isopropyl β-D-1-thiogalactopyranoside (IPTG) when the culture reached an OD_{600} of approximately 0.4, followed by an additional 4–6 hours of incubation at 37 °C with agitation. However, for the bat MZ1901 3CLpro, expression under these conditions yielded inactive protein, and the induction temperature was therefore reduced to 28 °C, with an extended 8–10 hour post-induction incubation to improve protease activity.

Cells were harvested by centrifugation and lysed using lysozyme followed by sonication, and 3CLpro was purified using the His-Buffer Purification Kit (Cytiva, Marlborough, MA, USA) according to the manufacturer's instructions. Purified proteins were dialyzed for 24 hours against a buffer containing 100 mM NaCl, 50 mM sodium phosphate, and 1 mM dithiothreitol (DTT) at pH 7.2. After dialysis, the proteins were centrifuged to remove any precipitates and stored at -80 °C until use. Successful expression and the molecular weights of recombinant 3CLpros were verified by sodium dodecyl sulfate–polyacrylamide gel electrophoresis (SDS–PAGE). Protease concentrations were measured by the Bradford assay. The enzymatic activities of the proteases were determined by the FRET-based enzymatic assay.

2.3.3 FRET (Fluorescence resonance energy transfer) assay

Enzymatic activity assay

Each expressed protease was serially diluted in an assay buffer composed of 30% glycerol, 120 mM NaCl, 50 mM HEPES, 4 mM DTT, and 0.4 mM EDTA at pH 6. The diluted protease was mixed with an equal volume of assay buffer containing the fluorogenic substrate (SAVLQSG) in a 96-well black microplate and incubated at room temperature for 30 min. The substrate, containing FAM as fluorophore and QXL5 as quencher, was synthesized by AnaSpec (Fremont, CA). Fluorescence was measured using a fluorescence microplate reader (FLx800; BioTek, Winooski, VT) set at an excitation wavelength of 485 nm and an emission wavelength of 526 nm. Relative fluorescence units (RFU) were calculated by subtracting the background fluorescence (from substrate-only wells) from the raw fluorescence values.

Enzymatic inhibition assay

A stock solution of each compound was prepared at a concentration of 10 mM. For the enzymatic inhibition assay, each protease was mixed with serial dilutions of the test compounds in 25µl of assay buffer and incubated at room temperature for 30 min. An equal volume assay buffer containing substrate was then added and the mixture was incubated for further 30 min. RFU values were determined for each compound dilution. The 50% inhibitory concentration (IC_{50}) of each compound was determined from dose-response curves using a variable-slope nonlinear regression analysis in GraphPad Prism

software. (GraphPad, La Jolla, CA, USA). Each assay was performed independently at least twice. The principle of the FRET-based inhibition assay is shown in Figure 7.

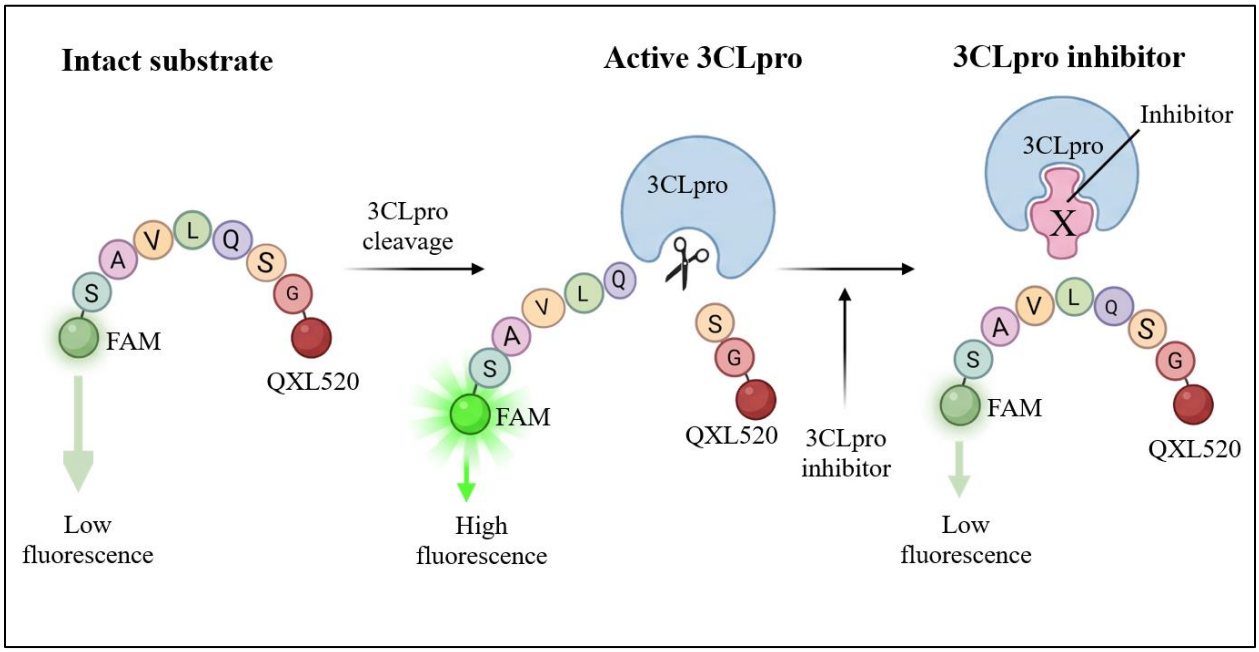


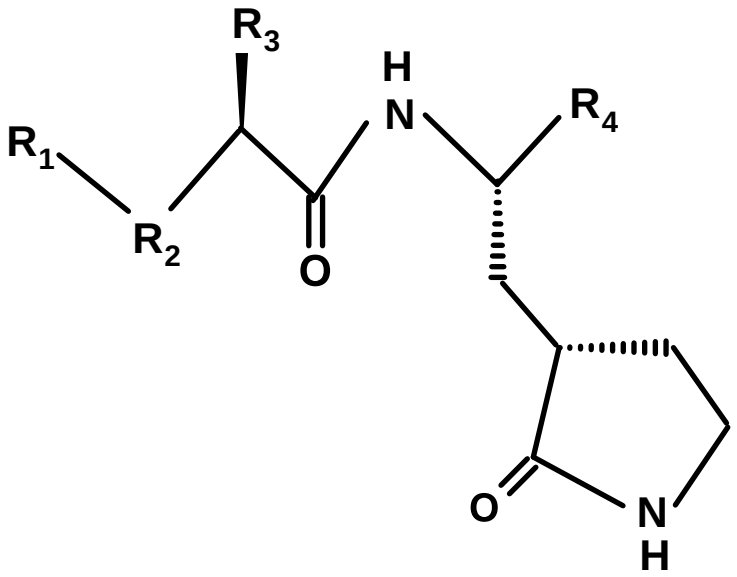
Figure 7. Principle of FRET- based 3CLpro inhibition assay

The fluorogenic peptide substrate contains the 3CLpro recognition sequence SAVLQ↓SG, flanked by the fluorophore FAM and the quencher QXL520. When 3CLpro is active and cleaves the Gln-Ser bond of the substrate, the fluorophore separates from the quencher and fluorescence increases. When an inhibitor binds 3CLpro, cleavage is blocked and fluorescence stays low. Figure created with BioRender.com.

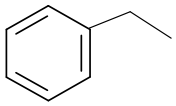
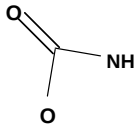
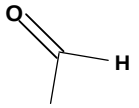
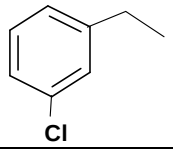
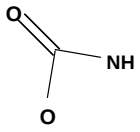
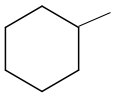
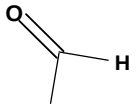
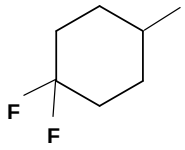
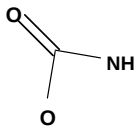
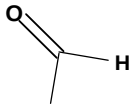
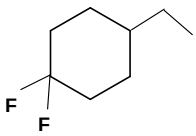
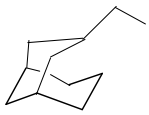
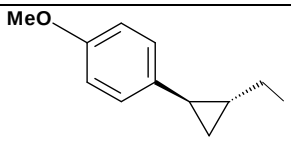
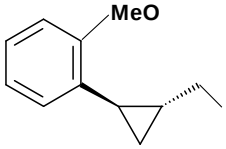
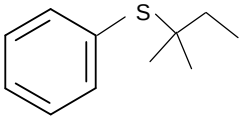
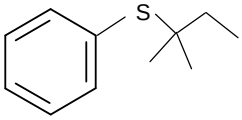
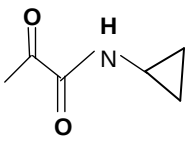
2.3.4 3CLpro inhibitors used in the FRET assay

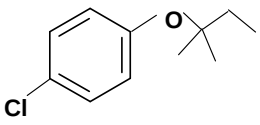
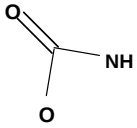
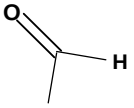
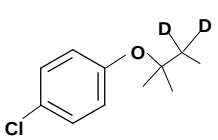
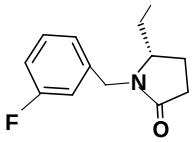
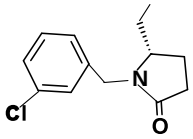
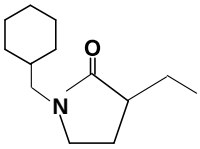
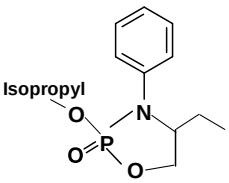
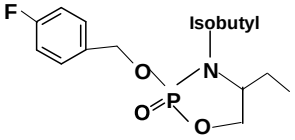
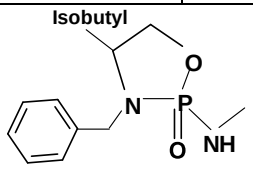
In this study, we evaluated inhibitory activity sixteen 3CLpro inhibitors from different series. The synthesis procedures for these inhibitors were previously reported by our research group (Table 2). All the inhibitors contain a glutamine surrogate at the P1 position with different functional groups. Nirmatrelvir, purchased from MedChemExpress (https://www.medchemexpress.com/), was also included as a control.

Table 2. Structure of 3CLpro inhibitors used in FRET assay



General scaffold of 3CLpro inhibitors used in FRET assay. R_1–R_4 indicate functional groups

Reference	Inhibitor	R_1(Cap)	R_2	R_3	R_4(Warhead)
Kim et al., 2012	GC376*				
Perera et al., 2018	GC583				
Rathnayake et al., 2020	GC1035*				
	GC1049*				
Dampalla et al., 2021a	GC1177*				
Dampalla et al., 2022	GC1326*				
	GC1320*				
Dampalla et al., 2023	GC1346*				
	GC1407				

Reference	Inhibitor	R_1(Cap)	R_2	R_3	R_4(Warhead)
Dampalla et al., 2023	GC1213*				
	GC1207*				
Dampalla et al., 2024	GC1400*				
	GC1406*				
	GC1399*				
Nguyen et al., 2026	GC1448*				
	GC1352*				
	GC1474*				

*These inhibitors are bisulfite adduct that convert in solution to the free aldehyde depicted here.

2.3.5 X-ray crystallography

Purified bat coronavirus 3CLpros NL140422 and MZ190138, in 100mM NaCl and 20mM Tris at pH 8.0 (with 5% glycerol added for MZ190138), were concentrated to 8.3 mg/mL (0.25 mM) and 10.13 mg/mL (0.3 mM), respectively, for crystallization screening. All crystallization experiments were set up using an NT8 drop-setting robot (Formulatrix Inc.) and UVXPO MRC (Molecular Dimensions) sitting-drop vapor-diffusion plates at 18 °C, with 100 nL of protein and 100 nL of crystallization solution dispensed and equilibrated against 50 µl of the latter. A stock solution of 100 mM GC376 was prepared in DMSO and protease inhibitor complexes were prepared by mixing 1µl of the ligand (2 mM) with 49 µl of the protease (0.28 mM) and incubating on ice for 1 h. Crystals of the NL140422-GC376 complex were obtained after 2 weeks from PACT HT screen (Molecular Dimensions) condition C3 (20% (w/v) PEG 6000, 100 mM HEPES pH 7.0, 200 mM lithium chloride), while crystals of the MZ190138-GC376 complex formed within 1-2 days from PACT HT screen condition B2 (15% (w/v) PEG 1500, 100 mM MIB pH 5.0). Prior to data collection, NL140422 crystals were cryoprotected in 80% (v/v) well solution supplemented with 20% (v/v) ethylene glycol, and MZ190138 crystals in 80% (v/v) well solution supplemented with 20% (v/v) PEG 200. X-ray diffraction data for both complexes were collected at the National Synchrotron Light Source II (NSLS-II), beamline 19-ID (NYX), using a Dectris Eiger2 XE 9M pixel-array detector. Diffraction intensities for both the NL1404 and MZ190138 complexes were processed and integrated with XDS (Kabsch, 2010, 1988) via Autoproc (Vonrhein et al., 2011), and Aimless (Evans, 2011) was used to assess the Laue class and scale the data. Structure solution was conducted by

molecular replacement in Phaser (McCoy et al., 2007) using a NL14022 3CLpro search model to solve NL140422 complex structure and a MZ190138 3Clpro search model to solve MZ190138 structure, each generated using the AlphaFold (Thompson and Petrić Howe, 2024). The resulting models were refined with Phenix (Adams, 2009) and manual model rebuilding carried out in Coot (Emsley et al., 2010) for each structure. The final models were validated using MolProbity (Chen et al., 2010) and structural figures were prepared with CCP4MG package (Potterton et al., 2004). The crystallographic studies and analyses were performed by our collaborator at Protein Structure and X-ray Crystallography Laboratory at the University of Kansas.

2.4 Result

2.4.1 Multiple sequence alignment and phylogenetic analysis of bat coronavirus 3CLpros

Multiple amino acid sequence alignments of bat coronavirus 3CLpros showed that bat sarbecoviruses shared 87.58%–99.67% amino acid identity in 3CLpro sequences, despite they were collected from different geographical locations and bat species. SARS-CoV and SARS-CoV-2 3CLpro amino acid sequences shared 91.50%–100% and 91.50%–99.67% of amino acid identity with bat sarbecovirus 3CLpro sequences, respectively. Among the analyzed bat merbecoviruses, 3CLpro amino acid sequence identity ranged from 78.10% to 99.67%. These 3CLpro sequences shared 80.72%–96.73% identity with MERS-CoV. The amino acid identity of bat coronavirus 3CLpro between the subgenera *Sarbecovirus* and *Merbecovirus* ranged from 48.84% to 53.80%. Analyzed alphacoronavirus 3CLpros shared 40.73–47.02% and 45.70–48.01% identity with bat sarbecovirus and bat merbecovirus 3CLpros, respectively.

Consistent with the reference sequences, the multiple sequence alignment of bat coronavirus 3CLpro showed conservation of the catalytic dyad: His41 paired with Cys144 in bat alphacoronaviruses, Cys145 in bat sarbecoviruses, and Cys148 in bat merbecoviruses (Figure 8).

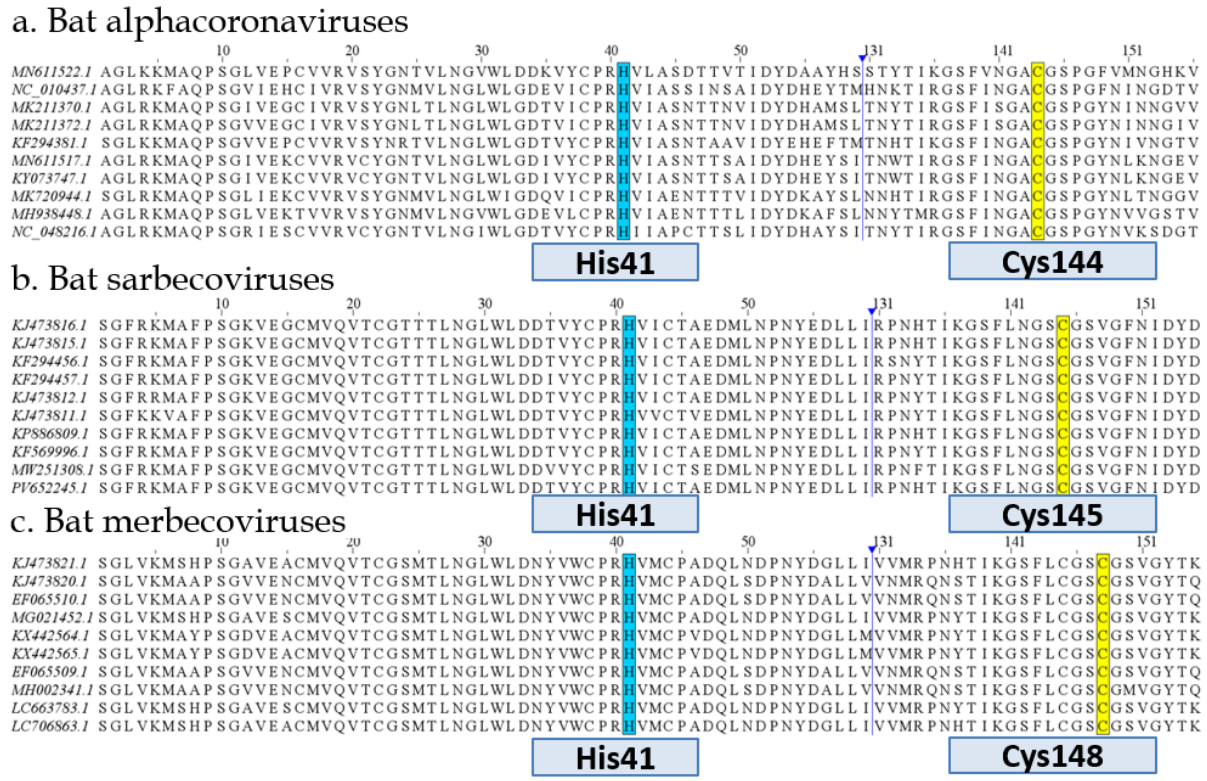


Figure 8. Conservation of the catalytic dyad in bat coronavirus 3CLpro sequences

Multiple sequence alignments of 3CLpro from a. bat alphacoronaviruses b. bat sarbecoviruses c. bat merbecoviruses demonstrate conservation of the catalytic histidine (His) and cysteine (Cys) residues. His41 is highlighted in blue, whereas the cysteine in the catalytic site is highlighted in yellow. This figure is showing ten representative bat coronavirus 3CLpro sequences from each group.

Sequence logos generated from the 3CLpro cleavage sites in bat coronavirus polyproteins showed glutamine was conserved at the P1 position in all analyzed bat coronaviruses (Figure 9). The P2 position was occupied by a hydrophobic residue, predominantly leucine, across all three groups. The P1' position was occupied by small amino acids such as serine, alanine, and glycine.

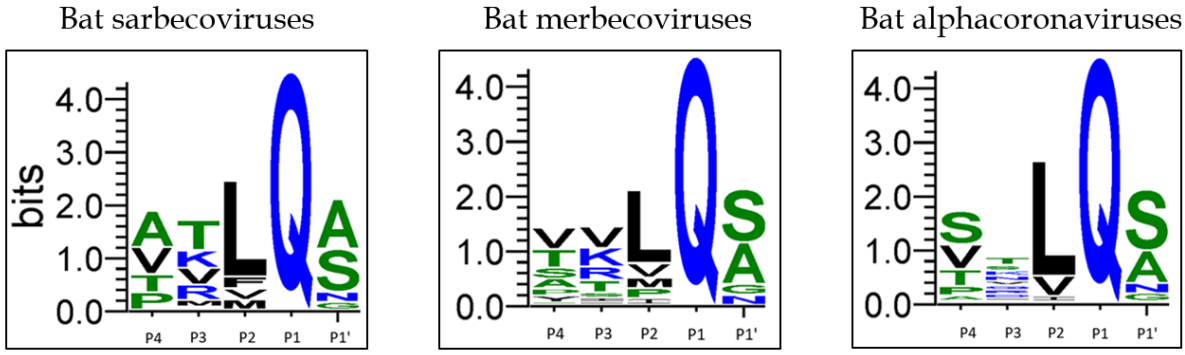


Figure 9. Sequence conservation at 3CLpro cleavage sites in bat coronaviruses

Sequence logos were generated with WebLogo (version 3.9) from 484 cleavage sites of bat sarbecovirus 3CLpros, 572 cleavage sites of bat merbecovirus 3CLpros, and 1,078 cleavage sites of bat alphacoronavirus 3CLpros, manually identified in their polyprotein sequences. Positions are numbered according to the Schechter–Berger as P4–P3–P2–P1↓P1' (Schechter and Berger, 1967). At each position, the total stack height (bits) reflects the degree of sequence conservation, and the height of each single-letter amino acid symbol within a stack is proportional to its relative frequency. Amino acids are colored according to their hydrophobicity: blue indicates hydrophilic residues, green indicates neutral residues, and black indicates hydrophobic residues.

Phylogenetic analysis of the bat coronavirus 3CLpro sequences revealed that bat alphacoronaviruses and betacoronaviruses formed distinct clades consistent with their established taxonomic classification and shared evolutionary ancestry (Figure 10). All bat alphacoronavirus 3CLpro sequences clustered within a single major clade and the analyzed betacoronavirus 3CLpro sequences formed two distinct clades, comprising bat sarbecoviruses and bat merbecoviruses. SARS-CoV and SARS-CoV-2 clustered with bat sarbecoviruses, supporting a close evolutionary relationship between them. Similarly, MERS-CoV clustered with bat merbecoviruses, supporting the evolutionary relatedness of their 3CLpro sequences. Within each major clade, sequences were further resolved into several sub–clades, reflecting genetic variation among the bat coronavirus 3CLpro sequences included in the analysis.

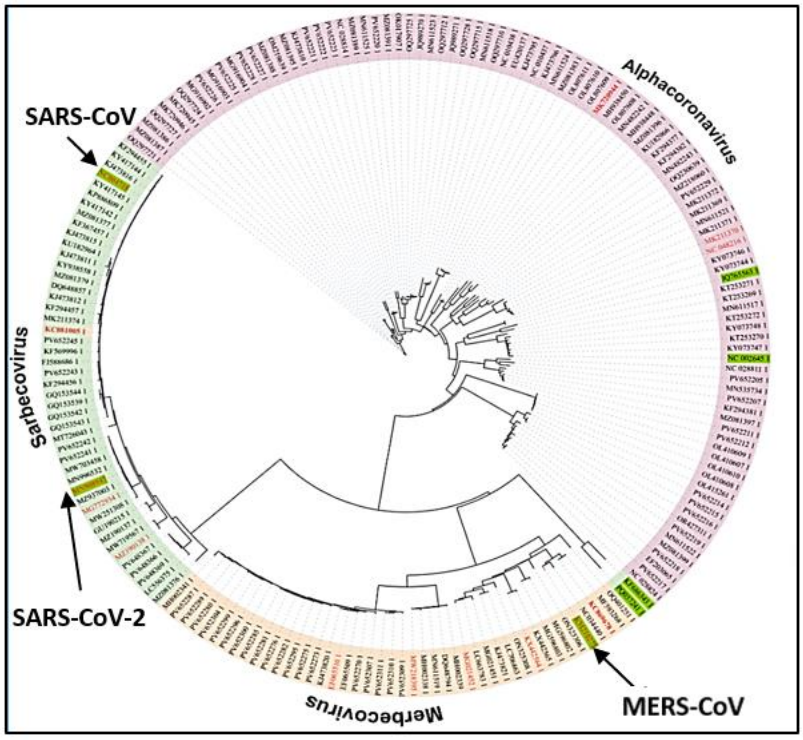


Figure 10. Phylogenetic tree of coronavirus 3CLpro amino acid sequences

Tree was generated by using the neighbor-joining method on the MAFFT web server and annotated using iTOL (version 6.4). Coronaviruses are colored by taxonomic group: the *Betacoronavirus* subgenera *Sarbecovirus* (light green) and *Merbecovirus* (light orange), and the genus *Alphacoronavirus* (light purple). Accession numbers highlighted in green correspond to human coronavirus 3CLpros.

2.4.2 FRET assay of 3CLpro inhibitors against expressed recombinant bat coronavirus 3CLpros

The activity of the expressed bat coronavirus 3CLpros was determined prior to the inhibition assay. The fluorescence signals from all the expressed proteases increased over time, following a similar trend, indicating that all expressed 3CLpros were enzymatically active.

The inhibitory activity of different series of 3CLpro inhibitors was evaluated against the expressed bat coronavirus 3CLpros. Because our research group had previously characterized these inhibitors against SARS-CoV-2, MERS-CoV, and/or SARS-CoV, and/or FIPV, the corresponding 3CLpros were included as reference controls. The FDA-approved SARS-CoV-2 3CLpro inhibitor nirmatrelvir was also included for comparison. The resulting IC_{50} values are summarized in Table 3 and 4.

All tested compounds showed nanomolar to submicromolar activity against SARS-CoV-2, MERS-CoV, and FIPV 3CLpros, consistent with the previous data from our group, confirming the validity of our FRET assay conditions. GC376 was highly active against bat merbecovirus 3CLpros (IC_{50} = 0.60–1.95 μM), showed high to moderate activity against bat sarbecovirus 3CLpros (IC_{50} = 2.95–8.36 μM) and was relatively less active against bat alphacoronavirus 3CLpros.

GC583 contains an *m*-chlorobenzyl group at R1, a Cha (cyclohexylmethyl) group at R3, and an aldehyde (CHO) warhead. Compared with GC376, GC583 showed markedly decreased activity against bat merbecovirus 3CLpros, whereas activity against bat

sarbecovirus 3CLpros remained comparable to that of GC376. A similar trend was observed against human coronavirus 3CLpros. Notably, GC583 showed high potency against FIPV 3CLpro (IC_{50} = 0.06 μM), but had no or very weak activity against tested bat alphacoronavirus 3CLpros.

Both GC1035 (bearing a 4,4-difluorocyclohexyl group at R1) and GC1049 (bearing a one-carbon-extended (4,4-difluorocyclohexyl) methyl group at R1) showed activity against all the tested 3CLpros, with the highest potency against bat merbecovirus 3CLpros (IC_{50} < 4.00 μM for both compounds). The IC_{50} values against bat sarbecovirus 3CLpros ranged from 1.89 to 7.41 μM for GC1035, approximately 2 to 2.5 fold higher than the corresponding values for GC1049. Both compounds showed high to moderate activity against bat alphacoronavirus 3CLpros (IC_{50} = 1.49–6.50 μM).

GC1177, in which the benzyl group of GC376 at R1 is replaced with a conformationally constrained bicyclo[3.3.1]nonan-3-ylmethyl group, showed an activity trend similar to that of GC376, with high activity against bat merbecovirus 3CLpros, moderate activity against bat sarbecovirus 3CLpros, and relatively lower activity against bat alphacoronavirus 3CLpros.

The cyclopropane inhibitors GC1320 and GC1326, bearing an *ortho*-and *para*-methoxyphenyl cyclopropylmethyl groups, respectively, at R1 in place of the benzyl group of GC376, showed high activity against bat betacoronavirus 3CLpros, with IC_{50} values ranging from 0.61 to 3.65 μM against bat sarbecovirus 3CLpros and 0.24–1.80 μM against bat merbecovirus 3CLpros. Activity against bat alphacoronavirus 3CLpros was

moderate to low with GC1320 (IC_{50}= 4.02–15.71 μM). GC1326 showed variable activity against bat alphacoronavirus 3CLpros, with high activity against KYNL 3CLpro (IC_{50} = 1.53 μM) but very weak activity against HKU33 3CLpro (IC_{50} > 25 μM).

Inhibitors bearing the *gem*-dimethyl scaffold showed broad-spectrum activity against all tested bat coronavirus 3CLpros. GC1346 (bearing a 2-methyl-2-(phenylthio)propyl group at R1) and GC1407 (with an α-ketoamide as warhead) showed IC_{50} values below 5.2 μM against all tested bat coronavirus 3CLpros. GC1213 (2-(4-chlorophenoxy)-2-methylpropyl group at R1) and its deuterated form GC1207 showed potent activity against all tested bat coronavirus 3CLpros, with IC_{50} values at or below 2.5 μM. Overall, the deuterated GC1207 tended to be slightly more active than GC1213.

Among the tested inhibitors with a pyrrolidinone-based R1 scaffold, GC1400 (bearing a 3-fluorophenyl substituent) and GC1406 (bearinga 3-chlorobenzyle substituent) showed potent broad-spectrum inhibitory activity against all tested bat coronavirus 3CLpros, with IC_{50} values ranging from 0.28 to 3.36 μM. In GC1399 the aromatic benzyl group is replaced with a saturated cyclohexylmethyl group, showed comparable activity against bat merbecovirus 3CLpros but decreased activity against bat sarbecovirus 3CLpros compared with GC1400 and GC1406. Its activity against bat alphacoronavirus 3CLpros ranged from low to very weak.

Compounds with a 1,3,2-oxazaphospholidin-3-one scaffold (GC1352, GC1448, and GC1474) showed potent activity against both bat sarbecovirus 3CLpros and bat merbecovirus 3CLpros. Against bat alphacoronavirus 3CLpros, inhibitors GC1352 and

GC1448 showed high to moderate activity (IC_{50} =1.14–6.21 μM), whereas GC1474 showed variable activity, ranging from high against KYNL to very weak against HKU33.

Nirmatrelvir showed high inhibitory activity against bat merbecovirus 3CLpros (IC_{50} = 0.36–3.48 μM) and bat sarbecovirus 3CLpros (IC_{50} = 1.28–4.07 μM), but low to very weak activity against bat alphacoronavirus 3CLpros. IC_{50} values against tested the human coronavirus and FIPV 3CLpros were submicromolar.

Overall, thirteen of the tested 3CLpro inhibitors demonstrated broad-spectrum inhibitory activity against 3CLpros of all three bat coronavirus groups tested. Across the panel, inhibitory activity was consistently higher against bat merbecovirus 3CLpros than against bat sarbecovirus 3CLpros (except for GC583). This trend was also observed with the tested human coronavirus 3CLpros, as every compound tested was more potent against MERS-CoV 3CLpro than against SARS-CoV and SARS-CoV-2 3CLpros. The activity against bat alphacoronavirus 3CLpros was reduced compare to the bat betacoronavirus 3CLpors for most compounds.

Table 3. IC_{50} values of 3CLpro inhibitors against MERS-CoV, SARS-CoV, SARS-CoV-2 and FIPV 3CLPro, determined by FRET assay

	IC50(μM) (Mean ± SE) [a]			
Inhibitors	**MERS-CoV**	**SARS-CoV**	**SARS-CoV-2**	**FIPV**
GC376	0.18±0.02	1.70±0.11	0.70±0.05	0.22±0.02
GC583	0.60±0.08	1.65±0.21	0.75±0.02	0.06±0.00
GC1035	0.2±0.00	1.34±0.07	0.76±0.08	0.25±0.05
GC1049	0.11±0.01	0.73±0.08	0.25±0.02	0.22±0.18
GC1177	0.25±0.04	1.55±0.08	0.35±0.05	0.22±0.02
GC1320	0.09±0.01	0.45±0.07	0.24±0.02	0.10±0.01
GC1326	0.10±0.00	0.66±0.04	0.26±0.02	0.20±0.02
GC1346	0.12±0.02	0.70±0.06	0.26±0.00	0.17±0.02
GC1407	0.10±0.00	0.76±0.07	0.38±0.04	0.59±0.05
GC1213	0.11±0.01	0.84±0.02	0.30±0.07	0.12±0.02
GC1207	0.10±0.02	0.69±0.09	0.17±0.06	0.11±0.01
GC1399	0.12±0.00	2.16±0.22	0.88±0.13	0.28±0.06
GC1400	0.09±0.02	0.79±0.10	0.28±0.01	0.15±0.01
GC1406	0.07±0.00	0.46±0.05	0.18±0.01	0.11±0.01
GC1352	0.15±0.03	2.4±0.32	0.51±0.02	0.27±0.07
GC1448	0.17±0.03	1.13±0.01	0.35±0.07	0.17±0.02
GC1474	0.17±0.03	1.3±0.11	0.43±0.02	0.27±0.00
Nirmatrelvir	0.04±0.01	0.96±0.16	0.40±0.04	0.88±0.09

[a] IC_{50} value is reported as the mean ± standard error (SE) of the mean from two or more independent experiments.

Table 4. IC_{50} values of 3CLpro inhibitors against bat coronavirus 3CLpros, determined by FRET assay

	IC_{50}(μM) (Mean ± SE) [a]										
	Bat Betacoronavirus								Bat Alphacoronaviruses		
	Bat Merbecoviruses					Bat Sarbecoviruses					
Inhibitors	**NL1404**	**HKU5.2**	**YD1313**	**SM3A**	**NeoPML**	**RsSHC**	**ZXC21**	**MZ1901**	**GX2018**	**HKU33**	**KYNL**
GC376	0.80±0.11	0.60±0.16	1.95±0.43	1.57±0.28	1.12±0.10	4.18±0.67	2.95±0.39	8.36±0.11	4.45±0.81	12.74±1.29	9.33±1.48
GC583	4.71±0.85	2.30±0.08	17.74±2.64	6.76±0.66	7.84±0.19	5.10±0.53	2.04±0.36	9.03±0.07	>25	>25	16.07±0.17
GC1035	0.85±0.12	0.59±0.03	2.16±0.15	3.81±0.47	1.84±0.07	4.35±0.09	1.89±0.09	7.41±0.78	4.57±0.81	2.27±0.37	3.02±0.15
GC1049	0.51±0.01	0.29±0.03	1.51±0.10	1.34±0.13	0.64±0.04	1.97±0.09	0.74±0.06	3.12±0.42	6.50±0.71	1.49±0.14	1.71±0.27
GC1177	0.56±0.04	0.41±0.08	2.54±0.38	2.24±0.50	1.67±0.10	3.85±0.39	1.72±0.01	6.31±0.14	11.93±0.67	7.47±1.20	2.10±0.11
GC1326	0.38±0.03	0.24±0.02	0.52±0.03	1.3±0.00	0.66±0.02	1.71±0.12	0.61±0.02	2.38±0.26	4.69±0.45	>25	1.53±0.22
GC1320	0.35±0.03	0.27±0.05	1.20±0.22	1.80±0.35	0.92±0.05	1.89±0.15	0.72±0.01	3.65±0.57	15.71±2.37	7.3±0.59	4.24±0.42
GC1346	0.65±0.13	0.50±0.09	1.36±0.00	2.48±0.68	1.54±0.40	2.30±0.29	0.74±0.04	3.19±0.55	5.11±0.64	3.68±0.25	1.06±0.23
GC1407	0.64±0.13	0.32±0.05	3.09±0.39	1.87±0.06	0.97±0.10	1.67±0.23	1.03±0.09	2.66±0.91	4.59±0.42	2.32±0.75	2.46±0.31
GC1213	0.29±0.09	0.20±0.03	0.58±0.07	1.29±0.18	0.56±0.12	2.00±0.22	0.80±0.12	2.03±0.23	1.32±0.10	1.36±0.07	0.68±0.09
GC1207	0.24±0.09	0.15±0.02	0.62±0.12	0.98±0.16	0.46±0.08	1.67±0.20	0.65±0.05	2.50±0.34	0.97±0.17	1.29±0.10	0.57±0.08
GC1399	0.70±0.10	0.61±0.04	1.85±0.12	1.53±0.19	1.74±0.11	6.06±0.67	3.13±0.26	4.93±0.65	24.57±4.96	>25	6.77±1.03
GC1400	0.63±0.11	0.40±0.03	1.36±0.01	1.89±0.12	1.13±0.03	2.63±0.29	0.75±0.01	3.36±0.55	2.78±0.40	2.65±0.70	0.90±0.05
GC1406	0.35±0.00	0.28±0.05	0.70±0.13	1.1±0.17	0.56±0.08	1.14±0.07	0.45±0.01	1.79±0.22	1.73±0.18	1.52±0.10	0.45±0.05
GC1352	0.59±0.06	0.54±0.02	2.41±0.07	3.03±0.08	1.03±0.12	4.65±0.31	2.73±0.33	6.07±0.29	6.21±0.71	2.29±0.06	1.14±0.11
GC1448	0.38±0.03	0.32±0.04	1.65±0.10	1.13±0.04	0.84±0.09	2.39±0.01	1.24±0.11	3.84±0.10	6.20±1.10	3.61±0.32	1.67±0.12
GC1474	0.53±0.04	0.61±0.02	3.05±0.63	1.3±0.01	1.17±0.08	3.35±0.05	1.55±0.03	3.73±0.27	10.53±1.01	20±4.5	1.01±0.02
Nirmatrelvir	0.67±0.10	0.36±0.01	3.07±0.17	3.48±0.76	1.5±0.04	2.58±0.13	1.28±0.10	4.07±0.97	>25	>25	15.71±0.62

[a] IC_{50} value is reported as the mean ± standard error (SE) of the mean from two or more independent experiments

2.4.3 X-ray crystallography structure of bat coronavirus 3CLpro in complex with GC376

2.4.3.1 Structure of NL1404 3CLpro in complex with GC376

We determined the crystal structure of bat coronavirus NL140422 (BtCoV NL1404) 3CLpro as a representative of bat merbecovirus 3CLpro. The protease formed a homodimer, with each subunit comprising three domains (domains I–III). The GC376 ligand was bound within the active site of each subunit. Examination of the active site revealed a prominent difference in electron density (F_o–F_c), contoured at 3σ, in each subunit, consistent with the presence of GC376. GC376 formed a covalent bond with Cys148. The electron density at the resulting stereocenter was consistent with the formation of both R and S enantiomers, which were modeled at an occupancy of 0.5 each. GC376 formed hydrogen bonds with the side chains of His41, His166, Glu169, and Gln192, and the backbone of Phe143, Gln167, and Glu169 (Figure 11).

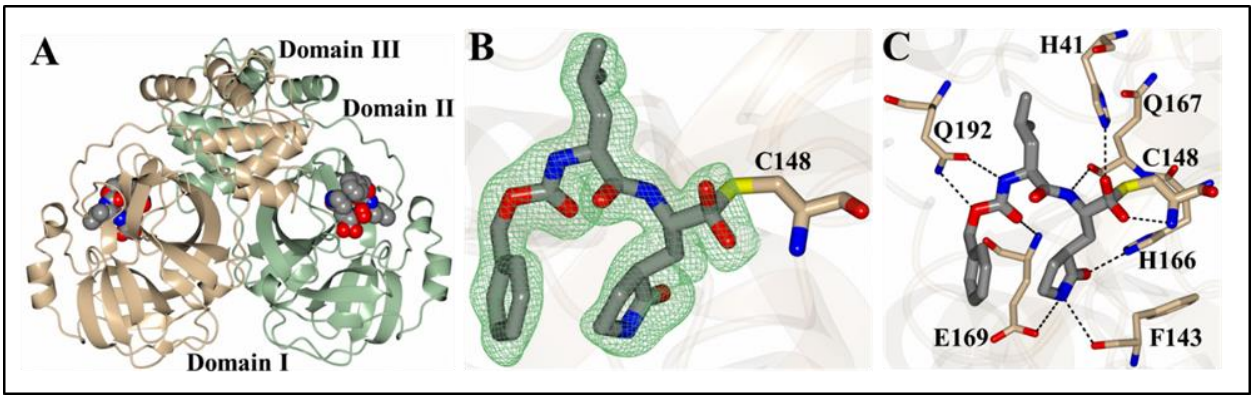


Figure 11. Structure of bat coronavirus NL140422 3CLpro in complex with GC376

A) Dimer showing subunits A(tan) and B (green) with GC376 ligand rendered as spheres in each subunit. B) F_o-F_c omit map (green mesh) contoured at 3σ. C) Hydrogen bond interaction between the protease and GC376, indicated by dashed lines.

Superposition of subunit A of BtCoV NL1404 3CLpro with MERS-CoV 3CLpro (PDB ID: 5WKJ) yielded root-mean-square deviation (RMSD) of 0.83 Å (282 residues) between Cα atoms and GC376 adopted a nearly identical binding mode in between two proteases (Figure 12).

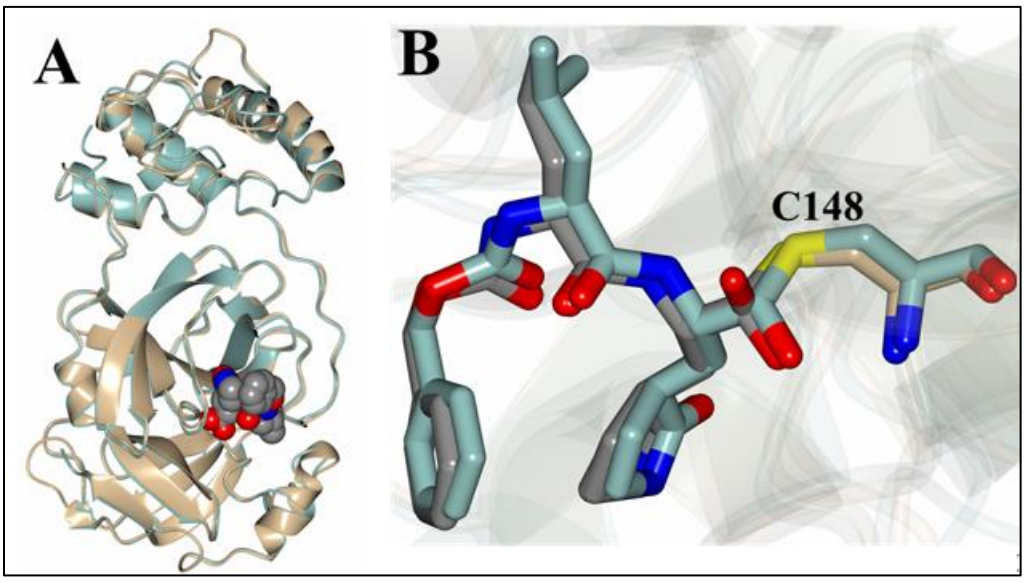


Figure 12. Comparison of Bat coronavirus NL1404 3CLpro with MERS-CoV 3CLpro

BtCoV NL1404 3CLpro (tan) and MERS 3CLpro (green). Panel A show the superposition of the proteases and the comparative GC376 binding modes are depicted in panel B.

Comparison of the electrostatic surface representations revealed a high degree of similarity in the binding pockets of BtCoV NL1404 and MERS-CoV 3CLpro, with glutamine surrogate ring and leucine of GC376 occupying the S1 and S2 subsites (Figure 13).

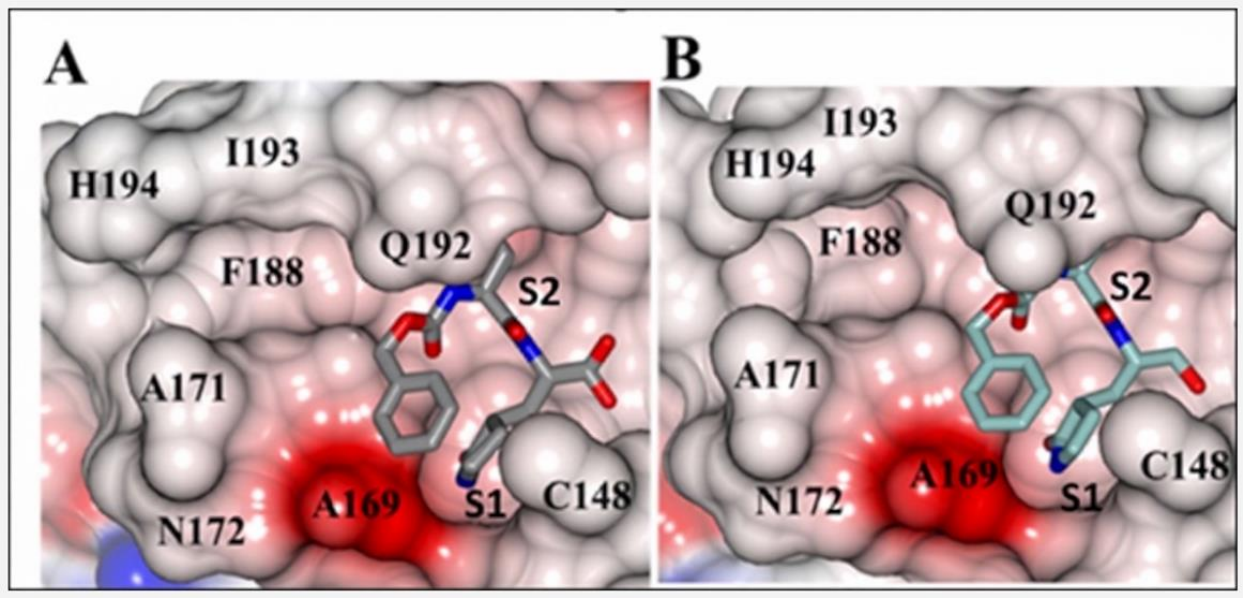


Figure 13. Electrostatic surface of bat coronavirus NL1404 3CLpro and MERS-CoV 3CLpro

Electrostatic surface representations showing the ligand binding pockets of A) BtCoV NL1404 3CLpro and B) MERS-CoV 3CLpro.

2.4.3.2 Structure of BtCoV MZ1901 3CLpro in complex with GC376

As a representative of bat sarbecovirus 3CLpro, we determined the crystal structure of bat coronavirus MZ190138 (BtCoV MZ1901) in complex with inhibitor GC376. The MZ1901 structure contained a monomer in the asymmetric unit, with each subunit comprising three domains (domains I-III) and the biologically relevant dimer generated by crystallographic symmetry. Examination of the active site revealed prominent difference electron density (F_o-F_c), contoured at 3σ in each subunit, consistent with GC376 covalently bound to Cys145. GC376 formed hydrogen bonds with Phe140, His163, His164, Glu166, and Gln189. Superposition of MZ1901 3CLpro with SARS-CoV-2 3CLpro (PDB ID: 7K0G) in complex with GC376 yielded an RMSD of 0.95Å (295 residues) between Cα atoms. GC376 adopted a nearly identical binding mode between the two proteases (Figure 14).

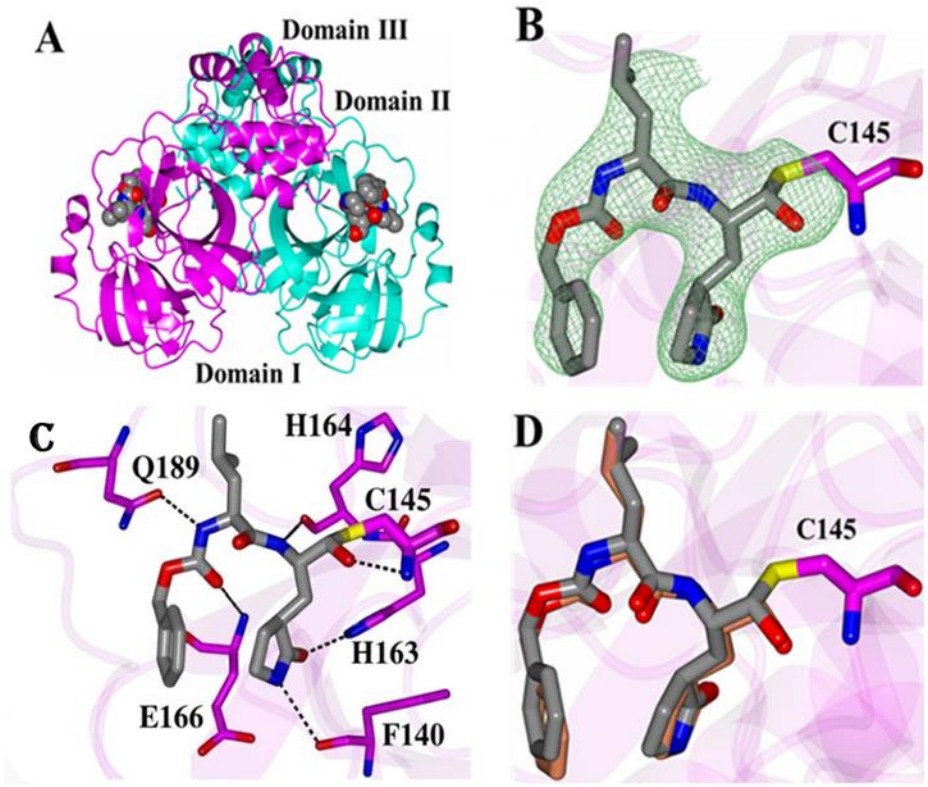


Figure 14. Structure of bat coronavirus MZ1901 3CLpro in complex with GC376

A) Dimer showing subunits A (magenta) and B (cyan) generated by crystallographic symmetry with the GC376 ligand rendered as spheres in each subunit. B) F_o-F_c omit map (green mesh) contoured at 3σ. C) Hydrogen bond interactions of GC376 and BtCoV MZ1901 3CLpro are indicated by dashed lines. D) Comparative binding mode of GC376 with SARS-CoV-2 and BtCoV MZ1901 3CLpros.

Table 5. Crystallographic data for bat coronavirus 3CLpro NL1404 and MZ1908 in complex with GC376

	NL1404 in complex with GC376	MZ1908 in complex with GC376
Data Collection		
Unit-cell parameters (Å, °)	*a*=58.28, *b*=92.02, *c*=63.09, β=112.4	*a*=109.74, *b*=79.54, *c*=52.84, β=102.7
Space group	$P2_1$	C2
Resolution (Å)[1]	49.28-1.85(1.89-1.85)	42.95-2.40 (2.49-2.40)
Wavelength (Å)	0.9786	0.9786
Temperature (K)	100	100
Observed reflections	193,815	118,046
Unique reflections	52,411	17,382
<I/□(I)>[1]	9.3(1.8)	21.0(2.3)
Completeness (%)[1]	99.7(99.7)	99.8(99.9)
Multiplicity[1]	3.7 (3.8)	6.8 (99.9)
R_{merge}(%)[1,2]	9.9 (77.8)	3.9 (78.5)
R_{means}(%)[1,4]	12.0(92.6)	4.2(86.6)
R_{pim}(%)[1,4]	5.9 (45.8)	1.6 (32.8)
$CC_{1/2}$[1,5]	0.997 (0.681)	1.000(0.911)
Refinement		
Resolution (Å)[1]	46.51-1.85	42.95-2.40
Reflections (working/test)[1]	49,881/2,499	16,418/879
R_{Factor}/R_{free} (%)[1,3]	15.4/19.7	21.5/25.5
No. of atoms (Protein/Ligand/Water)	4827/116/435	2365/29/-
Model Quality		
R.m.s deviations		
Bond lengths (Å)	0.010	0.003
Bond angles(Å)	1.048	0.586
Mean *B*-factor (Å^2)		
All atoms	26.2	105.3
Protein	25.7	105.3
Ligand	31.1	87.0
Water	32.6	-
Coordinate error (maximum likelihood) (Å)	0.21	0.39
Ramachandran Plot		
Most favored (%)	99.2	96.7
Additionally allowed (%)	0.8	3.3

2.5 Discussion

Coronaviruses are important pathogens of both humans and animals, causing respiratory, enteric, and hepatic diseases (Cui et al., 2019; V'kovski et al., 2021). SARS-CoV, MERS-CoV, and SARS-CoV-2 have caused major human outbreaks associated with substantial morbidity, mortality, and global economic disruption (Zaki et al., 2012; Zhu et al., 2020). Bats harbor diverse alphacoronaviruses and betacoronaviruses, and are considered potential natural hosts of most human coronaviruses (Woo et al., 2012). Some bat coronaviruses can utilize bat and/or human ACE2 receptors (Ge et al., 2013; Hu et al., 2017; Seifert et al., 2022; Temmam et al., 2022; Yang et al., 2016) or bat and/or human DPP4 receptors (Lau et al., 2021, 2018; Luo et al., 2018). The ability of some bat coronaviruses to utilize these receptors highlights their potential for zoonotic spillover. Continued surveillance and characterization of bat coronaviruses, and of the antiviral countermeasures that might be effective against them, is an important component of pandemic preparedness.

Coronavirus 3CLpro, given its essential role in viral polyprotein processing and replication, and its contribution to immune evasion, its conserved structure and function across coronaviruses (Anand et al., 2002; Jin et al., 2020) and the absence of a closely related human homolog, remains an attractive target for the development of direct-acting antivirals capable of addressing both circulating human coronaviruses and coronaviruses with zoonotic potential. Coronavirus 3CLpro shows a strong substrate preference for glutamine at the P1 position and a hydrophobic residue, most often leucine, at P2. GC376,

a peptidomimetic 3CLpro inhibitor, bears a P1 glutamine surrogate that occupies the S1 pocket and a P2 leucine residue that engages the S2 pocket, recognizing this conserved substrate specificity. It was originally developed by our group (Kim et al., 2012) and has demonstrated efficacy against FIPV, in both experimentally infected laboratory cats (Kim et al., 2016) and cats with naturally occurring FIP (Pedersen et al., 2018). These findings demonstrate biochemical inhibition of a coronavirus 3CLpro protease can translate into therapeutic activity *in vivo*. Subsequent work by our group extended this scaffold to a series of analogs bearing structurally diverse R1 substituents designed to engage the S4 subsite, several of which have been shown to substantially increase potency against SARS-CoV-2 and MERS-CoV in biochemical and/or cell-based assays, and selected compounds also improved survival in transgenic mouse models of SARS-CoV-2 or MERS-CoV infection (Dampalla et al., 2024, 2023, 2021a; Perera et al., 2018; Rathnayake et al., 2020).

In the present study, we analyzed the amino acid sequences of bat coronavirus 3CLpro available in NCBI GenBank representing the *Sarbecovirus* and *Merbecovirus* subgenera and the genus *Alphacoronavirus*, to assess amino acid identity and conservation of the catalytic dyad and substrate-recognition patterns. Representative bat sarbecoviruses (n = 3) and merbecoviruses (n = 5) were selected for expression of their 3CLpros. Six of these viruses have demonstrated the ability to utilize bat and/or human ACE2 or DPP4 receptors. Bat alphacoronaviruses (n = 3) from different subgenera were also included to increase the phylogenetic diversity of the study and to determine whether inhibitors could retain

activity against more divergent coronavirus 3CLpro enzymes. We evaluated the inhibitory activity of different series of 3CLpro inhibitors against recombinant bat coronavirus 3CLpros using a FRET-based enzymatic inhibition assay, and determined the crystal structures of two representative bat coronavirus 3CLpro–GC376 complexes to characterize the binding mode of GC376 and the molecular determinants associated with the bindings.

Despite considerable divergence in overall bat coronavirus 3CLpro amino acid sequences, particularly between the analyzed subgenera and between genera, the catalytic dyad– histidine (His41) and cysteine (Cys144 in alphacoronaviruses, Cys145 in sarbecoviruses, and Cys148 in merbecoviruses), was conserved in all analyzed sequences. Cleavage-site analysis also showed a preference for glutamine at P1, a hydrophobic residue, predominantly leucine at P2, and small residues such as serine, alanine, or glycine at P1'. This conservation of the catalytic machinery and substrate-recognition determinants, despite substantial divergence elsewhere in the enzyme, provides a structural rationale for why a single class of peptidomimetic inhibitors might retain activity across such a genetically diverse group of viruses. These findings parallel our group's prior sequence and structural analyses of 3CLpro from feline, ferret, and mink coronaviruses and TGEV (Perera et al., 2018), in which the catalytic residues were similarly conserved despite divergence elsewhere in the sequence. The phylogenetic clustering of the human sarbecovirus 3CLpros (SARS-CoV and SARS-CoV-2) and MERS-

CoV 3CLpro within their respective bat sarbecovirus and merbecovirus clades further supports the close evolutionary relationships between these viral lineages.

Consistent with the conserved catalytic dyad and substrate-recognition determinants described above, most of the tested compounds inhibited 3CLpros from all three bat coronavirus groups with varying activity. This activity across phylogenetically divergent enzymes suggests that inhibitors built around a P1 glutamine surrogate and a P2 leucine residue can engage a conserved catalytic core even when the surrounding protease sequence has diverged substantially.

Interestingly, the potency of most tested compounds against the 3CLpros of bat betacoronaviruses was more tightly ranged, with IC_{50} values spanning from nanomolar to low micromolar concentrations. However, we observed greater variability of these compounds against the 3CL pros of bat alphacoronaviruses.

A subset of compounds departed from this trend. GC1207 and GC1213, bearing the *gem*-dimethyl scaffold, and GC1400 and GC1406, bearing the pyrrolidinone-based scaffold, retained potent activity against all three tested bat alphacoronaviruses, with IC_{50} values below 2.80 μM. These findings suggest that particular structural features of these compounds favor inhibition of alphacoronavirus 3CLpros, potentially through differences in how their R_1 substituents interact with the binding pocket. GC1207, GC1213, GC1400, and GC1406 accordingly represent the most promising broad-spectrum inhibitors in this panel, showing consistently high potency across nearly all tested bat coronavirus 3CLpros. In contrast, GC1399, which carries a cyclohexylmethyl group at R1

in place of the benzyl group of GC1400 and GC1406, showed markedly low to very weak activity against all three bat alphacoronavirus 3CLpros. These data suggest that the R1 substituent may influence inhibitory activity against the more divergent Alphacoronavirus 3CLpros. The R1 change in GC1399 may also alter binding interactions at the S4 subsite. In our cyclopropane-based series, co-crystal structures showed, subtle modifications to the substituents that interact with the S4 subsite had dramatic effect on binding affinity to SARS-CoV-2 and MERS-CoV 3CLpros (Dampalla et al., 2022).

Previous studies have shown that optimal 3CLpro inhibitor potency requires a glutamine surrogate at P1 and leucine at P2; replacement of the P2 Leu with cyclohexylalanine (Cha) has been reported to reduce potency. In a related dipeptidyl series, Leu-containing compounds were more potent against MERS-CoV 3CLpro than their Cha-substituted counterparts (Rathnayake et al., 2020). However, Perera et al. (2018) found that the same Leu-to-Cha substitution did not reduce activity against feline, ferret, or mink coronavirus 3CLpros (Perera et al., 2018), indicating that the penalty for replacing P2 Leu may be target-dependent. GC583 illustrates this target-dependence in present study. Relative to GC376, GC583 replaces the P2 Leu with Cha at R3, in addition to changing the R1 cap group and the R4 warhead. It showed markedly reduced activity against bat merbecovirus 3CLpros and very low activity against bat alphacoronavirus 3CLpros but retained high potency against FIPV 3CLpro.

Nirmatrelvir showed potent inhibitory activity against the tested merbecovirus and sarbecovirus 3CLpros, but very weak or no activity against the tested bat

alphacoronavirus 3CLpros. This low activity of nirmatrelvir against bat alphacoronavirus 3CLpros was an interesting finding as it exhibited good activity against FIPV 3CLpro in our study and has demonstrated antiviral activity against FECV, HCoV-229E and HCoV-NL63 in cell-based assays (Maryam et al., 2025; Weil et al., 2022) The bat alphacoronavirus 3CLpros included in the present study diverged by 55-68% in amino acid sequence from FIPV 3CLpro, despite shared genus classification. This activity difference may result from topographical differences within the binding pocket of bat alphacoronavirus and FIPV 3CLpros.

The co-crystal structures of BtCoV NL1404 and BtCoV MZ1901 3CLpros in complex with GC376 provided direct structural evidence for the conservation of 3CLpro active-site architecture between bat coronaviruses and their human orthologs. BtCoV NL1404 3CLpro (bat merbecorvius) exhibited a low Cα RMSD of 0.83 Å relative to MERS-CoV 3CLpro, and BtCoV MZ1901 (bat sarbecovirus) 3CLpro exhibited a Cα RMSD of 0.95 Å relative to SARS-CoV-2 3CLpro. These low RMSD values indicate strong conservation of the overall 3CLpro fold. In both structures, GC376 occupied the substrate- binding cleft, with its glutamine surrogate and leucine moieties positioned in the S1 and S2 subsites, respectively. It formed a covalent adduct with the catalytic cysteine: Cys148 in NL1404 and Cys145 in MZ1901. Structural superposition showed that GC376 adopted a nearly identical binding orientation in NL1404 3CLpro compared with MERS-CoV 3CLpro and in MZ1901 3CLpro compared with SARS-CoV-2 3CLpro. Although NL1404 and MZ1901 3CLpros share only 51.82% amino acid identity, GC376 adopted the similar mode in both

enzymes, occupying S1 subsite with its glutamine surrogate and S2 with its leucine and forming a covalent bond with the respective catalytic cysteine. These results suggest that the conserved active-site geometry allows GC376 to inhibit phylogenetically distinct 3CLpro through a common binding mechanism.

2.6 Conclusion

Bats harbor diverse coronaviruses, including viruses closely related to SARS-CoV, SARS-CoV-2, and MERS-CoV. Several bat coronaviruses have shown the ability to utilize bat and/or human ACE2 or DPP4 receptors, highlighting their potential for zoonotic spillover. As part of an ongoing screening effort for coronavirus 3CLpro inhibitors, we evaluated multiple previously developed 3CLpro inhibitor series against recombinant 3CLpros from eleven bat coronaviruses, using a FRET-based assay. Six of these 3CLpros were from bat coronaviruses with demonstrated bat and/or human ACE2 or DPP4 receptor usage. We also determined the crystal structures of two representative bat coronavirus 3CLpro–GC376 complexes to elucidate the binding mode of the GC376. Most of the tested compounds showed inhibitory activity across all tested bat coronavirus 3CLpros. Four inhibitors bearing *gem*-dimethyl (GC1207 and GC1213) or pyrrolidinone-based scaffolds (GC1400 and GC1406) showed potent broad-spectrum inhibition. Structural analyses revealed conserved active-site architecture and a similar binding mode of GC376 between human and bat coronavirus 3CLpros. Together, these findings support coronavirus 3CLpro as a promising target for broad-spectrum antiviral development against coronaviruses with zoonotic potential.

References

Adams, P.D., 2009. PHENIX: a comprehensive Python-based system for macromolecular structure solution. Acta Crystallogr Biol Crystallogr 65, 1074.

Al-Qaaneh, A.M., Alshammari, T., Aldahhan, R., Aldossary, H., Alkhalifah, Z.A., Borgio, J.F., 2021. Genome composition and genetic characterization of SARS-CoV-2. Saudi J. Biol. Sci. 28, 1978–1989. https://doi.org/10.1016/j.sjbs.2020.12.053

Amorim, V.M. de F., Soares, E.P., Ferrari, A.S. de A., Merighi, D.G.S., de Souza, R.F., Guzzo, C.R., de Souza, A.S., 2024. 3-Chymotrypsin-like Protease (3CLpro) of SARS-CoV-2: Validation as a Molecular Target, Proposal of a Novel Catalytic Mechanism, and Inhibitors in Preclinical and Clinical Trials. Viruses 16, 844. https://doi.org/10.3390/v16060844

Anand, K., Palm, G.J., Mesters, J.R., Siddell, S.G., Ziebuhr, J., Hilgenfeld, R., 2002. Structure of coronavirus main proteinase reveals combination of a chymotrypsin fold with an extra α-helical domain. EMBO J. 21, 3213–3224. https://doi.org/10.1093/emboj/cdf327

Anand, K., Ziebuhr, J., Wadhwani, P., Mesters, J.R., Hilgenfeld, R., 2003a. Coronavirus Main Proteinase (3CLpro) Structure: Basis for Design of Anti-SARS Drugs. Science 300, 1763–1767. https://doi.org/10.1126/science.1085658

Anand, K., Ziebuhr, J., Wadhwani, P., Mesters, J.R., Hilgenfeld, R., 2003b. Coronavirus Main Proteinase (3CLpro) Structure: Basis for Design of Anti-SARS Drugs. Science 300, 1763–1767. https://doi.org/10.1126/science.1085658

Aniana, A., Nashed, N.T., Ghirlando, R., Coates, L., Kneller, D.W., Kovalevsky, A., Louis, J.M., 2023. Insights into the mechanism of SARS-CoV-2 main protease autocatalytic maturation from model precursors. Commun. Biol. 6, 1159. https://doi.org/10.1038/s42003-023-05469-8

Baker, M.L., Schountz, T., Wang, L.-F., 2013. Antiviral Immune Responses of Bats: A Review. Zoonoses Public Health 60, 104–116. https://doi.org/10.1111/j.1863-2378.2012.01528.x

Bank, R.P.D., n.d. RCSB PDB - 6Y84: SARS-CoV-2 main protease with unliganded active site (2019-nCoV, coronavirus disease 2019, COVID-19) [WWW Document]. URL https://www.rcsb.org/structure/6Y84 (accessed 11.12.26).

Barretto, N., Jukneliene, D., Ratia, K., Chen, Z., Mesecar, A.D., Baker, S.C., 2005. The Papain-Like Protease of Severe Acute Respiratory Syndrome Coronavirus Has Deubiquitinating Activity. J. Virol. 79, 15189–15198. https://doi.org/10.1128/JVI.79.24.15189-15198.2005

Beigel, J.H., Tomashek, K.M., Dodd, L.E., Mehta, A.K., Zingman, B.S., Kalil, A.C., Hohmann, E., Chu, H.Y., Luetkemeyer, A., Kline, S., Lopez De Castilla, D., Finberg, R.W., Dierberg, K., Tapson, V., Hsieh, L., Patterson, T.F., Paredes, R., Sweeney, D.A., Short, W.R., Touloumi, G., Lye, D.C., Ohmagari, N., Oh, M., Ruiz-Palacios, G.M., Benfield, T., Fätkenheuer, G., Kortepeter, M.G., Atmar, R.L., Creech, C.B., Lundgren, J., Babiker, A.G., Pett, S., Neaton, J.D., Burgess, T.H.,

Bonnett, T., Green, M., Makowski, M., Osinusi, A., Nayak, S., Lane, H.C., 2020. Remdesivir for the Treatment of Covid-19 — Final Report. N. Engl. J. Med. 383, 1813–1826. https://doi.org/10.1056/NEJMoa2007764

Belouzard, S., Chu, V.C., Whittaker, G.R., 2009. Activation of the SARS coronavirus spike protein via sequential proteolytic cleavage at two distinct sites. Proc. Natl. Acad. Sci. 106, 5871–5876. https://doi.org/10.1073/pnas.0809524106

Bosch, B.J., van der Zee, R., de Haan, C.A.M., Rottier, P.J.M., 2003. The Coronavirus Spike Protein Is a Class I Virus Fusion Protein: Structural and Functional Characterization of the Fusion Core Complex. J. Virol. 77, 8801–8811. https://doi.org/10.1128/JVI.77.16.8801-8811.2003

Brant, A.C., Tian, W., Majerciak, V., Yang, W., Zheng, Z.-M., 2021. SARS-CoV-2: from its discovery to genome structure, transcription, and replication. Cell Biosci. 11, 136. https://doi.org/10.1186/s13578-021-00643-z

Brierley, I., Dos Ramos, F.J., 2006. Programmed ribosomal frameshifting in HIV-1 and the SARS–CoV. Virus Res., Translational Control During Virus Infections 119, 29–42. https://doi.org/10.1016/j.virusres.2005.10.008

Calisher, C.H., Childs, J.E., Field, H.E., Holmes, K.V., Schountz, T., 2006. Bats: Important Reservoir Hosts of Emerging Viruses. Clin. Microbiol. Rev. 19, 531–545. https://doi.org/10.1128/cmr.00017-06

CDC, 2026. Human Coronavirus Types [WWW Document]. Hum. Coronaviruses. URL https://www.cdc.gov/human-coronaviruses/php/types/index.html (accessed 11.15.26).

Chen, H., Zhu, Z., Qiu, Y., Ge, X., Zheng, H., Peng, Y., 2022. Prediction of coronavirus 3C-like protease cleavage sites using machine-learning algorithms. Virol. Sin. 37, 437–444. https://doi.org/10.1016/j.virs.2022.04.006

Chen, V.B., Arendall, W.B., Headd, J.J., Keedy, D.A., Immormino, R.M., Kapral, G.J., Murray, L.W., Richardson, J.S., Richardson, D.C., 2010. MolProbity: all-atom structure validation for macromolecular crystallography. Acta Crystallogr. D Biol. Crystallogr. 66, 12–21. https://doi.org/10.1107/S0907444909042073

Chuck, C.-P., Chow, H.-F., Wan, D.C.-C., Wong, K.-B., 2011. Profiling of Substrate Specificities of 3C-Like Proteases from Group 1, 2a, 2b, and 3 Coronaviruses. PLOS ONE 6, e27228. https://doi.org/10.1371/journal.pone.0027228

Corman, V.M., Muth, D., Niemeyer, D., Drosten, C., 2018. Chapter Eight - Hosts and Sources of Endemic Human Coronaviruses, in: Kielian, M., Mettenleiter, T.C., Roossinck, M.J. (Eds.), Advances in Virus Research. Academic Press, pp. 163–188. https://doi.org/10.1016/bs.aivir.2018.01.001

Coutard, B., Valle, C., de Lamballerie, X., Canard, B., Seidah, N.G., Decroly, E., 2020. The spike glycoprotein of the new coronavirus 2019-nCoV contains a furin-like cleavage site absent in CoV of the same clade. Antiviral Res. 176, 104742. https://doi.org/10.1016/j.antiviral.2020.104742

COVID-19 cases | WHO COVID-19 dashboard [WWW Document], n.d. . datadot. URL https://data.who.int/dashboards/covid19/cases (accessed 11.15.26).

Cruz, J.L.G., Sola, I., Becares, M., Alberca, B., Plana, J., Enjuanes, L., Zuñiga, S., 2011. Coronavirus Gene 7 Counteracts Host Defenses and Modulates Virus Virulence. PLOS Pathog. 7, e1002090. https://doi.org/10.1371/journal.ppat.1002090

Cui, J., Li, F., Shi, Z.-L., 2019a. Origin and evolution of pathogenic coronaviruses. Nat. Rev. Microbiol. 17, 181–192. https://doi.org/10.1038/s41579-018-0118-9

Cui, J., Li, F., Shi, Z.-L., 2019b. Origin and evolution of pathogenic coronaviruses. Nat. Rev. Microbiol. 17, 181–192. https://doi.org/10.1038/s41579-018-0118-9

Cui, J., Li, F., Shi, Z.-L., 2019c. Origin and evolution of pathogenic coronaviruses. Nat. Rev. Microbiol. 17, 181–192. https://doi.org/10.1038/s41579-018-0118-9

Dampalla, C.S., Kim, Y., Bickmeier, N., Rathnayake, A.D., Nguyen, H.N., Zheng, J., Kashipathy, M.M., Baird, M.A., Battaile, K.P., Lovell, S., Perlman, S., Chang, K.-O., Groutas, W.C., 2021. Structure-Guided Design of Conformationally Constrained Cyclohexane Inhibitors of Severe Acute Respiratory Syndrome Coronavirus-2 3CL Protease. J. Med. Chem. 64, 10047–10058. https://doi.org/10.1021/acs.jmedchem.1c00319

Dampalla, C.S., Kim, Y., Zabiegala, A., Howard, D.J., Nguyen, H.N., Madden, T.K., Thurman, H.A., Cooper, A., Liu, L., Battaile, K.P., Lovell, S., Chang, K.-O., Groutas, W.C., 2024. Structure-Guided Design of Potent Coronavirus Inhibitors with a 2-Pyrrolidone Scaffold: Biochemical, Crystallographic, and Virological Studies. J. Med. Chem. 67, 11937–11956. https://doi.org/10.1021/acs.jmedchem.4c00551

Dampalla, C.S., Miller, M.J., Kim, Y., Zabiegala, A., Nguyen, H.N., Madden, T.K., Thurman, H.A., Machen, A.J., Cooper, A., Liu, L., Battaile, K.P., Lovell, S., Chang, K.-O., Groutas, W.C., 2023. Structure-guided design of direct-acting antivirals that exploit the gem-dimethyl effect and potently inhibit 3CL proteases of severe acute respiratory syndrome Coronavirus-2 (SARS-CoV-2) and middle east respiratory syndrome coronavirus (MERS-CoV). Eur. J. Med. Chem. 254, 115376. https://doi.org/10.1016/j.ejmech.2023.115376

Dampalla, C.S., Nguyen, H.N., Rathnayake, A.D., Kim, Y., Perera, K.D., Madden, T.K., Thurman, H.A., Machen, A.J., Kashipathy, M.M., Liu, L., Battaile, K.P., Lovell, S., Chang, K.-O., Groutas, W.C., 2022. Broad-Spectrum Cyclopropane-Based Inhibitors of Coronavirus 3C-like Proteases: Biochemical, Structural, and Virological Studies. ACS Pharmacol. Transl. Sci. 6, 181–194. https://doi.org/10.1021/acsptsci.2c00206

Dampalla, C.S., Zheng, J., Perera, K.D., Wong, L.-Y.R., Meyerholz, D.K., Nguyen, H.N., Kashipathy, M.M., Battaile, K.P., Lovell, S., Kim, Y., Perlman, S., Groutas, W.C., Chang, K.-O., 2021. Postinfection treatment with a protease inhibitor increases survival of mice with a fatal SARS-CoV-2 infection. Proc. Natl. Acad. Sci. 118, e2101555118. https://doi.org/10.1073/pnas.2101555118

Delmas, B., Gelfi, J., L'Haridon, R., Vogel, Sjöström, H., Norén, Laude, H., 1992. Aminopeptidase N is a major receptor for the enteropathogenic coronavirus TGEV. Nature 357, 417–420. https://doi.org/10.1038/357417a0

Deng, X., StJohn, S.E., Osswald, H.L., O'Brien, A., Banach, B.S., Sleeman, K., Ghosh, A.K., Mesecar, A.D., Baker, S.C., 2014. Coronaviruses Resistant to a 3C-Like Protease

Inhibitor Are Attenuated for Replication and Pathogenesis, Revealing a Low Genetic Barrier but High Fitness Cost of Resistance. J. Virol. 88, 11886–11898. https://doi.org/10.1128/JVI.01528-14

Edridge, A.W.D., Kaczorowska, J., Hoste, A.C.R., Bakker, M., Klein, M., Loens, K., Jebbink, M.F., Matser, A., Kinsella, C.M., Rueda, P., Ieven, M., Goossens, H., Prins, M., Sastre, P., Deijs, M., van der Hoek, L., 2020. Seasonal coronavirus protective immunity is short-lasting. Nat. Med. 26, 1691–1693. https://doi.org/10.1038/s41591-020-1083-1

Emsley, P., Lohkamp, B., Scott, W.G., Cowtan, K., 2010. Features and development of Coot. Acta Crystallogr. D Biol. Crystallogr. 66, 486–501. https://doi.org/10.1107/S0907444910007493

Evans, P.R., 2011. An introduction to data reduction: space-group determination, scaling and intensity statistics. Acta Crystallogr. D Biol. Crystallogr. 67, 282–292. https://doi.org/10.1107/S090744491003982X

Fang, P., Fang, L., Hong, Y., Liu, X., Dong, N., Ma, P., Bi, J., Wang, D., Xiao, S., 2017. Discovery of a novel accessory protein NS7a encoded by porcine deltacoronavirus. J. Gen. Virol. 98, 173–178. https://doi.org/10.1099/jgv.0.000690

Fang, P., Fang, L., Zhang, H., Xia, S., Xiao, S., 2021a. Functions of Coronavirus Accessory Proteins: Overview of the State of the Art. Viruses 13, 1139. https://doi.org/10.3390/v13061139

Fehr, A.R., Perlman, S., 2015. Coronaviruses: An Overview of Their Replication and Pathogenesis, in: Maier, H.J., Bickerton, E., Britton, P. (Eds.), Coronaviruses: Methods and Protocols. Springer, New York, NY, pp. 1–23. https://doi.org/10.1007/978-1-4939-2438-7_1

Ferron, F., Subissi, L., Silveira De Morais, A.T., Le, N.T.T., Sevajol, M., Gluais, L., Decroly, E., Vonrhein, C., Bricogne, G., Canard, B., Imbert, I., 2018. Structural and molecular basis of mismatch correction and ribavirin excision from coronavirus RNA. Proc. Natl. Acad. Sci. 115, E162–E171. https://doi.org/10.1073/pnas.1718806115

Galasiti Kankanamalage, A.C., Kim, Y., Damalanka, V.C., Rathnayake, A.D., Fehr, A.R., Mehzabeen, N., Battaile, K.P., Lovell, S., Lushington, G.H., Perlman, S., Chang, K.-O., Groutas, W.C., 2018. Structure-guided design of potent and permeable inhibitors of MERS coronavirus 3CL protease that utilize a piperidine moiety as a novel design element. Eur. J. Med. Chem. 150, 334–346. https://doi.org/10.1016/j.ejmech.2018.03.004

Ge, X.-Y., Li, J.-L., Yang, X.-L., Chmura, A.A., Zhu, G., Epstein, J.H., Mazet, J.K., Hu, B., Zhang, W., Peng, C., Zhang, Y.-J., Luo, C.-M., Tan, B., Wang, N., Zhu, Y., Crameri, G., Zhang, S.-Y., Wang, L.-F., Daszak, P., Shi, Z.-L., 2013. Isolation and characterization of a bat SARS-like coronavirus that uses the ACE2 receptor. Nature 503, 535–538. https://doi.org/10.1038/nature12711

Gerhart, J., Draica, F., Benigno, M., Atkinson, J., Reimbaeva, M., Francis, D., Baillon-Plot, N., Sidhu, G.S., Damle, B.D., 2023. Real-World Evidence of the Top 100 Prescribed Drugs in the USA and Their Potential for Drug Interactions with Nirmatrelvir; Ritonavir. AAPS J. 25, 73. https://doi.org/10.1208/s12248-023-00832-3

Ghai, R.R., Carpenter, A., Liew, A.Y., Martin, K.B., Herring, M.K., Gerber, S.I., Hall, A.J., Sleeman, J.M., VonDobschuetz, S., Behravesh, C.B., n.d. Animal Reservoirs and Hosts for Emerging Alphacoronaviruses and Betacoronaviruses - Volume 27, Number 4—April 2021 - Emerging Infectious Diseases journal - CDC. https://doi.org/10.3201/eid2704.203945

Guan, Y., Zheng, B.J., He, Y.Q., Liu, X.L., Zhuang, Z.X., Cheung, C.L., Luo, S.W., Li, P.H., Zhang, L.J., Guan, Y.J., Butt, K.M., Wong, K.L., Chan, K.W., Lim, W., Shortridge, K.F., Yuen, K.Y., Peiris, J.S.M., Poon, L.L.M., 2003. Isolation and Characterization of Viruses Related to the SARS Coronavirus from Animals in Southern China. Science 302, 276–278. https://doi.org/10.1126/science.1087139

Hagemeijer, M.C., Verheije, M.H., Ulasli, M., Shaltiël, I.A., de Vries, L.A., Reggiori, F., Rottier, P.J.M., de Haan, C.A.M., 2010. Dynamics of Coronavirus Replication-Transcription Complexes. J. Virol. 84, 2134–2149. https://doi.org/10.1128/jvi.01716-09

Hammond, J., Leister-Tebbe, H., Gardner, A., Abreu, P., Bao, W., Wisemandle, W., Baniecki, M., Hendrick, V.M., Damle, B., Simón-Campos, A., Pypstra, R., Rusnak, J.M., 2022. Oral Nirmatrelvir for High-Risk, Nonhospitalized Adults with Covid-19. N. Engl. J. Med. 386, 1397–1408. https://doi.org/10.1056/NEJMoa2118542

Hamre, D., Procknow, J.J., 1966. A new virus isolated from the human respiratory tract. Proc. Soc. Exp. Biol. Med. Soc. Exp. Biol. Med. 121, 190–193. https://doi.org/10.3181/00379727-121-30734

Heilmann, E., Costacurta, F., Moghadasi, S.A., Ye, C., Pavan, M., Bassani, D., Volland, A., Ascher, C., Weiss, A.K.H., Bante, D., Harris, R.S., Moro, S., Rupp, B., Martinez-Sobrido, L., Von Laer, D., 2023. SARS-CoV-2 $3CL^{pro}$ mutations selected in a VSV-based system confer resistance to nirmatrelvir, ensitrelvir, and GC376. Sci. Transl. Med. 15, eabq7360. https://doi.org/10.1126/scitranslmed.abq7360

Hilgenfeld, R., Peiris, M., 2013. From SARS to MERS: 10 years of research on highly pathogenic human coronaviruses. Antiviral Res. 100, 286–295. https://doi.org/10.1016/j.antiviral.2013.08.015

Hillen, H.S., Kokic, G., Farnung, L., Dienemann, C., Tegunov, D., Cramer, P., 2020. Structure of replicating SARS-CoV-2 polymerase. Nature 584, 154–156. https://doi.org/10.1038/s41586-020-2368-8

Hoffmann, M., Kleine-Weber, H., Pöhlmann, S., 2020a. A Multibasic Cleavage Site in the Spike Protein of SARS-CoV-2 Is Essential for Infection of Human Lung Cells. Mol. Cell 78, 779-784.e5. https://doi.org/10.1016/j.molcel.2020.04.022

Hoffmann, M., Kleine-Weber, H., Schroeder, S., Krüger, N., Herrler, T., Erichsen, S., Schiergens, T.S., Herrler, G., Wu, N.-H., Nitsche, A., Müller, M.A., Drosten, C., Pöhlmann, S., 2020b. SARS-CoV-2 Cell Entry Depends on ACE2 and TMPRSS2 and Is Blocked by a Clinically Proven Protease Inhibitor. Cell 181, 271-280.e8. https://doi.org/10.1016/j.cell.2020.02.052

Hofmann, H., Pyrc, K., van der Hoek, L., Geier, M., Berkhout, B., Pöhlmann, S., 2005. Human coronavirus NL63 employs the severe acute respiratory syndrome

coronavirus receptor for cellular entry. Proc. Natl. Acad. Sci. 102, 7988–7993. https://doi.org/10.1073/pnas.0409465102

Hu, B., Zeng, L.-P., Yang, X.-L., Ge, X.-Y., Zhang, W., Li, B., Xie, J.-Z., Shen, X.-R., Zhang, Y.-Z., Wang, N., Luo, D.-S., Zheng, X.-S., Wang, M.-N., Daszak, P., Wang, L.-F., Cui, J., Shi, Z.-L., 2017. Discovery of a rich gene pool of bat SARS-related coronaviruses provides new insights into the origin of SARS coronavirus. PLOS Pathog. 13, e1006698. https://doi.org/10.1371/journal.ppat.1006698

Hu, Y., Lewandowski, E.M., Tan, H., Zhang, Xiaoming, Morgan, R.T., Zhang, Xiujun, Jacobs, L.M.C., Butler, S.G., Gongora, M.V., Choy, J., Deng, X., Chen, Y., Wang, J., 2023. Naturally Occurring Mutations of SARS-CoV-2 Main Protease Confer Drug Resistance to Nirmatrelvir. ACS Cent. Sci. 9, 1658–1669. https://doi.org/10.1021/acscentsci.3c00538

Huang, C., Wang, Y., Li, X., Ren, L., Zhao, J., Hu, Y., Zhang, L., Fan, G., Xu, J., Gu, X., Cheng, Z., Yu, T., Xia, J., Wei, Y., Wu, W., Xie, X., Yin, W., Li, H., Liu, M., Xiao, Y., Gao, H., Guo, L., Xie, J., Wang, G., Jiang, R., Gao, Z., Jin, Q., Wang, J., Cao, B., 2020. Clinical features of patients infected with 2019 novel coronavirus in Wuhan, China. The Lancet 395, 497–506. https://doi.org/10.1016/S0140-6736(20)30183-5

Iketani, S., Mohri, H., Culbertson, B., Hong, S.J., Duan, Y., Luck, M.I., Annavajhala, M.K., Guo, Y., Sheng, Z., Uhlemann, A.-C., Goff, S.P., Sabo, Y., Yang, H., Chavez, A., Ho, D.D., 2023. Multiple pathways for SARS-CoV-2 resistance to nirmatrelvir. Nature 613, 558–564. https://doi.org/10.1038/s41586-022-05514-2

Irving, A.T., Ahn, M., Goh, G., Anderson, D.E., Wang, L.-F., 2021. Lessons from the host defences of bats, a unique viral reservoir. Nature 589, 363–370. https://doi.org/10.1038/s41586-020-03128-0

Jackson, C.B., Farzan, M., Chen, B., Choe, H., 2022. Mechanisms of SARS-CoV-2 entry into cells. Nat. Rev. Mol. Cell Biol. 23, 3–20. https://doi.org/10.1038/s41580-021-00418-x

Jaimes, J.A., André, N.M., Chappie, J.S., Millet, J.K., Whittaker, G.R., 2020. Phylogenetic Analysis and Structural Modeling of SARS-CoV-2 Spike Protein Reveals an Evolutionary Distinct and Proteolytically Sensitive Activation Loop. J. Mol. Biol. 432, 3309–3325. https://doi.org/10.1016/j.jmb.2020.04.009

Jantraphakorn, Y., Viriyakitkosol, R., Jongkaewwattana, A., Kaewborisuth, C., 2021. Interaction Between PEDV and Its Hosts: A Closer Look at the ORF3 Accessory Protein. Front. Vet. Sci. 8. https://doi.org/10.3389/fvets.2021.744276

Jia, Z., Yan, L., Ren, Z., Wu, L., Wang, J., Guo, J., Zheng, L., Ming, Z., Zhang, L., Lou, Z., Rao, Z., 2019. Delicate structural coordination of the Severe Acute Respiratory Syndrome coronavirus Nsp13 upon ATP hydrolysis. Nucleic Acids Res. 47, 6538–6550. https://doi.org/10.1093/nar/gkz409

Jiang, S., Yuan, J., Li, Q., Song, Ziyan, Cao, L., Song, Zhenhui, Zhang, X., n.d. The structure and function of membrane protein in coronavirus infection and its applications in the development of vaccines and therapeutic drugs. Front. Microbiol. 17, 1762041. https://doi.org/10.3389/fmicb.2026.1762041

Jiao, Z., Yan, Y., Chen, Y., Wang, G., Wang, X., Li, L., Yang, M., Hu, X., Guo, Y., Shi, Y., Peng, G., 2022. Adaptive Mutation in the Main Protease Cleavage Site of Feline Coronavirus Renders the Virus More Resistant to Main Protease Inhibitors. J. Virol. 96, e00907-22. https://doi.org/10.1128/jvi.00907-22

Jin, Z., Du, X., Xu, Y., Deng, Y., Liu, M., Zhao, Y., Zhang, B., Li, X., Zhang, L., Peng, C., Duan, Y., Yu, J., Wang, L., Yang, K., Liu, F., Jiang, R., Yang, Xinglou, You, T., Liu, Xiaoce, Yang, Xiuna, Bai, F., Liu, H., Liu, Xiang, Guddat, L.W., Xu, W., Xiao, G., Qin, C., Shi, Z., Jiang, H., Rao, Z., Yang, H., 2020. Structure of Mpro from SARS-CoV-2 and discovery of its inhibitors. Nature 582, 289–293. https://doi.org/10.1038/s41586-020-2223-y

Jochmans, D., Liu, C., Donckers, K., Stoycheva, A., Boland, S., Stevens, S.K., De Vita, C., Vanmechelen, B., Maes, P., Trüeb, B., Ebert, N., Thiel, V., De Jonghe, S., Vangeel, L., Bardiot, D., Jekle, A., Blatt, L.M., Beigelman, L., Symons, J.A., Raboisson, P., Chaltin, P., Marchand, A., Neyts, J., Deval, J., Vandyck, K., 2023. The Substitutions L50F, E166A, and L167F in SARS-CoV-2 3CLpro Are Selected by a Protease Inhibitor In Vitro and Confer Resistance To Nirmatrelvir. mBio 14, e02815-22. https://doi.org/10.1128/mbio.02815-22

Kabsch, W., 2010. XDS. Acta Crystallogr. D Biol. Crystallogr. 66, 125–132. https://doi.org/10.1107/S0907444909047337

Kabsch, W., 1988. Automatic indexing of rotation diffraction patterns. J. Appl. Crystallogr. 21, 67–72. https://doi.org/10.1107/S0021889887009737

Karamitros, T., Papadopoulou, G., Bousali, M., Mexias, A., Tsiodras, S., Mentis, A., 2020. SARS-CoV-2 exhibits intra-host genomic plasticity and low-frequency polymorphic quasispecies. J. Clin. Virol. 131, 104585. https://doi.org/10.1016/j.jcv.2020.104585

Katoh, K., Standley, D.M., 2013. MAFFT Multiple Sequence Alignment Software Version 7: Improvements in Performance and Usability. Mol. Biol. Evol. 30, 772–780. https://doi.org/10.1093/molbev/mst010

Kazi, L., Lissenberg, A., Watson, R., de Groot, R.J., Weiss, S.R., 2005. Expression of Hemagglutinin Esterase Protein from Recombinant Mouse Hepatitis Virus Enhances Neurovirulence. J. Virol. 79, 15064–15073. https://doi.org/10.1128/JVI.79.24.15064-15073.2005

Khan, M.A., Daiello, L.A., Berry, S.D., Harris, D.A., Mehta, H.B., Hsu, Y.-C. (Sam), Leonard, C.E., McConeghy, K.W., Zullo, A.R., 2026. Potential Drug-Drug Interactions With Nirmatrelvir/Ritonavir Among Long-Term Care Facility Residents. J. Am. Med. Dir. Assoc. 27, 106365. https://doi.org/10.1016/j.jamda.2026.106365

Kiemer, L., Lund, O., Brunak, S., Blom, N., 2004. Coronavirus 3CLproproteinase cleavage sites: Possible relevance to SARS virus pathology. BMC Bioinformatics 5, 72. https://doi.org/10.1186/1471-2105-5-72

Kifer, A., Pina, F., Codallos, N., Hermann, A., Ziegler, L., Niwa, M., Altan, -Bonnet Nihal, 2025. Orchestration of SARS-CoV-2 Nsp4 and host cell ESCRT proteins induces

morphological changes of the endoplasmic reticulum. Mol. Biol. Cell 36, ar40. https://doi.org/10.1091/mbc.E24-12-0542

Killerby, M.E., Biggs, H.M., Haynes, A., Dahl, R.M., Mustaquim, D., Gerber, S.I., Watson, J.T., 2018. Human coronavirus circulation in the United States 2014–2017. J. Clin. Virol. 101, 52–56. https://doi.org/10.1016/j.jcv.2018.01.019

Kim, Y., Liu, H., Galasiti Kankanamalage, A.C., Weerasekara, S., Hua, D.H., Groutas, W.C., Chang, K.-O., Pedersen, N.C., 2016. Reversal of the Progression of Fatal Coronavirus Infection in Cats by a Broad-Spectrum Coronavirus Protease Inhibitor. PLOS Pathog. 12, e1005531. https://doi.org/10.1371/journal.ppat.1005531

Kim, Y., Lovell, S., Tiew, K.-C., Mandadapu, S.R., Alliston, K.R., Battaile, K.P., Groutas, W.C., Chang, K.-O., 2012. Broad-Spectrum Antivirals against 3C or 3C-Like Proteases of Picornaviruses, Noroviruses, and Coronaviruses. J. Virol. 86, 11754–11762. https://doi.org/10.1128/JVI.01348-12

Koch, J., Uckeley, Z.M., Doldan, P., Stanifer, M., Boulant, S., Lozach, P., 2021. TMPRSS2 expression dictates the entry route used by SARS-CoV-2 to infect host cells. EMBO J. 40, EMBJ2021107821. https://doi.org/10.15252/embj.2021107821

Kumar, V., Shin, J.S., Shie, J.-J., Ku, K.B., Kim, C., Go, Y.Y., Huang, K.-F., Kim, M., Liang, P.-H., 2017. Identification and evaluation of potent Middle East respiratory syndrome coronavirus (MERS-CoV) 3CLPro inhibitors. Antiviral Res. 141, 101–106. https://doi.org/10.1016/j.antiviral.2017.02.007

Kung, Y.-A., Chuang, C.-H., Chen, Y.-C., Yang, H.-P., Li, H.-C., Chen, C.-L., Janapatla, R.P., Chen, C.-J., Shih, S.-R., Chiu, C.-H., 2025. Worldwide SARS-CoV-2 Omicron variant infection: Emerging sub-variants and future vaccination perspectives. J. Formos. Med. Assoc. 124, 592–599. https://doi.org/10.1016/j.jfma.2024.08.021

Laing, E.D., Sterling, S.L., Weir, D.L., Beauregard, C.R., Smith, I.L., Larsen, S.E., Wang, L.-F., Snow, A.L., Schaefer, B.C., Broder, C.C., 2019. Enhanced Autophagy Contributes to Reduced Viral Infection in Black Flying Fox Cells. Viruses 11, 260. https://doi.org/10.3390/v11030260

Lam, T.T.-Y., Jia, N., Zhang, Y.-W., Shum, M.H.-H., Jiang, J.-F., Zhu, H.-C., Tong, Y.-G., Shi, Y.-X., Ni, X.-B., Liao, Y.-S., Li, W.-J., Jiang, B.-G., Wei, W., Yuan, T.-T., Zheng, K., Cui, X.-M., Li, J., Pei, G.-Q., Qiang, X., Cheung, W.Y.-M., Li, L.-F., Sun, F.-F., Qin, S., Huang, J.-C., Leung, G.M., Holmes, E.C., Hu, Y.-L., Guan, Y., Cao, W.-C., 2020. Identifying SARS-CoV-2-related coronaviruses in Malayan pangolins. Nature 583, 282–285. https://doi.org/10.1038/s41586-020-2169-0

Lang, Y., Li, W., Li, Z., Koerhuis, D., van den Burg, A.C.S., Rozemuller, E., Bosch, B.-J., van Kuppeveld, F.J.M., Boons, G.-J., Huizinga, E.G., van der Schaar, H.M., de Groot, R.J., 2020. Coronavirus hemagglutinin-esterase and spike proteins coevolve for functional balance and optimal virion avidity. Proc. Natl. Acad. Sci. U. S. A. 117, 25759–25770. https://doi.org/10.1073/pnas.2006299117

LaTourrette, K., Holste, N.M., Rodriguez-Peña, R., Leme, R.A., Garcia-Ruiz, H., n.d. Genome-Wide Variation in Betacoronaviruses. J. Virol. 95, e00496-21. https://doi.org/10.1128/JVI.00496-21

Lau, S.K.P., Fan, R.Y.Y., Zhu, L., Li, K.S.M., Wong, A.C.P., Luk, H.K.H., Wong, E.Y.M., Lam, C.S.F., Lo, G.C.S., Fung, J., He, Z., Fok, F.C.H., Au-Yeung, R.K.H., Zhang, L., Kok, K.-H., Yuen, K.-Y., Woo, P.C.Y., 2021. Isolation of MERS-related coronavirus from lesser bamboo bats that uses DPP4 and infects human-DPP4-transgenic mice. Nat. Commun. 12, 216. https://doi.org/10.1038/s41467-020-20458-9

Lau, S.K.P., Li, K.S.M., Tsang, A.K.L., Lam, C.S.F., Ahmed, S., Chen, H., Chan, K.-H., Woo, P.C.Y., Yuen, K.-Y., 2013. Genetic Characterization of Betacoronavirus Lineage C Viruses in Bats Reveals Marked Sequence Divergence in the Spike Protein of Pipistrellus Bat Coronavirus HKU5 in Japanese Pipistrelle: Implications for the Origin of the Novel Middle East Respiratory Syndrome Coronavirus. J. Virol. 87, 8638–8650. https://doi.org/10.1128/jvi.01055-13

Lau, S.K.P., Lung, D.C., Wong, E.Y.M., Aw-Yong, K.L., Wong, A.C.P., Luk, H.K.H., Li, K.S.M., Fung, J., Chan, T.T.Y., Tang, J.Y.M., Zhu, L., Yip, C.C.Y., Wong, S.C.Y., Lee, R.A., Tsang, O.T.Y., Yuen, K.-Y., Woo, P.C.Y., 2021. Molecular Evolution of Human Coronavirus 229E in Hong Kong and a Fatal COVID-19 Case Involving Coinfection with a Novel Human Coronavirus 229E Genogroup. mSphere 6, 10.1128/msphere.00819-20. https://doi.org/10.1128/msphere.00819-20

Lau, S.K.P., Woo, P.C.Y., Li, K.S.M., Huang, Y., Tsoi, H.-W., Wong, B.H.L., Wong, S.S.Y., Leung, S.-Y., Chan, K.-H., Yuen, K.-Y., 2005. Severe acute respiratory syndrome coronavirus-like virus in Chinese horseshoe bats. Proc. Natl. Acad. Sci. 102, 14040–14045. https://doi.org/10.1073/pnas.0506735102

Lau, S.K.P., Zhang, L., Luk, H.K.H., Xiong, L., Peng, X., Li, K.S.M., He, X., Zhao, P.S.-H., Fan, R.Y.Y., Wong, A.C.P., Ahmed, S.S., Cai, J.-P., Chan, J.F.W., Sun, Y., Jin, D., Chen, H., Lau, T.C.K., Kok, R.K.H., Li, W., Yuen, K.-Y., Woo, P.C.Y., 2018. Receptor Usage of a Novel Bat Lineage C Betacoronavirus Reveals Evolution of Middle East Respiratory Syndrome-Related Coronavirus Spike Proteins for Human Dipeptidyl Peptidase 4 Binding. J. Infect. Dis. 218, 197–207. https://doi.org/10.1093/infdis/jiy018

Lednicky, J.A., Tagliamonte, M.S., White, S.K., Elbadry, M.A., Alam, M.M., Stephenson, C.J., Bonny, T.S., Loeb, J.C., Telisma, T., Chavannes, S., Ostrov, D.A., Mavian, C., Beau De Rochars, V.M., Salemi, M., Morris, J.G., 2021. Independent infections of porcine deltacoronavirus among Haitian children. Nature 600, 133–137. https://doi.org/10.1038/s41586-021-04111-z

Lee, J., Worrall, L.J., Vuckovic, M., Rosell, F.I., Gentile, F., Ton, A.-T., Caveney, N.A., Ban, F., Cherkasov, A., Paetzel, M., Strynadka, N.C.J., 2020. Crystallographic structure of wild-type SARS-CoV-2 main protease acyl-enzyme intermediate with physiological C-terminal autoprocessing site. Nat. Commun. 11, 5877. https://doi.org/10.1038/s41467-020-19662-4

Lei, F., Shu, J., Xia, C., Lei, Y., Zhang, Yajie, Zhang, Yang, Yuan, Z., Yi, Z., 2025. Viral determinants of cis- and trans-cleavage by SARS-CoV-2 Nsp3 and an on-off reporter for monitoring intracellular protease activity. Antiviral Res. 242, 106262. https://doi.org/10.1016/j.antiviral.2025.106262

Letunic, I., Bork, P., 2024. Interactive Tree of Life (iTOL) v6: recent updates to the phylogenetic tree display and annotation tool. Nucleic Acids Res. 52, W78–W82. https://doi.org/10.1093/nar/gkae268

Li, W., Moore, M.J., Vasilieva, N., Sui, J., Wong, S.K., Berne, M.A., Somasundaran, M., Sullivan, J.L., Luzuriaga, K., Greenough, T.C., Choe, H., Farzan, M., 2003. Angiotensin-converting enzyme 2 is a functional receptor for the SARS coronavirus. Nature 426, 450–454. https://doi.org/10.1038/nature02145

Li, W., Shi, Z., Yu, M., Ren, W., Smith, C., Epstein, J.H., Wang, H., Crameri, G., Hu, Z., Zhang, H., Zhang, J., McEachern, J., Field, H., Daszak, P., Eaton, B.T., Zhang, S., Wang, L.-F., 2005. Bats Are Natural Reservoirs of SARS-Like Coronaviruses. Science 310, 676–679. https://doi.org/10.1126/science.1118391

Liu, D.X., Fung, T.S., Chong, K.K.-L., Shukla, A., Hilgenfeld, R., 2014. Accessory proteins of SARS-CoV and other coronaviruses. Antiviral Res. 109, 97–109. https://doi.org/10.1016/j.antiviral.2014.06.013

Luis, A.D., Hayman, D.T.S., O'Shea, T.J., Cryan, P.M., Gilbert, A.T., Pulliam, J.R.C., Mills, J.N., Timonin, M.E., Willis, C.K.R., Cunningham, A.A., Fooks, A.R., Rupprecht, C.E., Wood, J.L.N., Webb, C.T., 2013. A comparison of bats and rodents as reservoirs of zoonotic viruses: are bats special? Proc. R. Soc. B Biol. Sci. 280, 20122753. https://doi.org/10.1098/rspb.2012.2753

Luo, C.-M., Wang, N., Yang, X.-L., Liu, H.-Z., Zhang, W., Li, B., Hu, B., Peng, C., Geng, Q.-B., Zhu, G.-J., Li, F., Shi, Z.-L., 2018. Discovery of Novel Bat Coronaviruses in South China That Use the Same Receptor as Middle East Respiratory Syndrome Coronavirus. J. Virol. 92, 10.1128/jvi.00116-18. https://doi.org/10.1128/jvi.00116-18

Ma, Juan, Zhu, F., Zhao, M., Shao, F., Yu, D., Ma, Jiangwen, Zhang, X., Li, W., Qian, Y., Zhang, Y., Jiang, D., Wang, S., Xia, P., 2021. SARS-CoV-2 nucleocapsid suppresses host pyroptosis by blocking Gasdermin D cleavage. EMBO J. 40, e108249. https://doi.org/10.15252/embj.2021108249

Madhugiri, R., Slanina, H., Saleem-Batcha, R., Ziebuhr, J., 2026. The Coronavirus Replication–Transcription Complex. https://doi.org/10.1146/annurev-biochem-052621-091439

Malone, B., Urakova, N., Snijder, E.J., Campbell, E.A., 2022. Structures and functions of coronavirus replication–transcription complexes and their relevance for SARS-CoV-2 drug design. Nat. Rev. Mol. Cell Biol. 23, 21–39. https://doi.org/10.1038/s41580-021-00432-z

Maryam, A., Moquin, S.A., Dovala, D., Kaur, J., Kurt Yilmaz, N., Shaqra, A.M., Schiffer, C.A., 2025. Structural Analysis of Inhibitor Binding to the Feline Enteric Coronavirus (FECV) Main Protease. Viruses 17, 1506. https://doi.org/10.3390/v17111506

McBride, R., Fielding, B.C., 2012. The Role of Severe Acute Respiratory Syndrome (SARS)-Coronavirus Accessory Proteins in Virus Pathogenesis. Viruses 4, 2902–2923. https://doi.org/10.3390/v4112902

McCoy, A.J., Grosse-Kunstleve, R.W., Adams, P.D., Winn, M.D., Storoni, L.C., Read, R.J., 2007. Phaser crystallographic software. J. Appl. Crystallogr. 40, 658–674. https://doi.org/10.1107/S0021889807021206

McWilliam, H., Li, W., Uludag, M., Squizzato, S., Park, Y.M., Buso, N., Cowley, A.P., Lopez, R., 2013. Analysis tool web services from the EMBL-EBI. Nucleic Acids Res. 41, W597–W600.

Menachery, V.D., Yount, B.L., Debbink, K., Agnihothram, S., Gralinski, L.E., Plante, J.A., Graham, R.L., Scobey, T., Ge, X.-Y., Donaldson, E.F., Randell, S.H., Lanzavecchia, A., Marasco, W.A., Shi, Z.-L., Baric, R.S., 2015. A SARS-like cluster of circulating bat coronaviruses shows potential for human emergence. Nat. Med. 21, 1508–1513. https://doi.org/10.1038/nm.3985

MHLW (Japan) grants full approval for Xocova (ensitrelvir) to treatSARS-CoV-2 infection in Japan [WWW Document], n.d. URL https://www.medthority.com/news/2024/3/mhlw-japan--grants-full-approval-for-xocova--ensitrelvir-to-treatsars-cov-2-infection-in-japan.--shionogi (accessed 11.12.26).

Middle East respiratory syndrome coronavirus (MERS-CoV) – Multi-country – Monthly update | European Centre for Disease Prevention and Control [WWW Document], n.d. URL https://www.ecdc.europa.eu/en/public-health-events/2012-eip-00049/2026-11-10#section-assessment (accessed 11.15.26).

Middleton, D.J., Morrissy, C.J., van der Heide, B.M., Russell, G.M., Braun, M.A., Westbury, H.A., Halpin, K., Daniels, P.W., 2007. Experimental Nipah Virus Infection in Pteropid Bats (*Pteropus poliocephalus*). J. Comp. Pathol. 136, 266–272. https://doi.org/10.1016/j.jcpa.2007.03.002

Millet, J.K., Whittaker, G.R., 2014. Host cell entry of Middle East respiratory syndrome coronavirus after two-step, furin-mediated activation of the spike protein. Proc. Natl. Acad. Sci. 111, 15214–15219. https://doi.org/10.1073/pnas.1407087111

Minigulov, N., Boranbayev, K., Bekbossynova, A., Gadilgereyeva, B., Filchakova, O., 2024. Structural proteins of human coronaviruses: what makes them different? Front. Cell. Infect. Microbiol. 14, 1458383. https://doi.org/10.3389/fcimb.2024.1458383

Moghadasi, S.A., Heilmann, E., Khalil, A.M., Nnabuife, C., Kearns, F.L., Ye, C., Moraes, S.N., Costacurta, F., Esler, M.A., Aihara, H., von Laer, D., Martinez-Sobrido, L., Palzkill, T., Amaro, R.E., Harris, R.S., 2023. Transmissible SARS-CoV-2 variants with resistance to clinical protease inhibitors. Sci. Adv. 9, eade8778. https://doi.org/10.1126/sciadv.ade8778

Nakagawa, K., Lokugamage, K.G., Makino, S., 2016. Viral and Cellular mRNA Translation in Coronavirus-Infected Cells. Adv. Virus Res. 96, 165–192. https://doi.org/10.1016/bs.aivir.2016.08.001

Needle, D., Lountos, G.T., Waugh, D.S., 2015. Structures of the Middle East respiratory syndrome coronavirus 3C-like protease reveal insights into substrate specificity. Acta Crystallogr. D Biol. Crystallogr. 71, 1102–1111. https://doi.org/10.1107/S1399004715003521

Nguyen, H.N., Ranasinghe, P.S., Ilesinghe, I.K.R.S., Dampalla, C.S., Rathnayake, A.D., Liska, Z., Jesri, A.-R.M., Azmi, Z., Nevonen, D.E., Kim, Y., Ung, A.R., Taylor, K.E., Cooper, A., Liu, L., Battaile, K.P., Thurman, H.A., Gusachenko, E., Lovell, S., Groutas, W.C., Chang, K.-O., 2026. Structure-guided design of broad-spectrum inhibitors of coronaviral proteases embodying a 1,3,2-oxazaphospholidin-3-one scaffold as a versatile design element. Eur. J. Med. Chem. 316, 119002. https://doi.org/10.1016/j.ejmech.2026.119002

Noske, G.D., Silva, E. de S., Godoy, M.O. de, Dolci, I., Fernandes, R.S., Guido, R.V.C., Sjö, P., Oliva, G., Godoy, A.S., 2023. Structural basis of nirmatrelvir and ensitrelvir activity against naturally occurring polymorphisms of the SARS-CoV-2 main protease. J. Biol. Chem. 299. https://doi.org/10.1016/j.jbc.2023.103004

Osipiuk, J., Azizi, S.-A., Dvorkin, S., Endres, M., Jedrzejczak, R., Jones, K.A., Kang, S., Kathayat, R.S., Kim, Y., Lisnyak, V.G., Maki, S.L., Nicolaescu, V., Taylor, C.A., Tesar, C., Zhang, Y.-A., Zhou, Z., Randall, G., Michalska, K., Snyder, S.A., Dickinson, B.C., Joachimiak, A., 2021. Structure of papain-like protease from SARS-CoV-2 and its complexes with non-covalent inhibitors. Nat. Commun. 12, 743. https://doi.org/10.1038/s41467-021-21060-3

Otieno, J.R., Cherry, J.L., Spiro, D.J., Nelson, M.I., Trovão, N.S., 2022. Origins and Evolution of Seasonal Human Coronaviruses. Viruses 14, 1551. https://doi.org/10.3390/v14071551

Owen, D.R., Allerton, C.M.N., Anderson, A.S., Aschenbrenner, L., Avery, M., Berritt, S., Boras, B., Cardin, R.D., Carlo, A., Coffman, K.J., Dantonio, A., Di, L., Eng, H., Ferre, R., Gajiwala, K.S., Gibson, S.A., Greasley, S.E., Hurst, B.L., Kadar, E.P., Kalgutkar, A.S., Lee, J.C., Lee, J., Liu, W., Mason, S.W., Noell, S., Novak, J.J., Obach, R.S., Ogilvie, K., Patel, N.C., Pettersson, M., Rai, D.K., Reese, M.R., Sammons, M.F., Sathish, J.G., Singh, R.S.P., Steppan, C.M., Stewart, A.E., Tuttle, J.B., Updyke, L., Verhoest, P.R., Wei, L., Yang, Q., Zhu, Y., 2021. An oral SARS-CoV-2 M^{pro} inhibitor clinical candidate for the treatment of COVID-19. Science 374, 1586–1593. https://doi.org/10.1126/science.abl4784

Pablos, I., Machado, Y., de Jesus, H.C.R., Mohamud, Y., Kappelhoff, R., Lindskog, C., Vlok, M., Bell, P.A., Butler, G.S., Grin, P.M., Cao, Q.T., Nguyen, J.P., Solis, N., Abbina, S., Rut, W., Vederas, J.C., Szekely, L., Szakos, A., Drag, M., Kizhakkedathu, J.N., Mossman, K., Hirota, J.A., Jan, E., Luo, H., Banerjee, A., Overall, C.M., 2021. Mechanistic insights into COVID-19 by global analysis of the SARS-CoV-2 3CLpro substrate degradome. Cell Rep. 37, 109892. https://doi.org/10.1016/j.celrep.2021.109892

Pedersen, N.C., Kim, Y., Liu, H., Galasiti Kankanamalage, A.C., Eckstrand, C., Groutas, W.C., Bannasch, M., Meadows, J.M., Chang, K.-O., 2018. Efficacy of a 3C-like protease inhibitor in treating various forms of acquired feline infectious peritonitis. J. Feline Med. Surg. 20, 378–392. https://doi.org/10.1177/1098612X17729626

Pensaert, M.B., de Bouck, P., 1978. A new coronavirus-like particle associated with diarrhea in swine. Arch. Virol. 58, 243–247. https://doi.org/10.1007/BF01317606

Perera, K.D., Galasiti Kankanamalage, A.C., Rathnayake, A.D., Honeyfield, A., Groutas, W., Chang, K.-O., Kim, Y., 2018. Protease inhibitors broadly effective against feline, ferret and mink coronaviruses. Antiviral Res. 160, 79–86. https://doi.org/10.1016/j.antiviral.2018.10.015

Perera, K.D., Rathnayake, A.D., Liu, H., Pedersen, N.C., Groutas, W.C., Chang, K.-O., Kim, Y., 2019. Characterization of amino acid substitutions in feline coronavirus 3C-like protease from a cat with feline infectious peritonitis treated with a protease inhibitor. Vet. Microbiol. 237, 108398. https://doi.org/10.1016/j.vetmic.2019.108398

Potterton, L., McNicholas, S., Krissinel, E., Gruber, J., Cowtan, K., Emsley, P., Murshudov, G.N., Cohen, S., Perrakis, A., Noble, M., 2004. Developments in the CCP4 molecular-graphics project. Acta Crystallogr. D Biol. Crystallogr. 60, 2288–2294. https://doi.org/10.1107/S0907444904023716

Rafique, S., Jabeen, Z., Pervaiz, T., Rashid, F., Luo, S., Xie, L., Xie, Z., 2024. Avian infectious bronchitis virus (AIBV) review by continent. Front. Cell. Infect. Microbiol. 14. https://doi.org/10.3389/fcimb.2024.1325346

Raj, V.S., Mou, H., Smits, S.L., Dekkers, D.H.W., Müller, M.A., Dijkman, R., Muth, D., Demmers, J.A.A., Zaki, A., Fouchier, R.A.M., Thiel, V., Drosten, C., Rottier, P.J.M., Osterhaus, A.D.M.E., Bosch, B.J., Haagmans, B.L., 2013. Dipeptidyl peptidase 4 is a functional receptor for the emerging human coronavirus-EMC. Nature 495, 251–254. https://doi.org/10.1038/nature12005

Rathnayake, A.D., Zheng, J., Kim, Y., Perera, K.D., Mackin, S., Meyerholz, D.K., Kashipathy, M.M., Battaile, K.P., Lovell, S., Perlman, S., Groutas, W.C., Chang, K.-O., 2020. 3C-like protease inhibitors block coronavirus replication in vitro and improve survival in MERS-CoV–infected mice. Sci. Transl. Med. 12, eabc5332. https://doi.org/10.1126/scitranslmed.abc5332

Rohaim, M.A., El Naggar, R.F., Clayton, E., Munir, M., 2021. Structural and functional insights into non-structural proteins of coronaviruses. Microb. Pathog. 150, 104641. https://doi.org/10.1016/j.micpath.2020.104641

SARS-Associated Coronavirus Quasispecies in Individual Patients | New England Journal of Medicine [WWW Document], n.d. URL https://www.nejm.org/doi/full/10.1056/NEJMc032421 (accessed 11.13.26).

Schechter, I., Berger, A., 1967. On the size of the active site in proteases. I. Papain. Biochem. Biophys. Res. Commun. 27, 157–162. https://doi.org/10.1016/S0006-291X(67)80055-X

Schoeman, D., Fielding, B.C., 2019. Coronavirus envelope protein: current knowledge. Virol. J. 16, 69. https://doi.org/10.1186/s12985-019-1182-0

Seifert, S.N., Bai, S., Fawcett, S., Norton, E.B., Zwezdaryk, K.J., Robinson, J., Gunn, B., Letko, M., 2022. An ACE2-dependent Sarbecovirus in Russian bats is resistant to SARS-CoV-2 vaccines. PLOS Pathog. 18, e1010828. https://doi.org/10.1371/journal.ppat.1010828

Shamsi, A., Mohammad, T., Anwar, S., Amani, S., Khan, M.S., Husain, F.M., Rehman, Md.T., Islam, A., Hassan, M.I., 2021. Potential drug targets of SARS-CoV-2: From

genomics to therapeutics. Int. J. Biol. Macromol. 177, 1–9. https://doi.org/10.1016/j.ijbiomac.2021.02.071

Shimizu, R., Sonoyama, T., Fukuhara, T., Kuwata, A., Matsuzaki, T., Matsuo, Y., Kubota, R., 2023. Evaluation of the Drug–Drug Interaction Potential of Ensitrelvir Fumaric Acid with Cytochrome P450 3A Substrates in Healthy Japanese Adults. Clin. Drug Investig. 43, 335–346. https://doi.org/10.1007/s40261-023-01265-8

Shin, D., Mukherjee, R., Grewe, D., Bojkova, D., Baek, K., Bhattacharya, A., Schulz, L., Widera, M., Mehdipour, A.R., Tascher, G., Geurink, P.P., Wilhelm, A., van der Heden van Noort, G.J., Ovaa, H., Müller, S., Knobeloch, K.-P., Rajalingam, K., Schulman, B.A., Cinatl, J., Hummer, G., Ciesek, S., Dikic, I., 2020. Papain-like protease regulates SARS-CoV-2 viral spread and innate immunity. Nature 587, 657–662. https://doi.org/10.1038/s41586-020-2601-5

Shionogi Announces FDA Approval of XOCOVA® (ensitrelvir), the First and Only Oral Option to Help Prevent COVID-19 Following Exposure [WWW Document], n.d. URL https://www.shionogi.com/global/en/news/2026/06/20260601.html (accessed 11.12.26).

Simmons, N.B. and A.L. Cirranello. 2026. Bat Species of the World: A taxonomic and geographic database. Version 1.11. Accessed on 11/17/2026.

Sipulwa, L.A., Ongus, J.R., Coldren, R.L., Bulimo, W.D., 2016. Molecular characterization of human coronaviruses and their circulation dynamics in Kenya, 2009–2012. Virol. J. 13, 18. https://doi.org/10.1186/s12985-016-0474-x

Sola, I., Almazán, F., Zúñiga, S., Enjuanes, L., 2015. Continuous and Discontinuous RNA Synthesis in Coronaviruses. Annu. Rev. Virol. 2, 265–288. https://doi.org/10.1146/annurev-virology-100114-055218

Statement on the fifteenth meeting of the IHR (2005) Emergency Committee on the COVID-19 pandemic [WWW Document], n.d. URL https://www.who.int/news/item/05-05-2023-statement-on-the-fifteenth-meeting-of-the-international-health-regulations-(2005)-emergency-committee-regarding-the-coronavirus-disease-(covid-19)-pandemic (accessed 11.15.26).

Stertz, S., Reichelt, M., Spiegel, M., Kuri, T., Martínez-Sobrido, L., García-Sastre, A., Weber, F., Kochs, G., 2007. The intracellular sites of early replication and budding of SARS-coronavirus. Virology 361, 304–315. https://doi.org/10.1016/j.virol.2006.11.027

Su, S., Wong, G., Shi, W., Liu, J., Lai, A.C.K., Zhou, J., Liu, W., Bi, Y., Gao, G.F., 2016. Epidemiology, Genetic Recombination, and Pathogenesis of Coronaviruses. Trends Microbiol. 24, 490–502. https://doi.org/10.1016/j.tim.2016.03.003

Summary of probable SARS cases with onset of illness from 1 November 2002 to 31 July 2003 [WWW Document], n.d. URL https://www.who.int/publications/m/item/summary-of-probable-sars-cases-with-onset-of-illness-from-1-november-2002-to-31-july-2003 (accessed 11.15.26).

Swanepoel, R., Leman, P.A., Burt, F.J., Zachariades, N.A., Braack, L.E., Ksiazek, T.G., Rollin, P.E., Zaki, S.R., Peters, C.J., 1996. Experimental inoculation of plants and

animals with Ebola virus. Emerg. Infect. Dis. 2, 321–325. https://doi.org/10.3201/eid0204.960407

Tai, W., He, L., Zhang, X., Pu, J., Voronin, D., Jiang, S., Zhou, Y., Du, L., 2020. Characterization of the receptor-binding domain (RBD) of 2019 novel coronavirus: implication for development of RBD protein as a viral attachment inhibitor and vaccine. Cell. Mol. Immunol. 17, 613–620. https://doi.org/10.1038/s41423-020-0400-4

Tao, Y., Shi, M., Chommanard, C., Queen, K., Zhang, J., Markotter, W., Kuzmin, I.V., Holmes, E.C., Tong, S., 2017. Surveillance of Bat Coronaviruses in Kenya Identifies Relatives of Human Coronaviruses NL63 and 229E and Their Recombination History. J. Virol. 91, 10.1128/jvi.01953-16. https://doi.org/10.1128/jvi.01953-16

Teeling, E.C., Springer, M.S., Madsen, O., Bates, P., O'Brien, S.J., Murphy, W.J., 2005. A Molecular Phylogeny for Bats Illuminates Biogeography and the Fossil Record. Science 307, 580–584. https://doi.org/10.1126/science.1105113

Tekes, G., Thiel, H.-J., 2016. Feline Coronaviruses. Adv. Virus Res. 96, 193–218. https://doi.org/10.1016/bs.aivir.2016.08.002

Temmam, S., Vongphayloth, K., Baquero, E., Munier, S., Bonomi, M., Regnault, B., Douangboubpha, B., Karami, Y., Chrétien, D., Sanamxay, D., Xayaphet, V., Paphaphanh, P., Lacoste, V., Somlor, S., Lakeomany, K., Phommavanh, N., Pérot, P., Dehan, O., Amara, F., Donati, F., Bigot, T., Nilges, M., Rey, F.A., van der Werf, S., Brey, P.T., Eloit, M., 2022. Bat coronaviruses related to SARS-CoV-2 and infectious for human cells. Nature 604, 330–336. https://doi.org/10.1038/s41586-022-04532-4

Thompson, B., Petrić Howe, N., 2024. Alphafold 3.0: the AI protein predictor gets an upgrade. Nature. https://doi.org/10.1038/d41586-024-01385-x

Tolah, A.M., Masaudi, S.B.A., El-Kafrawy, S.A., Mirza, A.A., Harakeh, S.M., Hassan, A.M., Alsaadi, M.A., Alzahrani, A.A., Alsaaidi, G.A., Amor, N.M.S., Alagaili, A.N., Hashem, A.M., Azhar, E.I., 2020. Cross-sectional prevalence study of MERS-CoV in local and imported dromedary camels in Saudi Arabia, 2016-2018. PLOS ONE 15, e0232790. https://doi.org/10.1371/journal.pone.0232790

Tyrrell, D.A., Bynoe, M.L., 1965. CULTIVATION OF A NOVEL TYPE OF COMMON-COLD VIRUS IN ORGAN CULTURES. Br. Med. J. 1, 1467–1470. https://doi.org/10.1136/bmj.1.5448.1467

Unoh, Y., Uehara, S., Nakahara, K., Nobori, H., Yamatsu, Y., Yamamoto, S., Maruyama, Y., Taoda, Y., Kasamatsu, K., Suto, T., Kouki, K., Nakahashi, A., Kawashima, S., Sanaki, T., Toba, S., Uemura, K., Mizutare, T., Ando, S., Sasaki, M., Orba, Y., Sawa, H., Sato, A., Sato, T., Kato, T., Tachibana, Y., 2022. Discovery of S-217622, a Noncovalent Oral SARS-CoV-2 3CL Protease Inhibitor Clinical Candidate for Treating COVID-19. J. Med. Chem. 65, 6499–6512. https://doi.org/10.1021/acs.jmedchem.2c00117

van der Hoek, L., Pyrc, K., Jebbink, M.F., Vermeulen-Oost, W., Berkhout, R.J.M., Wolthers, K.C., Wertheim-van Dillen, P.M.E., Kaandorp, J., Spaargaren, J.,

Berkhout, B., 2004. Identification of a new human coronavirus. Nat. Med. 10, 368–373. https://doi.org/10.1038/nm1024

van Huizen, M., Vendrell, X.M., de Gruyter, H.L.M., Boomaars-van der Zanden, A.L., van der Meer, Y., Snijder, E.J., Kikkert, M., Myeni, S.K., 2024. The Main Protease of Middle East Respiratory Syndrome Coronavirus Induces Cleavage of Mitochondrial Antiviral Signaling Protein to Antagonize the Innate Immune Response. Viruses 16, 256. https://doi.org/10.3390/v16020256

Vijgen, L., Keyaerts, E., Moës, E., Thoelen, I., Wollants, E., Lemey, P., Vandamme, A.-M., Van Ranst, M., 2005. Complete Genomic Sequence of Human Coronavirus OC43: Molecular Clock Analysis Suggests a Relatively Recent Zoonotic Coronavirus Transmission Event. J. Virol. 79, 1595–1604. https://doi.org/10.1128/jvi.79.3.1595-1604.2005

V'kovski, P., Kratzel, A., Steiner, S., Stalder, H., Thiel, V., 2021. Coronavirus biology and replication: implications for SARS-CoV-2. Nat. Rev. Microbiol. 19, 155–170. https://doi.org/10.1038/s41579-020-00468-6

Vlasova, A.N., Halpin, R., Wang, S., Ghedin, E., Spiro, D.J., Saif, L.J., 2011. Molecular characterization of a new species in the genus Alphacoronavirus associated with mink epizootic catarrhal gastroenteritis. J. Gen. Virol. 92, 1369–1379. https://doi.org/10.1099/vir.0.025353-0

Vonrhein, C., Flensburg, C., Keller, P., Sharff, A., Smart, O., Paciorek, W., Womack, T., Bricogne, G., 2011. Data processing and analysis with the autoPROC toolbox. Acta Crystallogr. D Biol. Crystallogr. 67, 293–302. https://doi.org/10.1107/S0907444911007773

Wacharapluesadee, S., Tan, C.W., Maneeorn, P., Duengkae, P., Zhu, F., Joyjinda, Y., Kaewpom, T., Chia, W.N., Ampoot, W., Lim, B.L., Worachotsueptrakun, K., Chen, V.C.-W., Sirichan, N., Ruchisrisarod, C., Rodpan, A., Noradechanon, K., Phaichana, T., Jantarat, N., Thongnumchaima, B., Tu, C., Crameri, G., Stokes, M.M., Hemachudha, T., Wang, L.-F., 2021. Evidence for SARS-CoV-2 related coronaviruses circulating in bats and pangolins in Southeast Asia. Nat. Commun. 12, 972. https://doi.org/10.1038/s41467-021-21240-1

Walls, A.C., Park, Y.-J., Tortorici, M.A., Wall, A., McGuire, A.T., Veesler, D., 2020. Structure, Function, and Antigenicity of the SARS-CoV-2 Spike Glycoprotein. Cell 181, 281-292.e6. https://doi.org/10.1016/j.cell.2020.02.058

Wan, Y., Shang, J., Graham, R., Baric, R.S., Li, F., 2020. Receptor Recognition by the Novel Coronavirus from Wuhan: an Analysis Based on Decade-Long Structural Studies of SARS Coronavirus. J. Virol. 94, 10.1128/jvi.00127-20. https://doi.org/10.1128/jvi.00127-20

Wang, F., Chen, C., Tan, W., Yang, K., Yang, H., 2016. Structure of Main Protease from Human Coronavirus NL63: Insights for Wide Spectrum Anti-Coronavirus Drug Design. Sci. Rep. 6, 22677. https://doi.org/10.1038/srep22677

Wang, W., Lin, X.-D., Guo, W.-P., Zhou, R.-H., Wang, M.-R., Wang, C.-Q., Ge, S., Mei, S.-H., Li, M.-H., Shi, M., Holmes, E.C., Zhang, Y.-Z., 2015. Discovery, diversity and

evolution of novel coronaviruses sampled from rodents in China. Virology 474, 19–27. https://doi.org/10.1016/j.virol.2014.10.017

Wasim, R., Sumaiya, Ahmad, A., 2025. Across-the-board review on Omicron SARS-CoV-2 variant. Inflammopharmacology 33, 1–10. https://doi.org/10.1007/s10787-024-01627-4

Watanabe, S., Masangkay, J.S., Nagata, N., Morikawa, S., Mizutani, T., Fukushi, S., Alviola, P., Omatsu, T., Ueda, N., Iha, K., Taniguchi, S., Fujii, H., Tsuda, S., Endoh, M., Kato, K., Tohya, Y., Kyuwa, S., Yoshikawa, Y., Akashi, H., 2010. Bat Coronaviruses and Experimental Infection of Bats, the Philippines. Emerg. Infect. Dis. 16, 1217–1223. https://doi.org/10.3201/eid1608.100208

Weil, T., Lawrenz, J., Seidel, A., Münch, J., Müller, J.A., 2022. Immunodetection assays for the quantification of seasonal common cold coronaviruses OC43, NL63, or 229E infection confirm nirmatrelvir as broad coronavirus inhibitor. Antiviral Res. 203, 105343. https://doi.org/10.1016/j.antiviral.2022.105343

WHO Director-General's opening remarks at the media briefing on COVID-19 - 11 March 2020 [WWW Document], n.d. URL https://www.who.int/news-room/speeches/item/who-director-general-s-opening-remarks-at-the-media-briefing-on-covid-19---11-march-2020 (accessed 11.15.26).

Williams, R., Hales, J., Collier, W., Gould, P., 2025. Coronavirus Replication: Genomes, Subgenomic RNAs, and Defective Viral Genomes. Viruses 17, 767. https://doi.org/10.3390/v17060767

Wong, A.C.P., Li, X., Lau, S.K.P., Woo, P.C.Y., 2019. Global Epidemiology of Bat Coronaviruses. Viruses 11, 174. https://doi.org/10.3390/v11020174

Woo, P.C.Y., de Groot, R.J., Haagmans, B., Lau, S.K.P., Neuman, B.W., Perlman, S., Sola, I., van der Hoek, L., Wong, A.C.P., Yeh, S.-H., 2023. ICTV Virus Taxonomy Profile: Coronaviridae 2023. J. Gen. Virol. 104, 001843. https://doi.org/10.1099/jgv.0.001843

Woo, P.C.Y., Lau, S.K.P., Lam, C.S.F., Lau, C.C.Y., Tsang, A.K.L., Lau, J.H.N., Bai, R., Teng, J.L.L., Tsang, C.C.C., Wang, M., Zheng, B.-J., Chan, K.-H., Yuen, K.-Y., 2012. Discovery of Seven Novel Mammalian and Avian Coronaviruses in the Genus Deltacoronavirus Supports Bat Coronaviruses as the Gene Source of Alphacoronavirus and Betacoronavirus and Avian Coronaviruses as the Gene Source of Gammacoronavirus and Deltacoronavirus. J. Virol. 86, 3995–4008. https://doi.org/10.1128/JVI.06540-11

Woo, P.C.Y., Lau, S.K.P., Li, K.S.M., Poon, R.W.S., Wong, B.H.L., Tsoi, H., Yip, B.C.K., Huang, Y., Chan, K., Yuen, K., 2006. Molecular diversity of coronaviruses in bats. Virology 351, 180–187. https://doi.org/10.1016/j.virol.2006.02.041

Wu, Z., Lu, L., Du, J., Yang, L., Ren, X., Liu, B., Jiang, J., Yang, J., Dong, J., Sun, L., Zhu, Y., Li, Y., Zheng, D., Zhang, C., Su, H., Zheng, Y., Zhou, H., Zhu, G., Li, H., Chmura, A., Yang, F., Daszak, P., Wang, J., Liu, Q., Jin, Q., 2018. Comparative analysis of rodent and small mammal viromes to better understand the wildlife origin of emerging infectious diseases. Microbiome 6, 178. https://doi.org/10.1186/s40168-018-0554-9

Xiao, K., Zhai, J., Feng, Y., Zhou, N., Zhang, X., Zou, J.-J., Li, N., Guo, Y., Li, X., Shen, X., Zhang, Zhipeng, Shu, F., Huang, W., Li, Y., Zhang, Ziding, Chen, R.-A., Wu, Y.-J., Peng, S.-M., Huang, M., Xie, W.-J., Cai, Q.-H., Hou, F.-H., Chen, W., Xiao, L., Shen, Y., 2020. Isolation of SARS-CoV-2-related coronavirus from Malayan pangolins. Nature 583, 286–289. https://doi.org/10.1038/s41586-020-2313-x

Xiong, M., Su, H., Zhao, W., Xie, H., Shao, Q., Xu, Y., 2021. What coronavirus 3C-like protease tells us: From structure, substrate selectivity, to inhibitor design. Med. Res. Rev. 41, 1965–1998. https://doi.org/10.1002/med.21783

Xiong, Q., Cao, L., Ma, C., Tortorici, M.A., Liu, C., Si, J., Liu, P., Gu, M., Walls, A.C., Wang, C., Shi, L., Tong, F., Huang, M., Li, J., Zhao, C., Shen, C., Chen, Y., Zhao, H., Lan, K., Corti, D., Veesler, D., Wang, X., Yan, H., 2022. Close relatives of MERS-CoV in bats use ACE2 as their functional receptors. Nature 612, 748–757. https://doi.org/10.1038/s41586-022-05513-3

Xu, G., Qiao, Z., Schraauwen, R., Avan, A., Peppelenbosch, M.P., Bijvelds, M.J.C., Jiang, S., Li, P., 2024. Evidence for cross-species transmission of human coronavirus OC43 through bioinformatics and modeling infections in porcine intestinal organoids. Vet. Microbiol. 293, 110101. https://doi.org/10.1016/j.vetmic.2024.110101

Yang, H., Yang, M., Ding, Y., Liu, Y., Lou, Z., Zhou, Z., Sun, L., Mo, L., Ye, S., Pang, H., Gao, G.F., Anand, K., Bartlam, M., Hilgenfeld, R., Rao, Z., 2003. The crystal structures of severe acute respiratory syndrome virus main protease and its complex with an inhibitor. Proc. Natl. Acad. Sci. U. S. A. 100, 13190–13195. https://doi.org/10.1073/pnas.1835675100

Yang, X.-L., Hu, B., Wang, B., Wang, M.-N., Zhang, Q., Zhang, W., Wu, L.-J., Ge, X.-Y., Zhang, Y.-Z., Daszak, P., Wang, L.-F., Shi, Z.-L., 2016. Isolation and Characterization of a Novel Bat Coronavirus Closely Related to the Direct Progenitor of Severe Acute Respiratory Syndrome Coronavirus. J. Virol. 90, 3253–3256. https://doi.org/10.1128/jvi.02582-15

Ye, Z.-W., Yuan, S., Yuen, K.-S., Fung, S.-Y., Chan, C.-P., Jin, D.-Y., 2020. Zoonotic origins of human coronaviruses. Int. J. Biol. Sci. 16, 1686–1697. https://doi.org/10.7150/ijbs.45472

Yeager, C.L., Ashmun, R.A., Williams, R.K., Cardellichio, C.B., Shapiro, L.H., Look, A.T., Holmes, K.V., 1992. Human aminopeptidase N is a receptor for human coronavirus 229E. Nature 357, 420–422. https://doi.org/10.1038/357420a0

Yusof, M.F., Queen, K., Eltahir, Y.M., Paden, C.R., Al Hammadi, Z.M.A.H., Tao, Y., Li, Y., Khalafalla, A.I., Shi, M., Zhang, J., Mohamed, M.S.A.E., Abd Elaal Ahmed, M.H., Azeez, I.A., Bensalah, O.K., Eldahab, Z.S., Al Hosani, F.I., Gerber, S.I., Hall, A.J., Tong, S., Al Muhairi, S.S., 2017. Diversity of Middle East respiratory syndrome coronaviruses in 109 dromedary camels based on full-genome sequencing, Abu Dhabi, United Arab Emirates. Emerg. Microbes Infect. 6, 1–10. https://doi.org/10.1038/emi.2017.89

Zaki, A.M., Boheemen, S. van, Bestebroer, T.M., Osterhaus, A.D.M.E., Fouchier, R.A.M., 2012. Isolation of a Novel Coronavirus from a Man with Pneumonia in Saudi Arabia. N. Engl. J. Med. 367, 1814–1820. https://doi.org/10.1056/NEJMoa1211721

Zhang, L., Lin, D., Sun, X., Curth, U., Drosten, C., Sauerhering, L., Becker, S., Rox, K., Hilgenfeld, R., 2020. Crystal structure of SARS-CoV-2 main protease provides a basis for design of improved α-ketoamide inhibitors. Science 368, 409–412. https://doi.org/10.1126/science.abb3405

Zhang, X.M., Kousoulas, K.G., Storz, J., 1991. The hemagglutinin/esterase glycoprotein of bovine coronaviruses: sequence and functional comparisons between virulent and avirulent strains. Virology 185, 847–852. https://doi.org/10.1016/0042-6822(91)90557-r

Zhang, Y., Ji, X., Huang, D., Lu, G., Chen, X., 2025a. The coronavirus 3CL protease: Unveiling its complex host interactions and central role in viral pathogenesis. Virol. Sin. 40, 509–519. https://doi.org/10.1016/j.virs.2025.07.002

Zhang, Z., Nomura, N., Muramoto, Y., Ekimoto, T., Uemura, T., Liu, K., Yui, M., Kono, N., Aoki, J., Ikeguchi, M., Noda, T., Iwata, S., Ohto, U., Shimizu, T., 2022. Structure of SARS-CoV-2 membrane protein essential for virus assembly. Nat. Commun. 13, 4399. https://doi.org/10.1038/s41467-022-32019-3

Zhao, M., Zhang, Y., Liang, Y., Lei, F., Han, Y., Yuan, Z., Yi, Z., 2025. SARS-CoV-2 polyprotein expression and the induction of double-membrane vesicles. J. Virol. 99, e01385-25. https://doi.org/10.1128/jvi.01385-25

Zhao, M.-M., Yang, W.-L., Yang, F.-Y., Zhang, L., Huang, W.-J., Hou, W., Fan, C.-F., Jin, R.-H., Feng, Y.-M., Wang, Y.-C., Yang, J.-K., 2021. Cathepsin L plays a key role in SARS-CoV-2 infection in humans and humanized mice and is a promising target for new drug development. Signal Transduct. Target. Ther. 6, 134. https://doi.org/10.1038/s41392-021-00558-8

Zheng, M., Zhao, X., Zheng, S., Chen, D., Du, P., Li, X., Jiang, D., Guo, J.-T., Zeng, H., Lin, H., n.d. Bat SARS-Like WIV1 coronavirus uses the ACE2 of multiple animal species as receptor and evades IFITM3 restriction via TMPRSS2 activation of membrane fusion. Emerg. Microbes Infect. 9, 1567–1579. https://doi.org/10.1080/22221751.2020.1787797

Zhou, P., Fan, H., Lan, T., Yang, X.-L., Shi, W.-F., Zhang, W., Zhu, Y., Zhang, Y.-W., Xie, Q.-M., Mani, S., Zheng, X.-S., Li, B., Li, J.-M., Guo, H., Pei, G.-Q., An, X.-P., Chen, J.-W., Zhou, L., Mai, K.-J., Wu, Z.-X., Li, D., Anderson, D.E., Zhang, L.-B., Li, S.-Y., Mi, Z.-Q., He, T.-T., Cong, F., Guo, P.-J., Huang, R., Luo, Y., Liu, X.-L., Chen, J., Huang, Y., Sun, Q., Zhang, X.-L.-L., Wang, Y.-Y., Xing, S.-Z., Chen, Y.-S., Sun, Y., Li, J., Daszak, P., Wang, L.-F., Shi, Z.-L., Tong, Y.-G., Ma, J.-Y., 2018. Fatal swine acute diarrhoea syndrome caused by an HKU2-related coronavirus of bat origin. Nature 556, 255–258. https://doi.org/10.1038/s41586-018-0010-9

Zhou, P., Tachedjian, M., Wynne, J.W., Boyd, V., Cui, J., Smith, I., Cowled, C., Ng, J.H.J., Mok, L., Michalski, W.P., Mendenhall, I.H., Tachedjian, G., Wang, L.-F., Baker, M.L., 2016. Contraction of the type I IFN locus and unusual constitutive expression

of IFN-α in bats. Proc. Natl. Acad. Sci. 113, 2696–2701. https://doi.org/10.1073/pnas.1518240113

Zhou, P., Yang, X.-L., Wang, X.-G., Hu, B., Zhang, L., Zhang, W., Si, H.-R., Zhu, Y., Li, B., Huang, C.-L., Chen, H.-D., Chen, J., Luo, Y., Guo, H., Jiang, R.-D., Liu, M.-Q., Chen, Y., Shen, X.-R., Wang, X., Zheng, X.-S., Zhao, K., Chen, Q.-J., Deng, F., Liu, L.-L., Yan, B., Zhan, F.-X., Wang, Y.-Y., Xiao, G.-F., Shi, Z.-L., 2020. A pneumonia outbreak associated with a new coronavirus of probable bat origin. Nature 579, 270–273. https://doi.org/10.1038/s41586-020-2012-7

Zhou, Y., Gammeltoft, K.A., Ryberg, L.A., Pham, L.V., Tjørnelund, H.D., Binderup, A., Duarte Hernandez, C.R., Fernandez-Antunez, C., Offersgaard, A., Fahnøe, U., Peters, G.H.J., Ramirez, S., Bukh, J., Gottwein, J.M., 2022. Nirmatrelvir-resistant SARS-CoV-2 variants with high fitness in an infectious cell culture system. Sci. Adv. 8, eadd7197. https://doi.org/10.1126/sciadv.add7197

Zhu, N., Zhang, D., Wang, W., Li, X., Yang, B., Song, J., Zhao, X., Huang, B., Shi, W., Lu, R., Niu, P., Zhan, F., Ma, X., Wang, D., Xu, W., Wu, G., Gao, G.F., Tan, W., 2020. A Novel Coronavirus from Patients with Pneumonia in China, 2019. N. Engl. J. Med. 382, 727–733. https://doi.org/10.1056/NEJMoa2001017